SYNTHESIS OF METAL AND SEMICONDUCTOR NANOPARTICLES:

PROGRESS TOWARDS UNDERSTANDING DIGESTIVE RIPENING

by

SREERAM CINGARAPU

B.Sc., KAKATIYA UNIVERSITY, ANDHRA PRADESH, INDIA, 1993
M.Sc., KAKATIYA UNIVERSITY, ANDHRA PRADESH, INDIA, 1998

AN ABSTRACT OF A DISSERTATION

submitted in partial fulfillment of the requirements for the degree

DOCTOR OF PHILOSOPHY

Department of Chemistry
College of Arts and Sciences

KANSAS STATE UNIVERSITY
Manhattan, Kansas

2010

Abstract

In recent years both metal and semiconductor nanoparticles have gained the attention of many research groups because of their unique properties. Synthesizing metal and semiconductor nanoparticles with narrow size distribution, uniform shape, and good crystalline nature represents a significant challenge.

Our research group has taken the synthesis procedure a step forward when we discovered that “when a polydispersed colloidal solution upon heating at or near the boiling point of the solvent in presence of excess surface active ligands, the particles evolve into a thermodynamic equilibrium size regime and this phenomenon was named “Digestive Ripening”. The ability to tune the nanoparticles size with a narrow size distribution after post - preparation in a reproducible fashion is remarkable.

The current dissertation research encompasses the field of metal and semiconductor nanoparticles and the major part of the work is devoted to understand the digestive ripening of gold-dodecanethiol system, and the effect of the nature of the ligand and solvent temperature on a low melting point indium metal – digestive ripening.

A noteworthy achievement of the current work is the ability to extent the digestive ripening to the semiconductor materials cadmium selenide and cadmium telluride by employing different ligands and by the use of different solvents. A diverse set of instrumental techniques is used for the characterization of both metal and semiconductor nanoparticles.

SYNTHESIS OF METAL AND SEMICONDUCTOR NANOPARTICLES:

PROGRESS TOWARDS UNDERSTANDING DIGESTIVE RIPENING

by

SREERAM CINGARAPU

B.Sc., KAKATIYA UNIVERSITY, ANDHRA PRADESH, INDIA, 1993
M.Sc., KAKATIYA UNIVERSITY, ANDHRA PRADESH, INDIA, 1998

A DISSERTATION

submitted in partial fulfillment of the requirements for the degree

DOCTOR OF PHILOSOPHY

Department of Chemistry
College of Arts and Sciences

KANSAS STATE UNIVERSITY
Manhattan, Kansas

2010

Approved by:

Major Professor
Kenneth J. Klabunde

Copyright

Abstract

In recent years both metal and semiconductor nanoparticles have gained the attention of many research groups because of their unique properties. Synthesizing metal and semiconductor nanoparticles with narrow size distribution, uniform shape, and good crystalline nature represents a significant challenge.

Our research group has taken the synthesis procedure a step forward when we discovered that “when a polydispersed colloidal solution upon heating at or near the boiling point of the solvent in presence of excess surface active ligands, the particles evolve into a thermodynamic equilibrium size regime and this phenomenon was named “Digestive Ripening”. The ability to tune the nanoparticles size with a narrow size distribution after post - preparation in a reproducible fashion is remarkable.

The current dissertation research encompasses the field of metal and semiconductor nanoparticles and the major part of the work is devoted to understand the digestive ripening of gold-dodecanethiol system, and the effect of the nature of the ligand and solvent temperature on a low melting point indium metal – digestive ripening.

A noteworthy achievement of the current work is the ability to extent the digestive ripening to the semiconductor materials cadmium selenide and cadmium telluride by employing different ligands and by the use of different solvents. A diverse set of instrumental techniques is used for the characterization of both metal and semiconductor nanoparticles.

Table of Contents

List of Figures

List of Tables

List of Schemes

Acknowledgements

First of all, I would like to express my sincere and heartfelt gratitude to my doctorate advisor, at Kansas State University, Professor Kenneth J. Klabunde, for the honor to work under his guidance. I greatly appreciate the freedom he gave me to pursue my research in my own way and the opportunity to work in collaboration with both inter-disciplinary and intra-disciplinary research groups. I would also like to thank him for taking his time in meeting my family members back home, during his trip to my home country, India. I greatly appreciate his outstanding support in my personal life, without which, my personal life equation could have been in imbalance. I tremendously enjoyed all the trips taken in the past few years; especially my trip to Bulgaria is a life lasting experience. The people I have met during these trips have made my life richer and my research better. Along those lines I would like to thank Linda Klabunde for her support, encouragement and especially for all those International Friends parties, which sparks every year at Mr & Mrs Klabunde's house.

Secondly, I would like to thank my undergraduate Professor, Nagabushanum, and my graduate Professor S. SriHari, Kakatiya University, who taught me in several classes. Along those lines I would also like to thank Phanindra Krishna Mohan Venukadasula and Dr. Battina K. Srinivas for introducing Department of Chemistry, Kansas State University to me. I would like to thank Professor Christer Aakeroy for the opportunity to come to K-State and attend graduate school and I would like to thank to Professor Christopher J. Levy.

I also want to thank Dr. Amit kumar, Mausam Kalita, Vinodh Reddy Sareddy, Naga Prasad Daggupati, and Aditya Gundugolavas (@ 1207 Kearney Street) for being good friends for the past five years.

I would like to thank my committee members: Prof. Kenneth J. Klabunde, Prof. Christopher M. Sorensen, Prof. Stefan H. Bossmann, and Prof. Viktor Chikan. Thank you for your time and valuable suggestions and discussions. I really appreciate Prof. Youqi Wang for accepting the role as the chair of my committee.

A special thanks to all the present and former group members of the KJK group during my time there: Dr. Shalini Rodrigues, Dr. Jeevanandam Pethaiyan, Dr. Igor Martyanov, Dr. Alexander Bedilo, Dr. Alexander Smetana, Dr. Dmytro Demydov, Dr. Aaron Yang, Dr. Johanna A. Haggstrom, Dr. Xiangxin Yang, Dr. Kennedy K. Kalebaila, Dr. Dambar Hamal, Erin Beavers, Luther Mahoney, Yen-Ting Kuo, Khadga Man Shrestha, Schuyler Baker, Manindu Peiris, Sheila, and Ashley Cetnar. The NIRT-NSF research team, Prof. Kenneth J. Klabunde, Prof. Christopher M. Sorensen, Prof. Christer Aakeroy, Prof. Bruce M. Law, Prof. Amit Chakrabarti, and Dr. Xiao-Min Lin for their valuable suggestions and discussions in every week research group meeting. Along those lines I would also like to thank Dr. Benjamin Scott, Dr. Hao Yan, Dr. Haeng Sub Wi, Brandon Lohman , Evan Pugh, Siddique J. Khan and Jeff Powell for their support. A special acknowledgement to Dr. Alexander Smetana, who helped me with SMAD technique.

Thank you Richard Bachamp, Tobe Eggers, Jim Hodgson, Ron Jackson for fixing my equipment whenever needed! Thank you, Earline Dikeman for helping in teaching lab course and thank you to all the ladies in the office for helping with all kinds of things! My

special thanks go to Linda Gibbs, who helped me to come across my home sickness in my initial days at KSU.

I would like to thank Dr. Dan Boyle and the Division of Biology for the assistance and use of the Transmission Electron Microscope, Dr. David Moore and Heather Shinogle, KU Microscopy & Analytical Imaging Lab for their help with HRTEM images. I am also thankful to Myles Ikenberry and Dr. Keith Hohn for the XPS measurements of my samples. Along the line, I would also like to thank Dr. Karen Gaskell, for the XPS measurements of my samples, Shared Experimental Facilities (SEF), Materials Research Science and Engineering Center, Maryland University. I would also like to thank all the lab members of Prof. Duy Hua, for their help with distilled solvents.

I thank Christopher Tuinenga, Sanmitra Barman, Lateef Syed, Fathima Ibrahim (Shaida), Prashant Chopade, Santanu Roy, and Safiyyah Forbes. My special thanks to Hicran Koç for her encouragement and support.

Lastly, I would like to thank my friends, especially Dr. Kondaji Gajulapati, Dr. Ravinder Kodela, Dr. Putta Prashanthi, Yannam Janardhan, Raghu Gundapuneni, Venu Madhav Venukadasula, Brahmareddy Gandra, Srinivasa R. Raju. Garikapati Satyanarayana (Taj Bakery), a person who stood with me in a very needy hr in my life. I would also like to thank Maganti Vijaya Bhasker. My cousin brother Srinivas Rao Rakonda, Ragu Avudurthi, Pampati Srinivas and to my family back home for all their support and for making it easier being far away from home. A very special acknowledgment to my Late. Grandmother Alagandula Ramulamma for her love and encouragement and I would like to thank my aunt Alagandula Ramanamma for her support.

Dedication

For their endless love and encouragement,

without which this journey could not be possible.

To my parents:

Cingarapu Laxmi Narsaiah (late)

Cingarapu Satyavathi

To my wife:

Vindhya Gudichuttu

And

To all my former teachers

.

Preface

Digestive Ripening Matters!

CHAPTER 1 - Gold-Dodecanethiol: Digestive Ripening, Effect of Ligand Concentration, and Reaction Intermediates

1.1 INTRODUCTION

Historically, colloidal gold is most often tracked back to Alchemy, where coloring glass and enamels were made from colloidal gold in the presence of tin. [1] In modern era the synthesis of colloidal gold was first reported by Michael Faraday in 1857,[2] where he discovered a ruby color from colloidal gold upon reduction of gold salts with a reducing solution such as phosphorus in carbon disulfide in a two phase system. [2] The objective of his investigations with gold was to examine the interaction of light with the metal particles and he concluded that the ruby fluid of gold was from the dispersion of small gold in the liquid and those small gold particles were not detected from any of the imaging microscopes in those days. Later, his idea of interaction of light with the metal particles was theoretically explained by Mie, who solved the Maxwell equation of electricity and magnetism for small metal nanoparticles [3] and after nearly 100 years of Faraday's first observations, it was Turkevich et al, investigation with transmission electron microscopy revealed that the ruby color colloid produced by Faraday was particles of gold with an average size in the rage of 6 – 8 nm. [4]

1.2 Gold Nanoparticles – Colloidal Synthesis Routes

1.2.1 Turkevich Method – 1951

A useful method for synthesis of metal colloids was reported by Turkevich and co-workers in 1951.[4] Figure 1.1 represents the schematic synthesis of colloid gold by

reduction of metal salts in aqueous phase, where the gold ions were reduced in the presence of citrate anions.

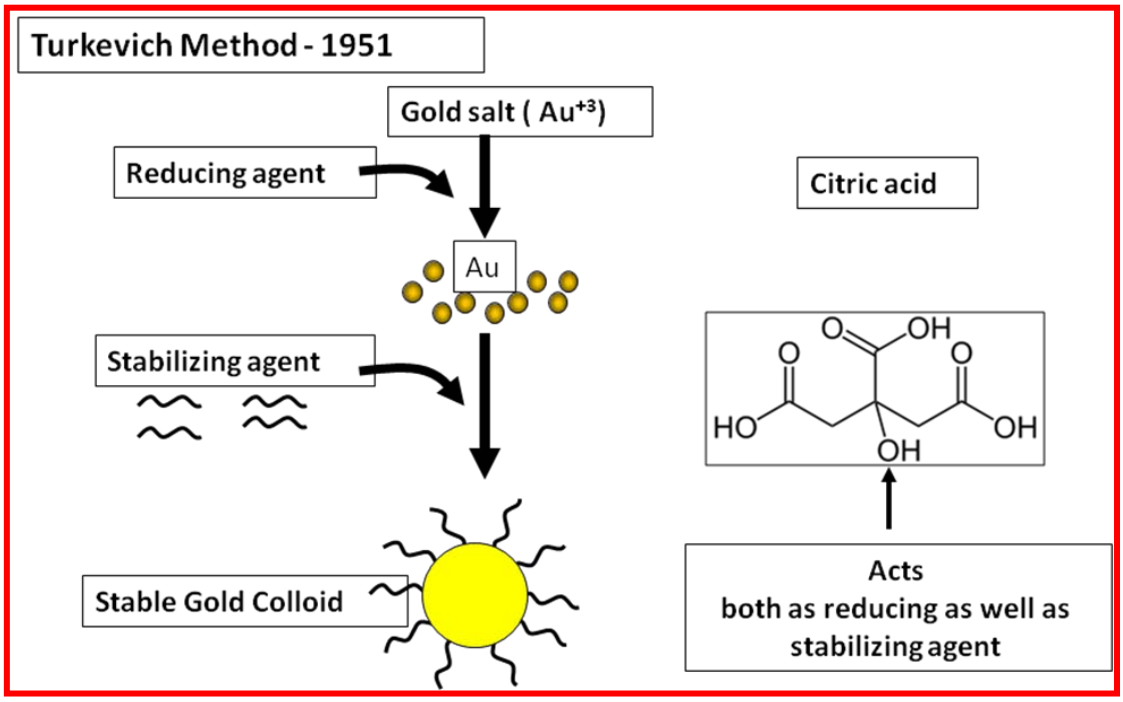

Figure 1.1 Schematic representation of synthesis of colloidal gold by Turkevich Method [4]

Even though this procedure is well established in practice, this method does not yield highly monodispersed nanoparticles.

1.2.2 Micelles and Inverse Micelle assemblies

An alternate method to synthesize colloidal gold is by reduction of gold salts in constrained environment created by a surfactant molecule. [5,6] [7] These surfactant molecules consist of hydrophilic head and a hydrophobic tail, by maintaining a delicate balance between a surfactant and two solvents of different polarities, surfactant

molecules order themselves into spherical micellar pockets separating the aqueous and organic phases. These micellar pockets acts as “microreactors”, where the reduction of metal salts takes place. Hence particles growth is somewhat limited and controlled within these microreactors. In these systems, the constituents undergo rapid exchange with time and therefore the number of metal ions available in the micellar pockets is not constant and hence these systems yields poly-dispersed particles. [6] Synthesis of nanomaterial by such method involves an extensive size – selective procedure to obtain mono-dispersed particles.[8] Figure 1. 2 represent a schematic overview of a typical inverse micelle method. [9]

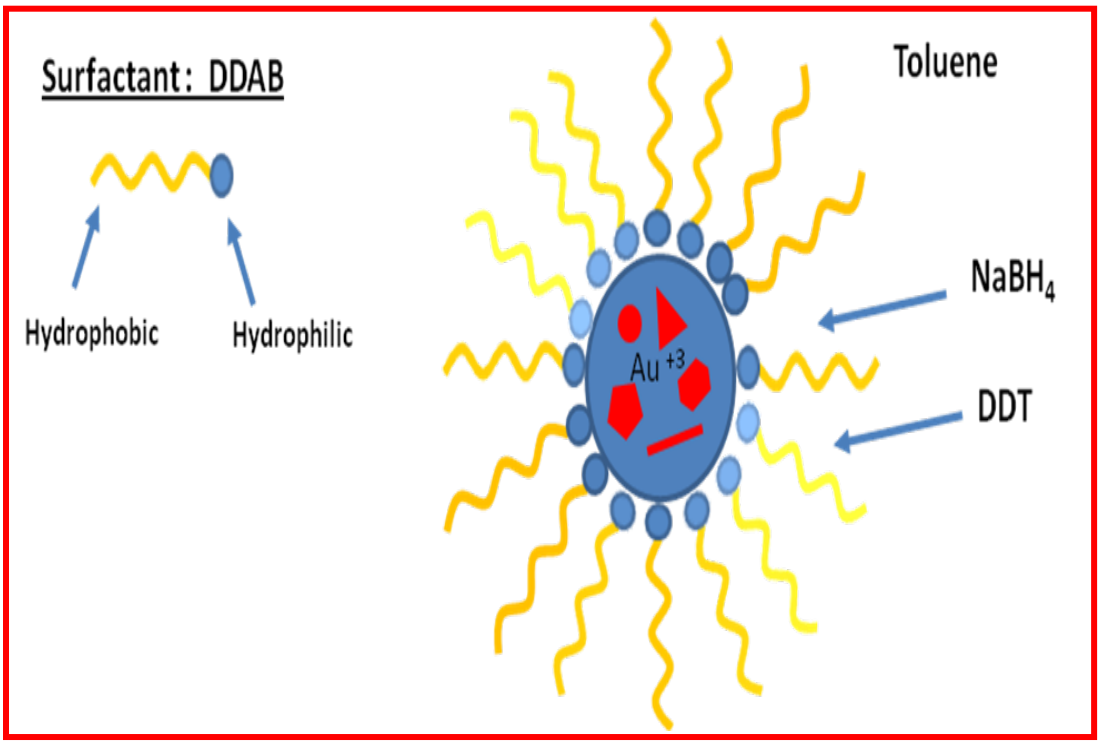

Figure 1.2 Schematic overview of a typical Inverse Micelle Method, (Didodecyl di methyl ammonium bromide (DDAB), Dodecane thiol (DDT)) [9] .

1.2.3 Brust Method

This method was reported by Brust and co-workers in 1994,[10] and is a single- step synthesis which utilizes a two-phase system to produce alkanethiol stabilized gold or silver nanoparticles. By employing a phase transfer agent tetraoctyl ammonium bromide (TOAB), transfer of unreduced gold salt ($AuCl_4^-$) from aqueous phase to organic phase was achieved, and the reduction of salt was carried by sodium borohydride. The formed nanoparticles were then quickly stabilized by alkanethiol ligand present in the organic phase. Indeed, a sulfur atom is a softer base and has a better interaction with the soft noble metal atoms compared to citrate stabilized particles by Turkevich method.

1.2.4 Sonochemical Method

In recent years a sonochemical method has emerged as an alternate method for the synthesis of nanoparticles. By employing ultrasonication in a liquid environment, enormous temperatures and pressures are created in a localized area within the solution and a unique reaction environment is induced by acoustic cavitation. These extreme conditions cause shock wave generation, and radical formation that can drive the reactions in unique ways.[11] Franz Grieser and co-workers found that the rate of sonochemical reduction of Au (III) to produce gold nanoparticles was strongly dependent upon the ultrasound frequency.[12]

1.2.5 Microwave Irradiation

The use of microwave for the synthesis of nanoparticles has gained attention beginning in 1986 due to its rapid heating and energy penetration, thereby reducing the reaction time.[13] Many microwave based synthesis routes were developed to synthesize gold nanoparticles, nanowires, nanoplates, and nanorods. [14-16] Recently, Kundal et al has achieved size-controlled gold (Au) nanoparticles in the presence of poly (N-vinyl-2-pyrrolidone) (PVP) under microwave heating for just 60 s in aqueous solutions by adjusting the PVP to Au (III) molar ratio, and by using different molecular weight PVP molecules. The reduction of Au (III) to Au (0) by PVP was attributed to favorable thermodynamics. [17]

1.2.6 Vaporization methods

There are several ways to create nanoparticles from atoms: In Physical Vapor Deposition (PVD) the source metal will be thermally heated under inert atmosphere using tungsten crucible and the evaporated metal atoms or clusters can be cooled by a carrier gas (such as helium), and then deposited on a cold finger. When the reaction is completed the powder can be scraped from the cold finger. [18]

Gram -scale synthesis of metal and semiconductor nanoparticles is possible by a modified vaporization technique known as the Solvated Metal Atom Dispersion (SMAD) developed by Klabunde et al.[19-22] in this technique the vaporized atoms / cluster were co-condensed with excess solvents (solvated at low temperature) and upon gentle warming and matrix melts, allowed to react with stabilizing ligands. The initial as-prepared SMAD product generally yields poly-dispersed particles due to little control

over the vaporization and condensation. But it is remarkable that these poly-dispersed particles can be converted into highly mono-dispersed particles by a unique post-preparative digestive ripening process. [9,19-22]

1.3 Digestive Ripening – a Post-Preparative process

Nanomaterials can be synthesized either by bottom-up or top-down approaches as described above. Though, there are many synthesis approaches, synthesizing metal nanoparticles with narrow size distribution, uniform shape, and good crystalline nature represents a significant challenge. Digestive ripening is a unique post-preparative process, where a poly-dispersed colloid material upon heating at or near the boiling temperature of the solvent in the presence of excess surface active ligand will bring these particles to an thermodynamically equilibrium size distribution.[9] This digestive ripening process was discovered in our laboratory, which is a simple, yet effective route to convert poly-dispersed nanoparticles into highly mono-disperse.

In contrast to the well-known Ostwald ripening process, where larger particles grow at the expense of smaller ones, in digestive ripening smaller particles will grow bigger and bigger particles will break down / dissolve and finally the system reaches a thermodynamic equilibrium size. This process could be more advantageous in synthesizing nanomaterial on gram-scale for practical applications. Further, this procedure was successfully employed to other metal nanoparticles silver, copper, magnesium, and palladium [21,23,24] [25] and in fact, different functional group ligands and ligand chain lengths have also been investigated by Stoeva and Prasad et al. [26,27]

1.4 Surface Plasmon Resonance

Metal nanoparticles like gold and silver posses a plasmonic band in the visible region of the electromagnetic spectrum. Thus spherical gold nanoparticles have a characteristic red color, while silver spheres are yellow. The d-electrons in these metals are free to travel through the material and the mean free path is ~ 50 nm. Therefore, in metal nanoparticles smaller than this mean free path, no scattering of light is observed, as in the case of bulk, larger particles. Thus, the interactions of light in resonance with the surface free electrons of metal nanoparticles create oscillations.[28] As a result of this optical effect, a new type of resonance called plasmon or surface plasmon resonance (SPR) localized between the metal nanoparticles and the surrounding dielectric medium produces an enhanced electromagnetic field at the interface and experimentally these resonances can be monitored by absorption spectroscopy.[28] The wavelength of the absorption peak maximum is found to depend on the shape, size and dielectric constant of the surrounding environment. [29] In fact, the capping material or stabilizing ligands, does influence the shift of the plasmon resonance, for example, thiol stabilized gold nanoparticles will give a surface plasmon resonance at 530 nm, whereas amine stabilized gold nanoparticles exhibit SPR at 540 nm. [27,29] If the particle size is smaller than the wavelength of the absorption light, the shift in SPR will be in a narrow range. In case of larger plasmonic metal nanoparticles they exhibit red shift. [30,31]

The purpose of this work is to evaluate the effect of ligand concentration on digestive ripening of the gold-dodecanethiol system and to explore possible intermediates, and a part of this work was devoted to ligand exchange reactions through digestive ripening.

1.5 Experimental Procedure

In a typical experiment, 0.104 gram (mol) of didodecylammonium bromide (DDAB, FLUKE) was dissolved in 10 mL of distilled and degassed toluene to form a 0.02 M inverse micelle solution and the entire solution was stirred continuously for 30 minutes to ensure complete dissolution of DDAB in toluene. After 30 minutes 0.034 g (mol) of $AuCl_3$ (99.99%, Sigma-Aldrich) was dissolved in the DDAB-toluene solution by vigorous stirring, followed by sonication. At this stage the solution becomes clear with a deep orange-red colored $AuCl_3$ –DDAB – toluene was obtained. Freshly prepared aqueous $NaBH_4$ solution (40 µl, 9.4 M) was then added by drop wise addition to the $AuCl_3$ – DDAB – toluene solution with continuous stirring for to ensure completed reduction. Upon complete reduction the solution turns into a deep purple-red in color.[26,27]

These particles were then precipitated by the addition of 30 mL of ethanol (200 proof, Fisher) and the system was left undisturbed overnight. On the following day particles were found precipitated. The supernatant was decanted and the solid precipitate was then vacuum dried and re-dissolved in 10 mL of distilled and degassed toluene solvent.

In order to understand the effect of ligand concentration on digestive ripening, different molar ratios of gold to ligand (1:8, 1: 16, 1:30 and 1:60.) were employed and then the samples were subjected to “Digestive Ripening”. Note: These ratios were employed to

replace the DDAB ligand and the same ligand ratio was added to the precipitated / re-dissolved particles before subjecting to digestive ripening.

Another set of reactions was carried out to understand the effect of digestive ripening on ligand exchange reactions. Mono-dispersed gold-dodecanethiol stabilized ~ 5 nm particles were prepared by the standard inverse micelle method, followed by digestive ripening. In order to remove the excess unbounded thiol ligand, the particles were precipitated with the addition of ethanol and then vacuum dried. The dry particles were then re-dissolved in 10 mL of distilled and degassed toluene. (I) One example, an exchange reaction with by dodecylamine ligand was carried by adding an excess of the amine, followed by digestive ripening again under argon. A similar procedure was adopted for gold-dodecylamine stabilized particles, where digestively ripened particles were precipitated, vacuum dried and re-dissolved in toluene but in this case excess dodecanethiol ligand was added. Scheme 1.1 shows the ligand-exchange procedure and digestive ripening.

1.6 Characterization

Ultraviolet-Visible-Near Infra Red (UV-Vis- NIR) spectra were collected on a Carry 500 Scan spectrophotometer equipped with a dual cell peltier accessory that allows temperature control of both the reference and the sample compartment.

Transmission electron microscopy (TEM) was performed with a Philips CM 100 operating at 100 kV. Particle size distribution was determined from a pool of minimum 300 particles from different parts of the TEM grid were observed.

A flash vaporization technique was used so as to quickly evaporate toluene solvent to restrict self-assembly of these particles (See Figure 1.3).

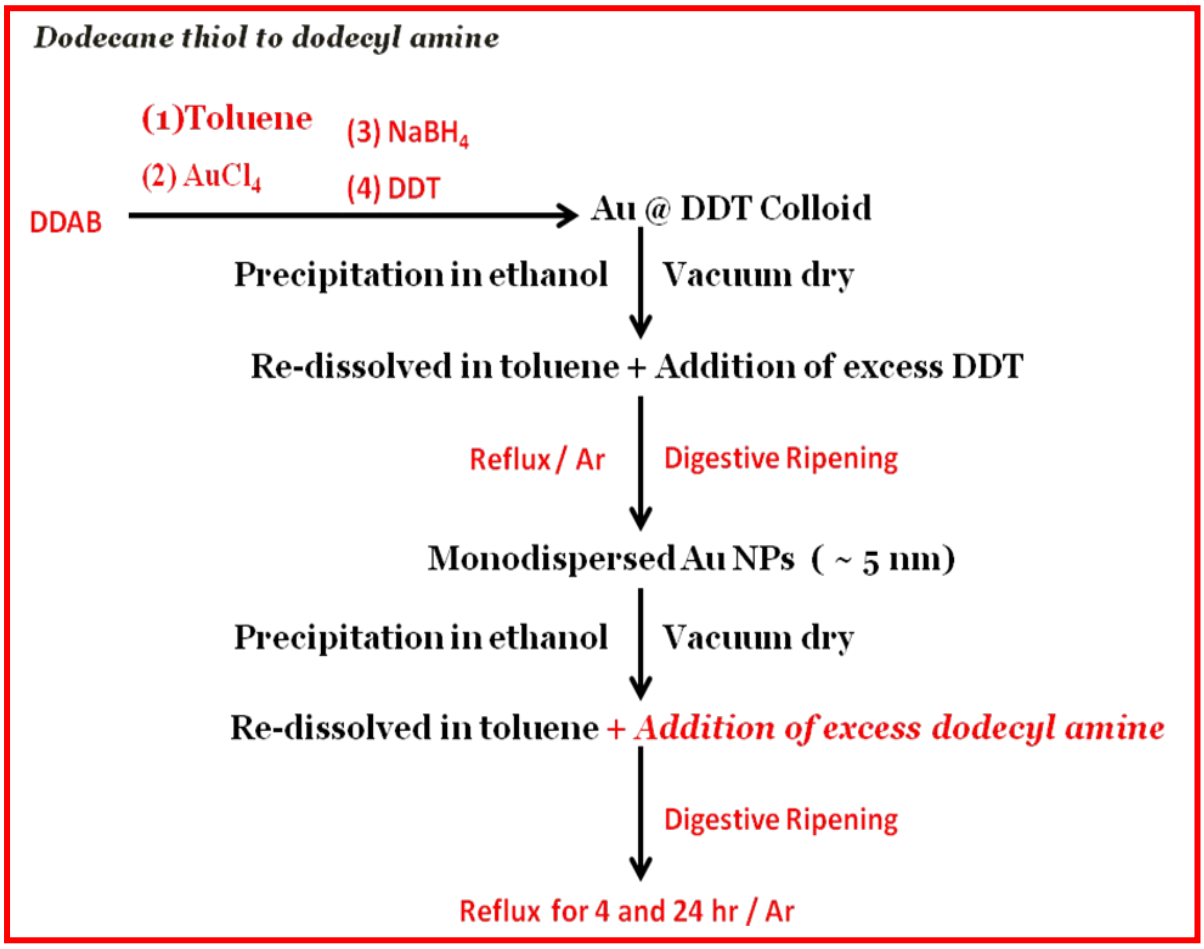

Scheme 1.1 Schematic representation of ligand-exchange and digestive ripening

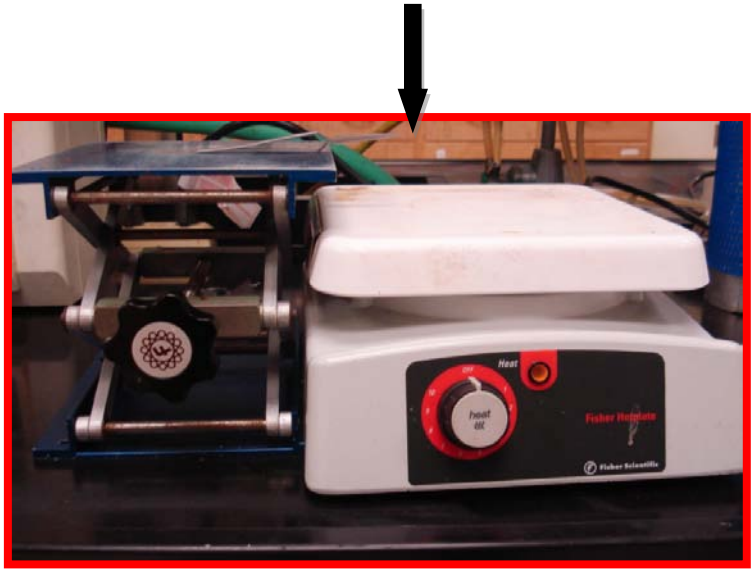

Figure 1.3 Flash vaporization of toluene from the Gold @ DDT colloid using a hot plate. The arrow showing the tweezers with the sample on TEM grid, placed near to the hot plate. The sample dries within 5 seconds, this procedure helps in restricting particles from aggregation, before examination by TEM.

1.7 Results and Discussion

Typically, before digestive ripening the surface plasmon resonance (SPR) peak of a poly-dispersed colloidal gold appears broad with a low absorption maximum, but as digestive ripening progresses, the SPR peak becomes sharper and the absorption maximum increases and finally reaches an equilibrium when the particles attain monodispersity as shown in the Figure 1.4. First we will discuss the gold: ligand ratios that were found not to be ideal, as can be observed in Figure 1.5 and 1. 6.

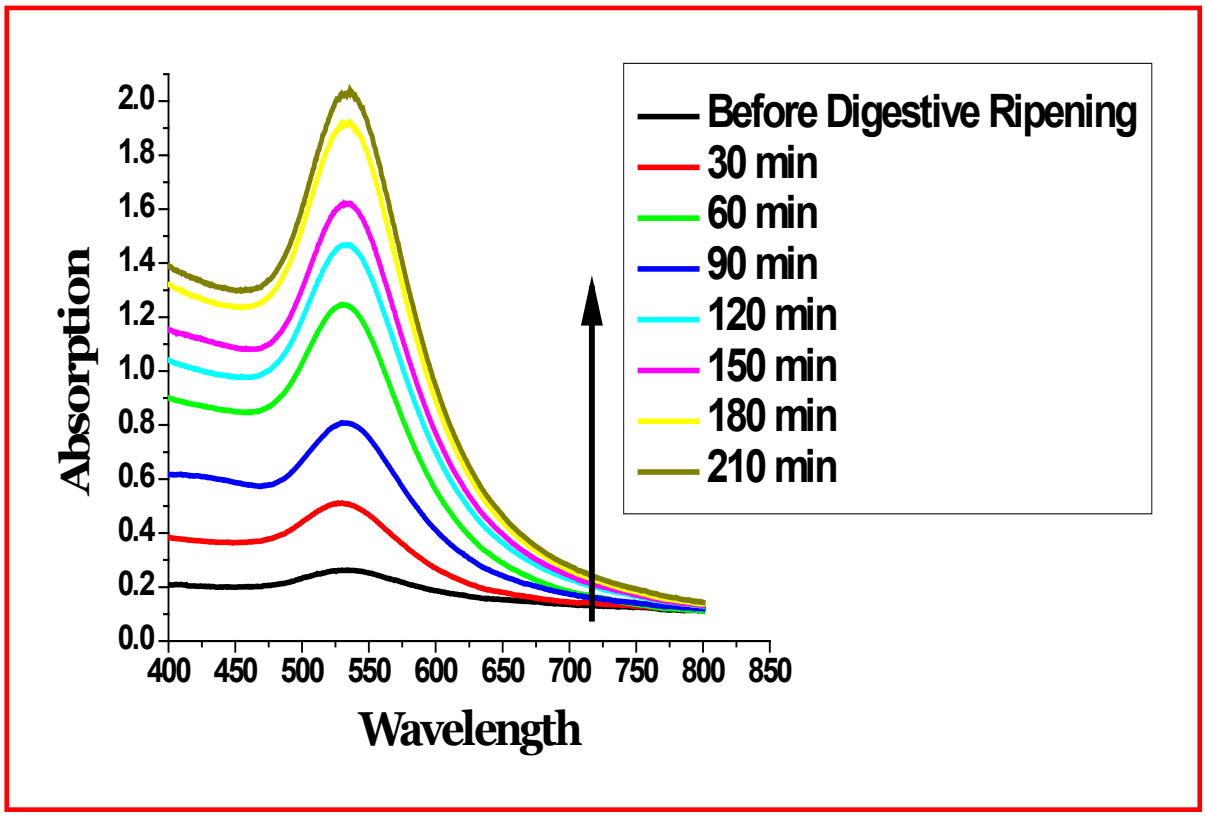

Figure 1.4 The surface plasmon peak of gold nanoparticles before digestive ripening is broad but as digestive ripening progresses, the surface plasmon peak becomes much sharper. Once particles attain a thermodynamic equilibrium size, the SPR also attains equilibrium. The increase in intensity is due to either breaking or dissolving of big crystals in solution.

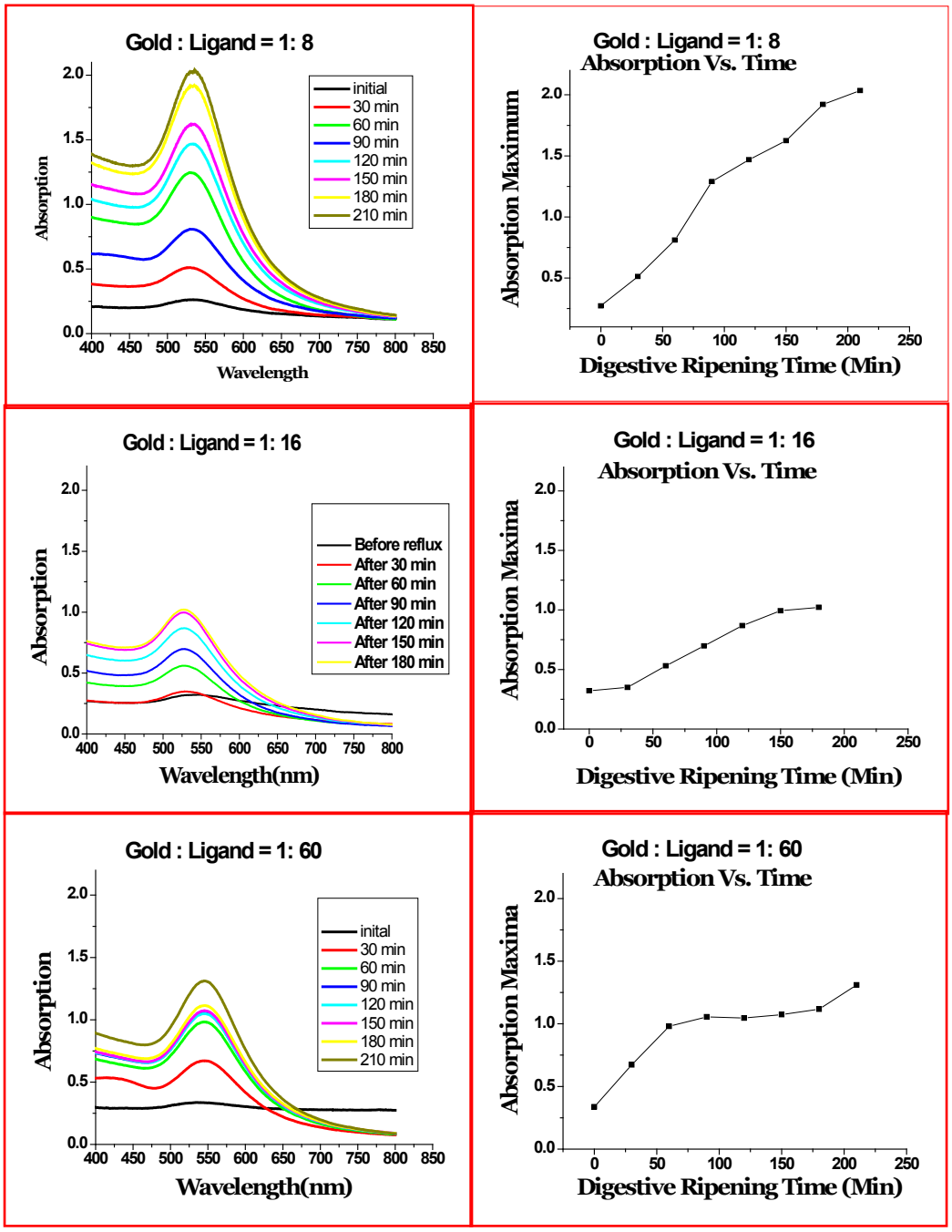

Figure 1.5 Comparison of SPR of colloidal gold with different ligand ratios with digestive ripening time and corresponding intensities of absorption maximums with digestive ripening time.

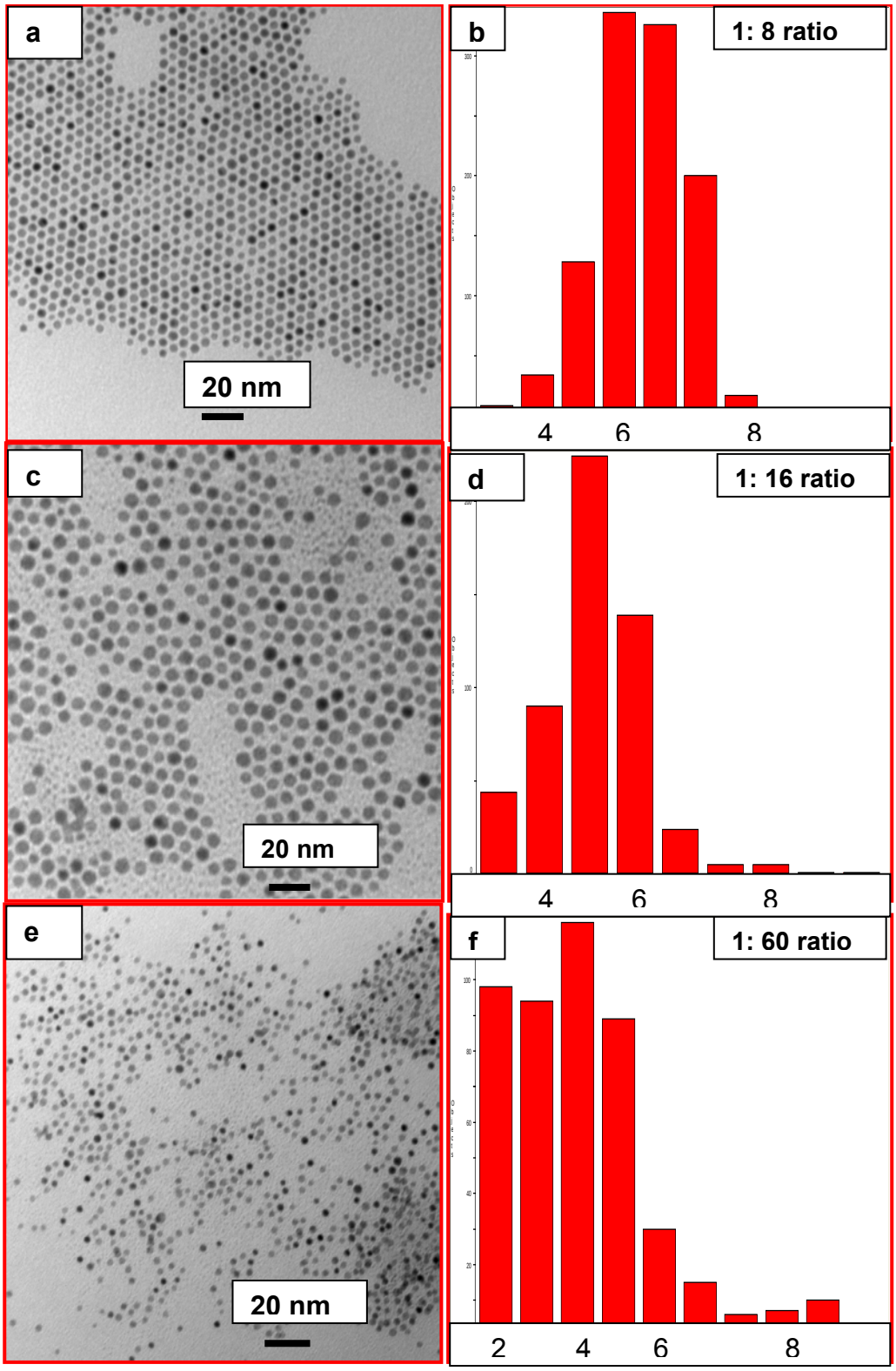

Figure 1.6 Corresponding TEM images colloidal gold with different ligand ratios with the histogram.

The corresponding absorption maxima versus digestive ripening time plot indicates that the particles described in Figure 1.4 and 1.5 did not yield an equilibrium size even after

a period of 3 hrs of digestive ripening. The average particle size measured after 3 hrs of digestive ripening with 1:8 ligand ratio is ~ 6 to 6.5 nm, whereas with 1: 16 ratio the average particle size is found to be 5 nm ± . 5 nm and with 1: 60 ratio they all tend to form smaller particles < 5 nm in size. This variation is size distribution with change in ligand ratio could have resulted from a change in the stability of these particles. For example, when glutathione- stabilized gold nanocrystals were etched in a hot solution in the presence of excess ligand; smaller particles were completely etched away leaving an Au (I): thiol polymer, where as larger particles reached a size that were especially thermodynamically stable.[32] Similar results have also been reported with different gold clusters. [33,34] It is worth noting that the particle size reported by Brust, et al[10] and Whetten, et al.[35] have produced multiply-peaked size. Figure 1.7 and Table 1.1 shows an overall comparison of the effect of ligand concentration on the absorption maxima of gold-dodecanethiol digestive ripening system.

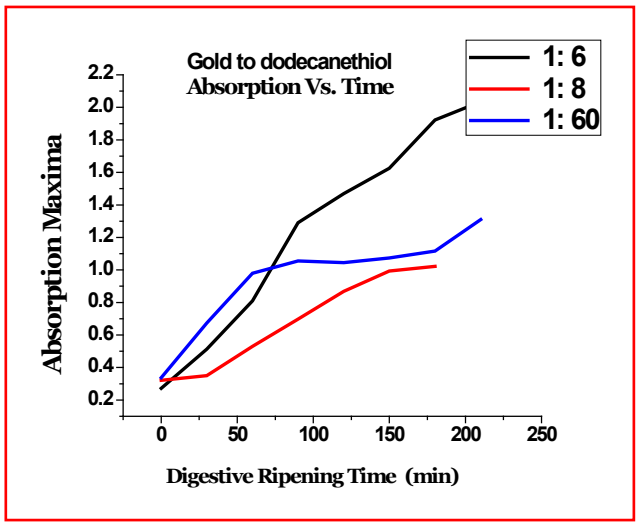

Gold :DDT Ratio	SPR peak position
1: 8	533 nm
1: 16	528 nm
1: 60	543 nm

Figure 1.7 Overall comparison of the effect of ligand concentration on the absorption maxima of gold-dodecanethiol digestive ripening system.

Table 1.1 Overall comparison of the effect of ligand concentration on the absorption maxima of gold-dodecanethiol digestive ripening system.

To investigate longer digestive ripening times, three different ligand ratios were investigated 1: 8, 1: 30, and 1:60, and were subjected to reflux for a period of 24 hrs (Figure 1.8). From the data it is evident that the 1:30 ligand ratio works best, and the absorption maxima attained equilibrium within 3 hrs of digestive ripening and it stays at equilibrium even after 24 hrs of reflux under the protection of argon. However, note that the 1:8 and 1:60 ratios did not achieve equilibrium. These results reaffirm that gold: ligand ratio is important in order to achieve a final thermodynamically stable state.

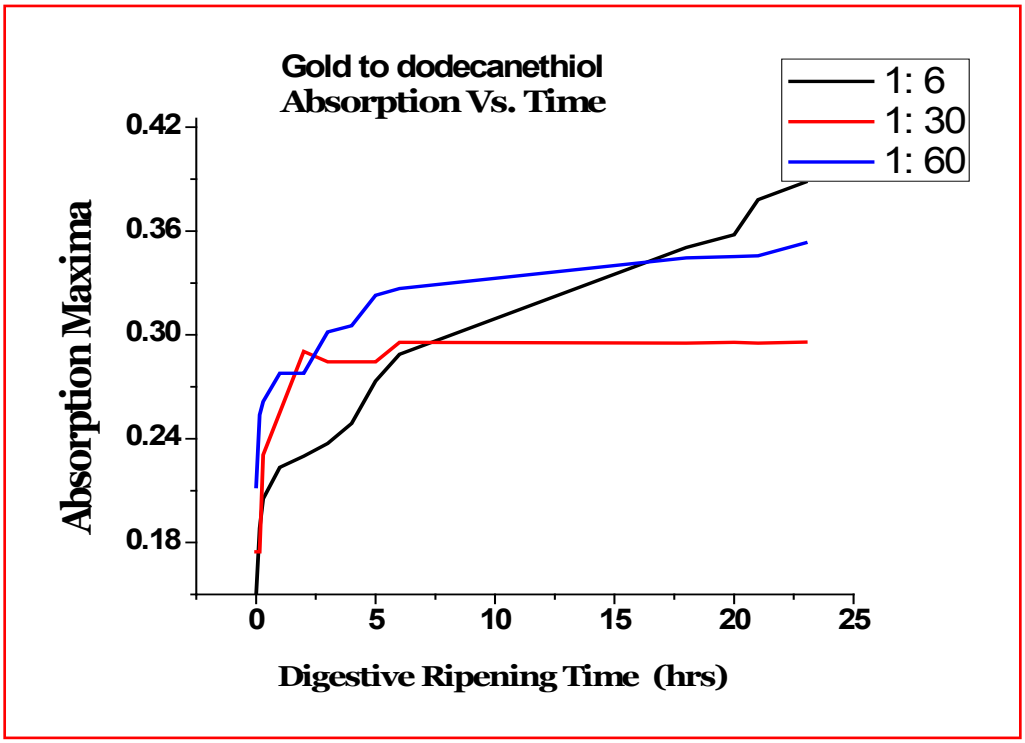

Figure 1.8 Comparison of corresponding intensities of absorption maximums with digestive ripening time for a period of 24 hrs for 1: 6, 1:30, and 1: 60 gold to dodecanethiol ratio. Where 1: 30 ration has reached an equilibrium absorption maximum.

From the absorption maxima data the 1:30 ligand ratio works best for the gold-dodecanethiol system so, in order to substantiate this, a complete particle size distribution with digestive ripening time was studied by analyzing particles from various parts of the TEM grid. Further, to eliminate the possibility of self-assembly of these digestively ripened particles, a flash vaporization technique was adopted. During this process 0.1 mL of hot colloid was initially diluted by 0.9 mL of hot toluene and from this diluted hot colloid .3μL was placed on the TEM grid, and the TEM grid was dried by flash vaporization as shown in Figure 1.3. A complete particle mean size distribution with digestive ripening is shown in Figure 1.9 with the corresponding TEM images.

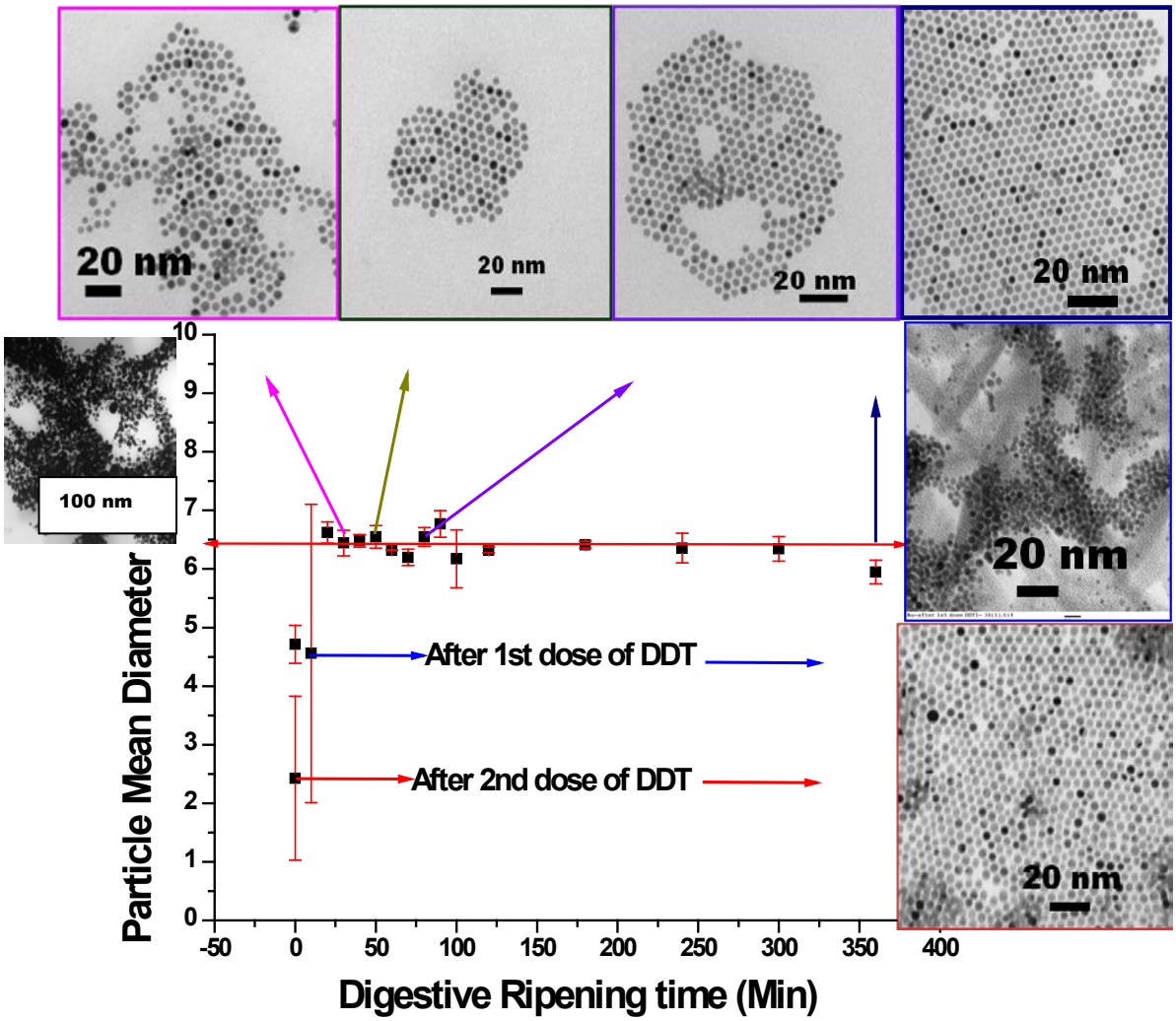

Figure 1.9 Particle mean size distribution after the addition of 1st dose, 2nd dose of dodecanethiol ligand at room temperature and with the progress of digestive ripening time with the error bars shows the particle size distribution analyzed from different parts of the TEM grid. The DDAB stabilized particles were also shown. (Please find the appendix 1 for additional TEM images

By analyzing the TEM image profile of the gold-dodecanethiol (1: 30), it is evident that the initial DDAB stabilized particles are polydispersed with particle size ranging 2-50 nm but when the first DDT ligand is added, the particles break down into a bi-model size

distribution with particles size ranging from 1 to 5 nm. After a few processing steps (precipitation, vacuum drying, and re-dissolving in toluene) when a second dose of DDT ligand (1:30) was added, the particle size was re-adjusted even at room temperature but upon digestive ripening the particles were further re-adjusted and such re-adjustment is possible because alkane thiols are well know etchants of the noble metal surface. [36] and thus DDT can enable mass transfer of atoms between particles and thereby adjusting overall narrowing of the particle size distribution, and eventually leading to a thermodynamic equilibrium size.

It is further interesting to note the interaction between the particles with digestive ripening time. Metal nanoparticles tend to self-organize into 2-D and 3-D super lattice structures and these interactions are found to depend on particle size, the nature, and the size of the organic ligand on the surface of the particle.[37-39] For example, when different chain lengths of thiol ligands are used, it was only thiols with C10, C12 chain length were found to form super lattices of gold, [26,27] Initially, tend to form some fractal structures form and with the progress of digestive ripening they tend to eventually form 3D super lattice structures and finally leading to more and more 3D super lattice formation, especially under slow evaporation conditions as shown in Figures 1.10 (a- f).

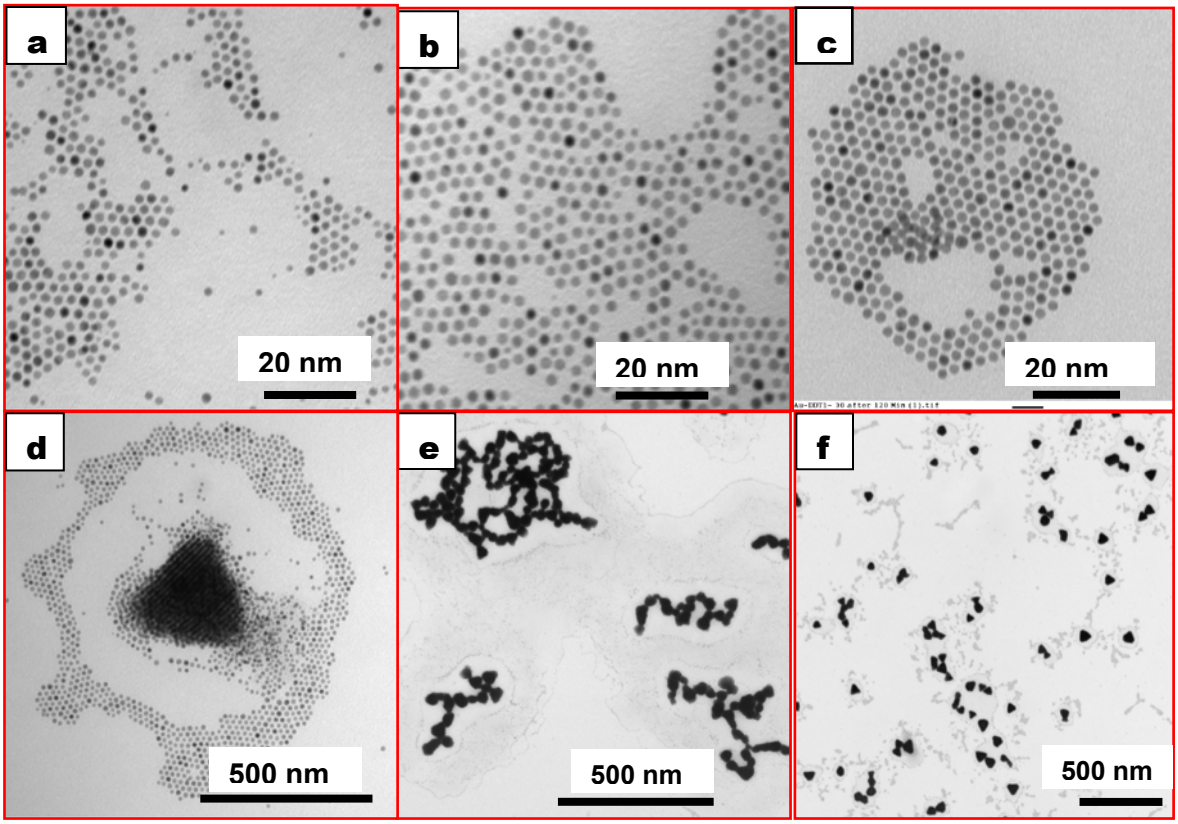

Figure 1.10 (a-f) are the samples collected at different interval of digestive ripening time for 1: 30 gold-dodecanethiol system, (a) after 10 min, (b) 30, (c) 60 min, (d) 90 min, (e) 120 min, and (f) 180 min of digestive ripening. Where the initial colloid show only fractal aggregations but with digestive ripening, more and more 3D super lattice structures were formed. The samples were prepared by slow evaporation.

1.7.1 Ligand Exchange reactions

It has been found that when thiol or amine ligand is added to a didodecyldimethyl ammonium bromide (DDAB) stabilized polyhedral gold nanoparticles (> 50 nm), the large polyhedral particles led to the break-up even at room temperature leading to small (2- 10 nm) spherical particles [40] and these smaller particles upon digestive

ripening spontaneously transform into monodispersed particles. Further it has been also found that the final particle size depends on the nature of the functional group. If thiol ligands were used, then the particle size adjusts to ~5 nm, whereas with amine, the polydispersed particles yield 9 nm. [40] Interestingly, a reversible transformation of gold nanoparticle morphology was achieved by nanomachining upon addition of DDAB to highly monodispersed gold nanoparticles, followed by digestive ripening. [41] Based on these observations; will it be possible to further adjust the particles size ~5 nm to ~9 nm and vice versa by ligand exchange through digestive ripening? Though there is no conclusive answer at this time, however some reasonable suggestions can be given. Starting with a highly monodispersed ~ 5 nm gold-dodecanethiol stabilized ligands (Figure 1.11), an excess (1:30) dodecayl amine ligand was added and then the system was subjected to digestive ripening. Figure 1.11 show the ligand exchange reaction of AU-DDA to Au-DDT ligand through an intermediate Au-DDA-DDT.

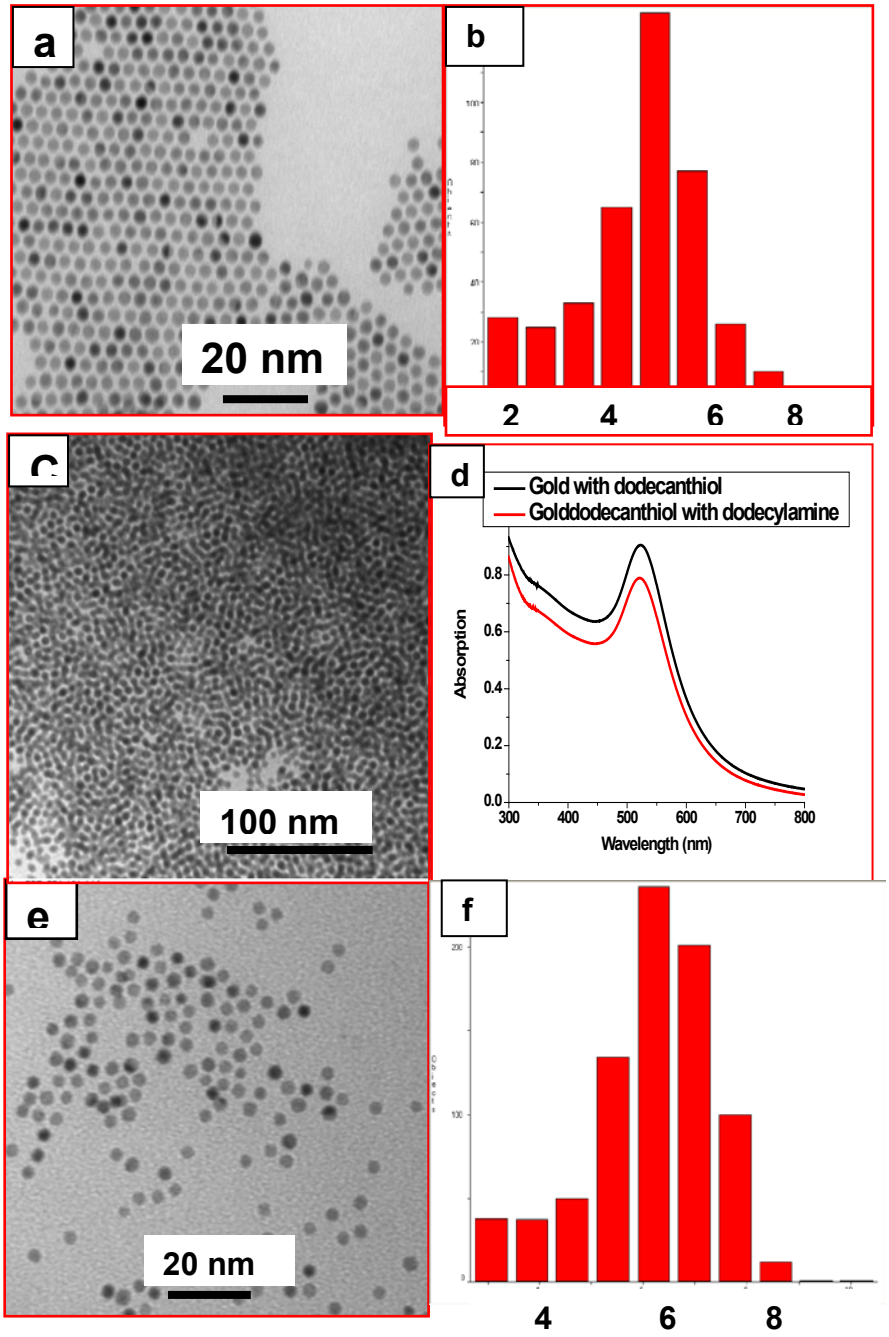

Figure 1.11 (a) DDT-stabilized gold nanoparticles,(b) corresponding histogram of particles, (c) TEM image of gold- DDT-DDA ligand exchange after 14 hrs, (d) UV-Vis before and after ligand exchange ,(e) TEM image of gold-DDT-DDA ligand exchange after 24 hrs of digestive ripening in toluene and (f) corresponding histogram.

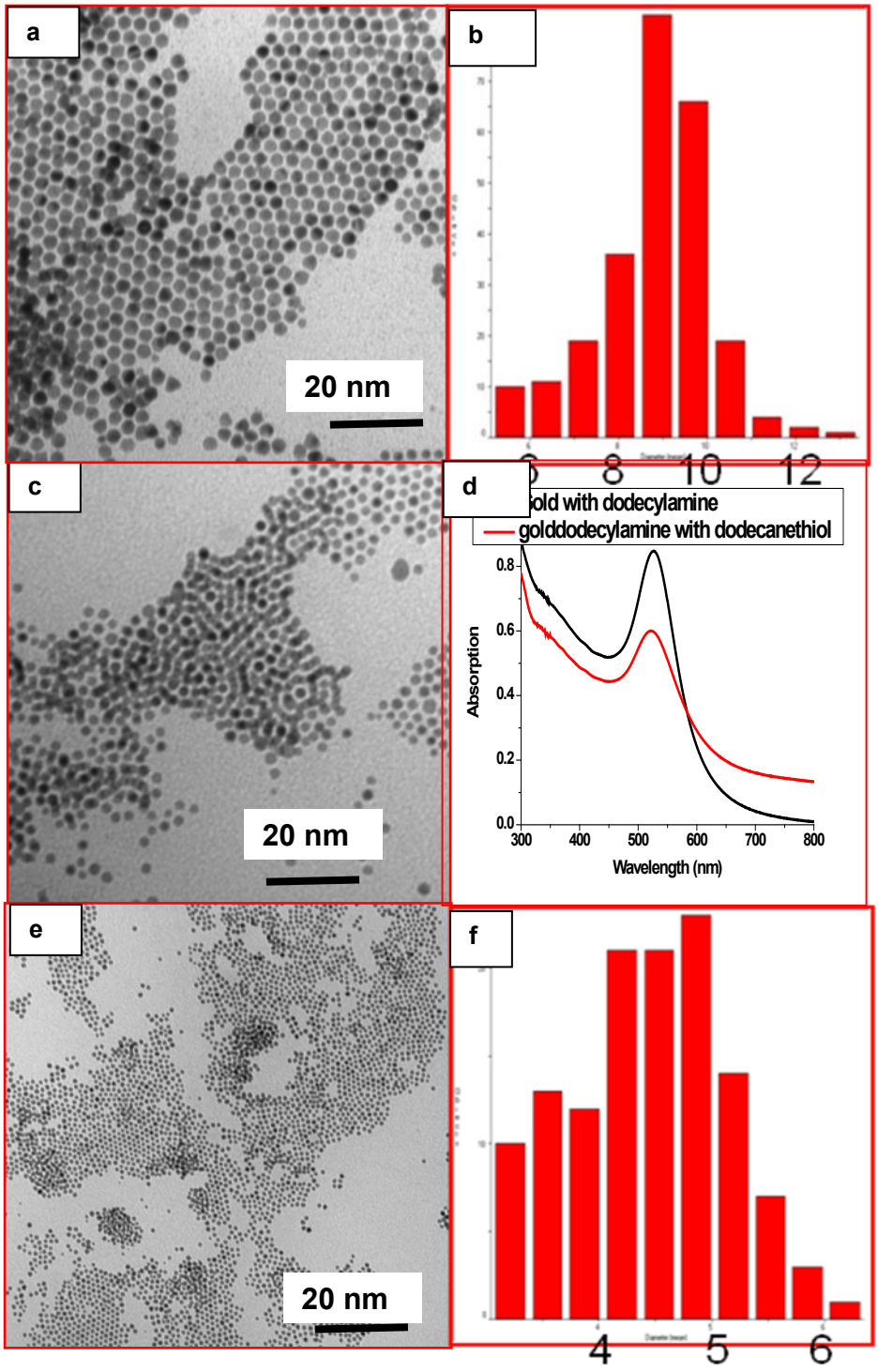

Figure 1.12 (a) DDA-stabilized gold nanoparticles,(b) corresponding histogram of particles, (c) TEM image of gold- DDA-DDT ligand exchange after 14 hrs, (d) UV-Vis before and after ligand exchange ,(e) TEM image of gold-DDA-DDT ligand exchange after 24 hrs of digestive ripening in toluene and (f) corresponding histogram.

In first ligand exchange reaction when gold-dodecanethiol stabilized gold nanoparticles were subjected to a ligand exchange with dodecylamine ligand by digestive ripening for 4 hours in toluene the particles were found to coalesce (Figure 1.11 c) but upon 24 hrs reflux at the boiling point of toluene, the particle size was adjusted from 5 nm (Figure 1.11b) to an 6.5 nm, a growth of 1.5 nm was achieved (Figure 1.11 f). The particles were well dispersed but there was no significant change in the surface plasmon absorption peak (Figure 1.11d).

In the second exchange reaction when gold-dodecylamine stabilized gold nanoparticles were subjected to a ligand exchange reaction with dodecanethiol ligand by digestive ripening, the well dispersed 9 nm (Figure 1.12a, b) gold particles were found coalesced as in the case of first ligand exchange reaction (Figure 1. 11c) but upon 24 hrs digestive ripening they yield smaller size particles, which are polydispersed with particle size ranging from 2-5 nm (Figure 1.11 e, f) and there was no significant change in the SPR before and after ligand exchange.

Based on previous finding with particle size adjustment (5 nm and 9 nm) with dodecanethiol and dodecylamine ligands, the metal to ligand interactions play an important role in adjusting the final size. Compared to nitrogen in amine ligands, sulfur in thiol ligand binds more strongly with the gold surface. Now, in ligand exchange reactions it's possible that atoms on different crystallographic facets might have different interaction strengths leading to different growth as found with polymeric and surfactant capping agent. [42,43] Therefore the leading to different particle size adjustments.

1.8 SUMMARY

1. Before digestive ripening the gold colloid has a broad UV-Vis SPR absorption peak, but during digestive ripening the SPR becomes sharper with an increase in intensity in the absorption maximum (Figure 1.4) and finally when particles attains an equilibrium size regime, the SPR reaches an equilibrium.

2. When 1:6 ligand ratio was employed, the average particle size was found to be 6.5 nm (Figure 1.5b) and it is possible that due to less ligand concentration the coalescence of neighboring crystals due to particles collisions might have resulted in particle size growth. However, they did not yield monodisperse particles as expected from digestive ripening.

3. In the case of 1: 16 gold to ligand ratio, though the average particles were found to be 5 nm but it is evident that still there are smaller particles (< 2nm) as could be seen from the TEM image (Figure 1.4 C). These results also emphasize the importance of ligand concentration on the digestive ripening.

4. When a higher ligand concentration was used (1:60) the particles were more polydispersed with < 5nm size.

5. Whereas when with 1:30 ligand ratio was used, highly monodispersed particles resulted. Upon a careful examination of particle size distribution upon the first DDT addition the system appear to be a bi-model.

6. Hence it can now be summarized that during digestive ripening the system transforms from a bi-model size distribution to a thermodynamically stable monodispersed size regime.

7. It is further interesting to note the interaction between the particles depending on the digestive ripening time under slow evaporation, where the initial digestive ripened particles formed fractal structure but with the progress of digestive ripening more and more superlattices were formed.

8. Flash vaporization techniques allowed better images of individual particles.

9. In ligand exchange reactions (With DDT to DDA and with DDA to DDT) the colloidal particles appear to coalescence upon initial digestive ripening process, and upon prolonged reflux the particle size was adjusted, and the intermediate coalescence might be due to difference in the crystallographic energies of the facets of the gold nanocrystal and the interaction of ligands with those facets.

1.9 References

(1) Hunt, L. B. *Gold Bull* **1976**, *9, 134*.

(2) Faraday, M. *Philos. Trans. R. Soc. London* **1857**, *147, 145*.

(3) Mie, G. *Ann. Phys.* **1908**, *25, 377.*

(4) Turkevich, J. S., P. S.; Hillier, *J. Discuss. Faraday Soc.* **1951**, *11, 58.*

(5) Bradley, J. S. *The chemistry of Transition Metal Colloids, G. Schmid, Ed., VCH,* **1994**, *459 - 544*.

(6) Pileni, M. P. *Collodal Assemblies Used as Microreactors in Handbook of Surface and Collodal Chemistry, J. S Bradley, Ed., CRC* **1997**, *495 - 532*.

(7) Pileni, M. P. *Adv. Colloid Interface Sci.* **1993**, *46*, 139 - 163.

(8) Murray, C. B.; Kagan, C. R.; Bawendi, M. G. *Annu. Rev. Mater. Sci.* **2000**, *30*, 545.

(9) Lin, X. M.; Sorensen, C. M.; Klabunde, K. J. *J. Nanopart. Res.* **2000**, *2*, 157-164.

(10) Brust, M. W., M.; Bethell, D.; Schiffrin, D. J.; Whyman, R. *J. Chem. Soc., Chem.Commun.* **1994**, 801.

(11) Zhang, j. H., B.; Liu, M.; Liu, D.; Dong, Z.; Liu, J.; Li, D.; Wang, J.; Dong, B.; Zhao, H.; Rong, L. *J. Phys. Chem. B* **2003**, *107*, 3679-3683.

(12) Okitsu, K.; Ashokkumar, M.; Grieser, F. *The Journal of Physical Chemistry B* **2005**, *109*, 20673-20675.

(13) Gao, F. L., Q.; Komarneni, S. *Chem. Mater* **2005**, *17*.

(14) Wang, J. W., Z. *Mater. Lett.* **2007**, *61*, 4149–4151.

(15) Tsuji, M. H., M.; Nishizawa,Y.; Tsuji,T. *Mater. Lett.* **2005**, *59*, 3856–3860.

(16) Li, C. C. C., W. P.; Cao, B.Q.; Sun, F. Q.; Li, Y.; Kan, C. X.; Zhang, L. D. *Adv. Funct. Mater* **2006**, *16*, 83–90.

(17) Kundu, S.; Wang, K.; Liang, H. *The Journal of Physical Chemistry C* **2009**, *113*, 5157-5163.

(18) Choy, K. L. *Academic Press* **2000**, *Handbook of Nanostructured Materials and Nanotechnology volume 1*.

(19) Stoeva, S.; Klabunde, K. J.; Sorensen, C. M.; Dragieva, I. *J. Am. Chem. Soc.* **2002**, *124*, 2305-2311.

(20) Stoeva, S. I.; Smetana, A. B.; Sorensen, C. M.; Klabunde, K. J. *J. Colloid Interface Sci.* **2007**, *309*, 94-98.

(21) Smetana, A. B.; Klabunde, K. J.; Sorensen, C. M. *J. Colloid Interface Sci.* **2005**, *284*, 521-526.

(22) Cingarapu, S.; Yang, Z.; Sorensen, C. M.; Klabunde, K. J. *Chem. Mater.* **2009**, *21*, 1248-1252.

(23) Kalidindi, S. B.; Jagirdar, B. R. *Inorg. Chem. (Washington, DC, U. S.)* **2009**, *48*, 4524-4529.

(24) Ponce, A. A.; Klabunde, K. J. *J. Mol. Catal. A: Chem.* **2005**, *225*, 1-6.

(25) Naoe, K.; Petit, C.; Pileni, M. P. *The Journal of Physical Chemistry C* **2007**, *111*, 16249-16254.

(26) Prasad, B. L. V.; Stoeva, S. I.; Sorensen, C. M.; Klabunde, K. J. *Langmuir* **2002**, *18*, 7515-7520.

(27) Prasad, B. L. V.; Stoeva, S. I.; Sorensen, C. M.; Klabunde, K. J. *Chemistry of Materials* **2003**, *15*, 935-942.

(28) Prasad, P. N. *Nanophotonics. John Wiley & Sons, Inc.:* **2004;**, *Vol. I.*

(29) Ghosh, S. K.; Nath, S.; Kundu, S.; Esumi, K.; Pal, T. *The Journal of Physical Chemistry B* **2004**, *108*, 13963-13971.

(30) Kelly, K. L.; Coronado, E.; Zhao, L. L.; Schatz, G. C. *The Journal of Physical Chemistry B* **2002**, *107*, 668-677.

(31) Willets, K. A.; Van Duyne, R. P. *Annual Review of Physical Chemistry* **2007**, *58*, 267-297.

(32) Shichibu, Y.; Negishi, Y.; Tsunoyama, H.; Kanehara, M.; Teranishi, T.; Tsukuda, T. *Small* **2007**, *3*, 835.

(33) Schaaff, T. G.; Whetten, R. L. *J. Phys. Chem. B* **1999**, *103*, 9394.

(34) Boyen, H. G.; KÃ¤stle, G.; Weigl, F.; Koslowski, B.; Dietrich, C.; Ziemann, P.; Spatz, J. P.; RiethmuÌˆller, S.; Hartmann, C.; MoÌˆller, M.; Schmid, G.; Garnier, M. G.; Oelhafen, P. *Science* **2002**, *297*, 1533.

(35) Whetten, R. L.; Khoury, J. T.; Alvarez, M. M.; Murthy, S.; Vezmar, I.; Wang, Z. L.; Stephens, P. W.; Cleveland, C. L.; Luedtke, W. D.; Landman, U. *Adv. Mater.* **1996**, *8*, 428.

(36) ScholÌˆnenberger, C.; Sondag-Huethorst, J. A. M.; Jorritsma, J.; Fokkink, L. G. J. *Langmuir* **1994**, *10*, 611.

(37) Ohara, P. C.; Leff, D. V.; Heath, J. R.; Gelbart, W. M. *Physical Review Letters* **1995**, *75*, 3466.

(38) Hamaker, H. C. *Physica (Utrecht)* **1937**, *4*, 1058.

(39) Bargeman, D.; Van Voorst Vaden, F. *J. Electroanal. Chem.* **1972**, *37*, 45.

(40) Prasad, B. L. V.; Stoeva, S. I.; Sorensen, C. M.; Klabunde, K. J. *Chem. Mater.* **2003**, *15*, 935-942.

(41) Stoeva, S. I.; Zaikovski, V.; Prasad, B. L. V.; Stoimenov, P. K.; Sorensen, C. M.; Klabunde, K. J. *Langmuir* **2005**, *21*, 10280-10283.

(42) Pradeep, T.; Mitra, S.; Nair, A. S.; Mukhopadhyay, R. *The Journal of Physical Chemistry B* **2004**, *108*, 7012-7020

(43) Liu, X.-Y.; Bennema, P. *Physical Review B* **1994**, *49*, 765.

1.10 APPENDIX

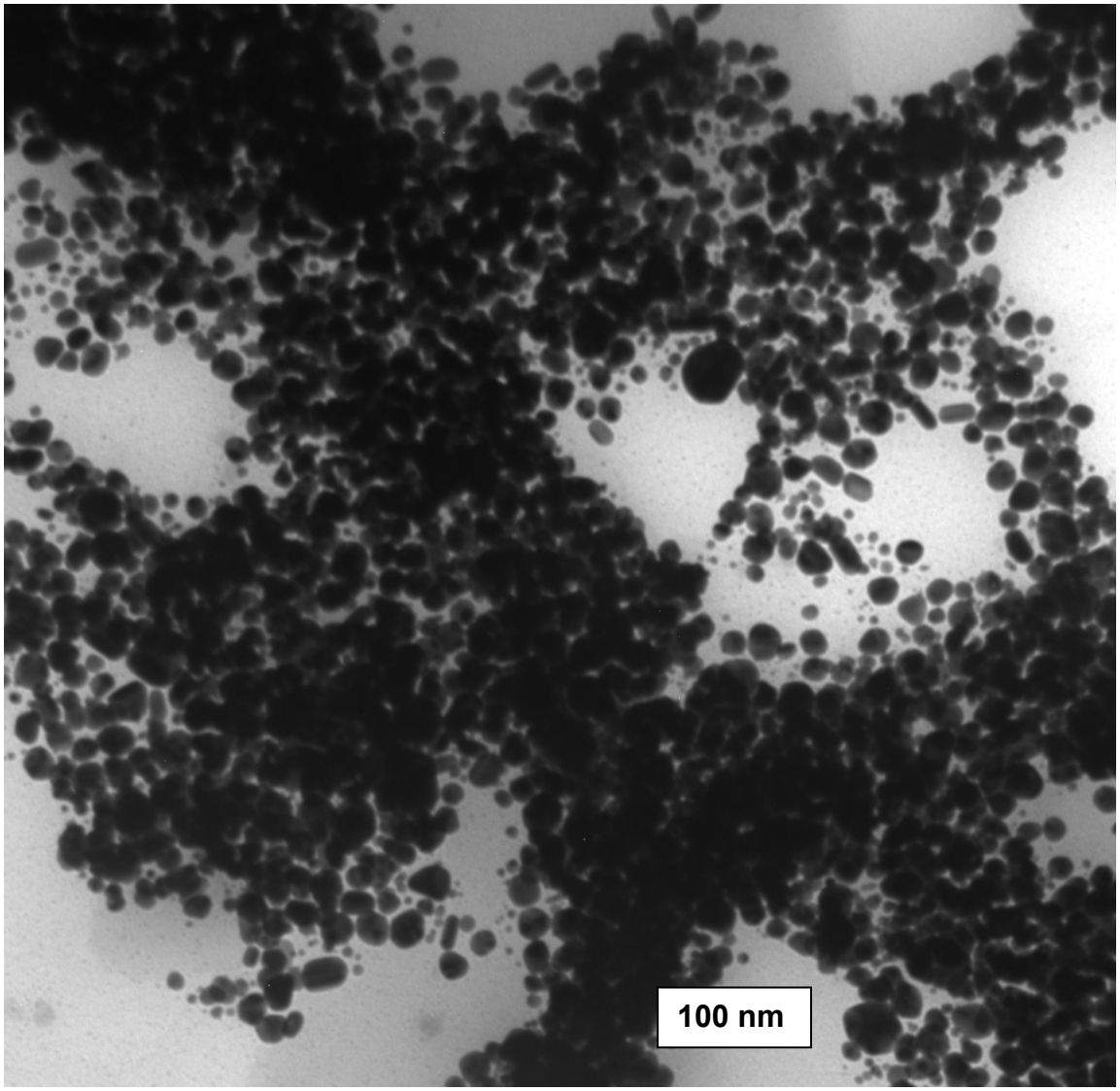

Figure 1.13 DDAB stabilized gold nanoparticles- Different morphology and show bigger particles.

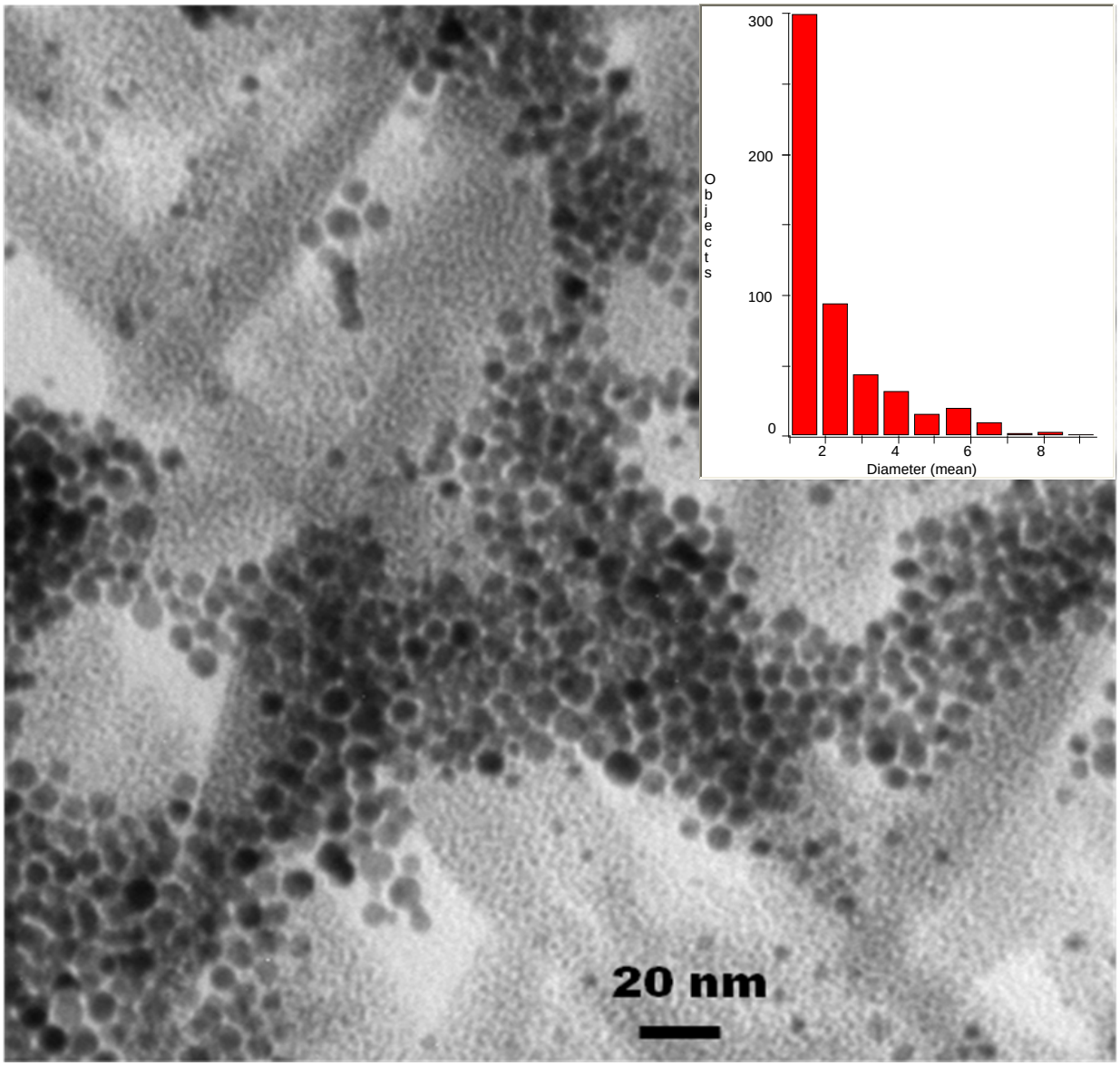

Figure 1.14 : Bi-model distribution of gold nanoparticles after addition of 1st dose of dodecanethiol ligand (metal to ligand ratio 1:30). Insert is particle histogram.

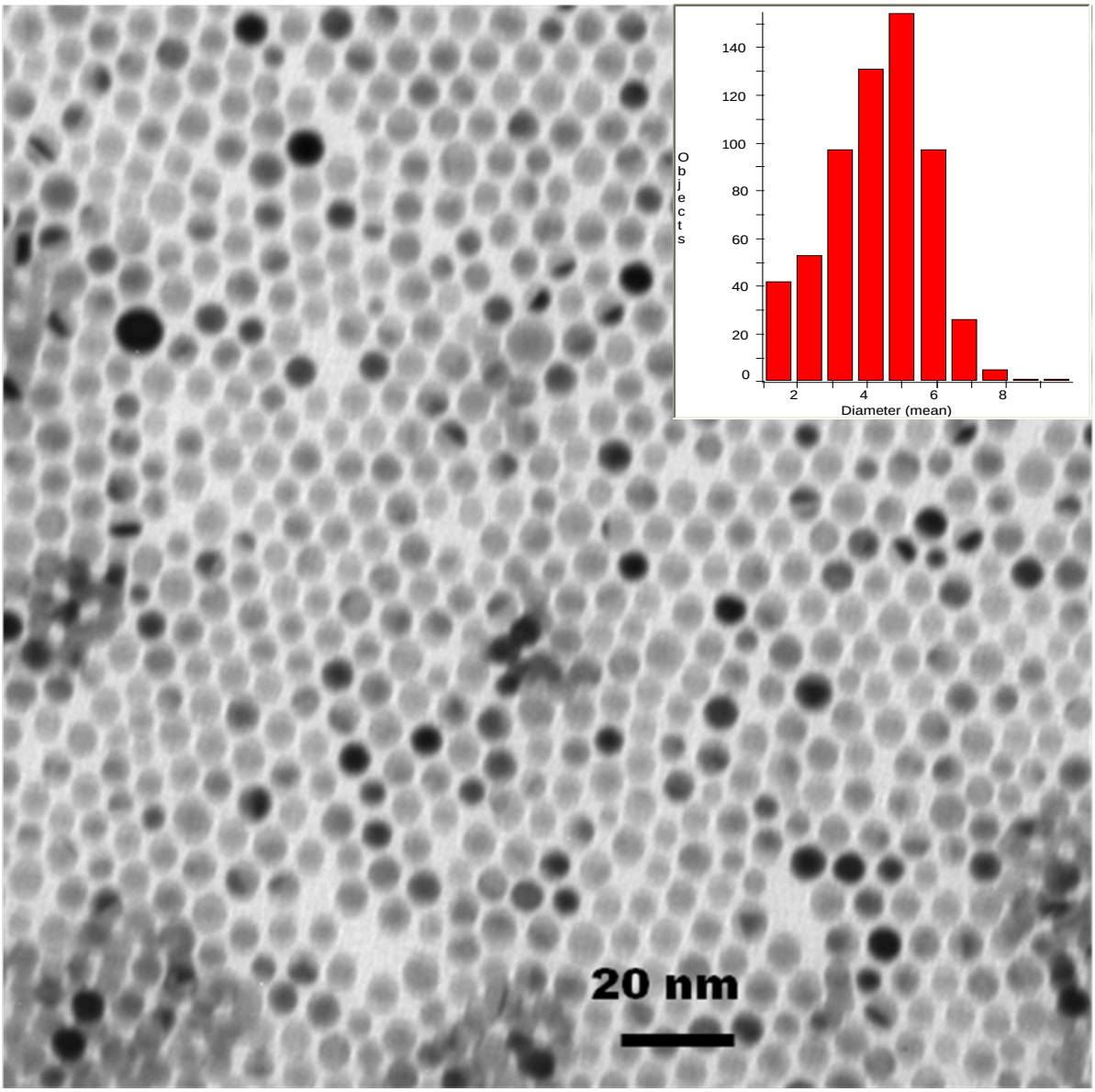

Figure 1.15 After 2nd dose of dodecanethiol ligand addition (metal to ligand ratio 1:30). Insert is particle histogram.

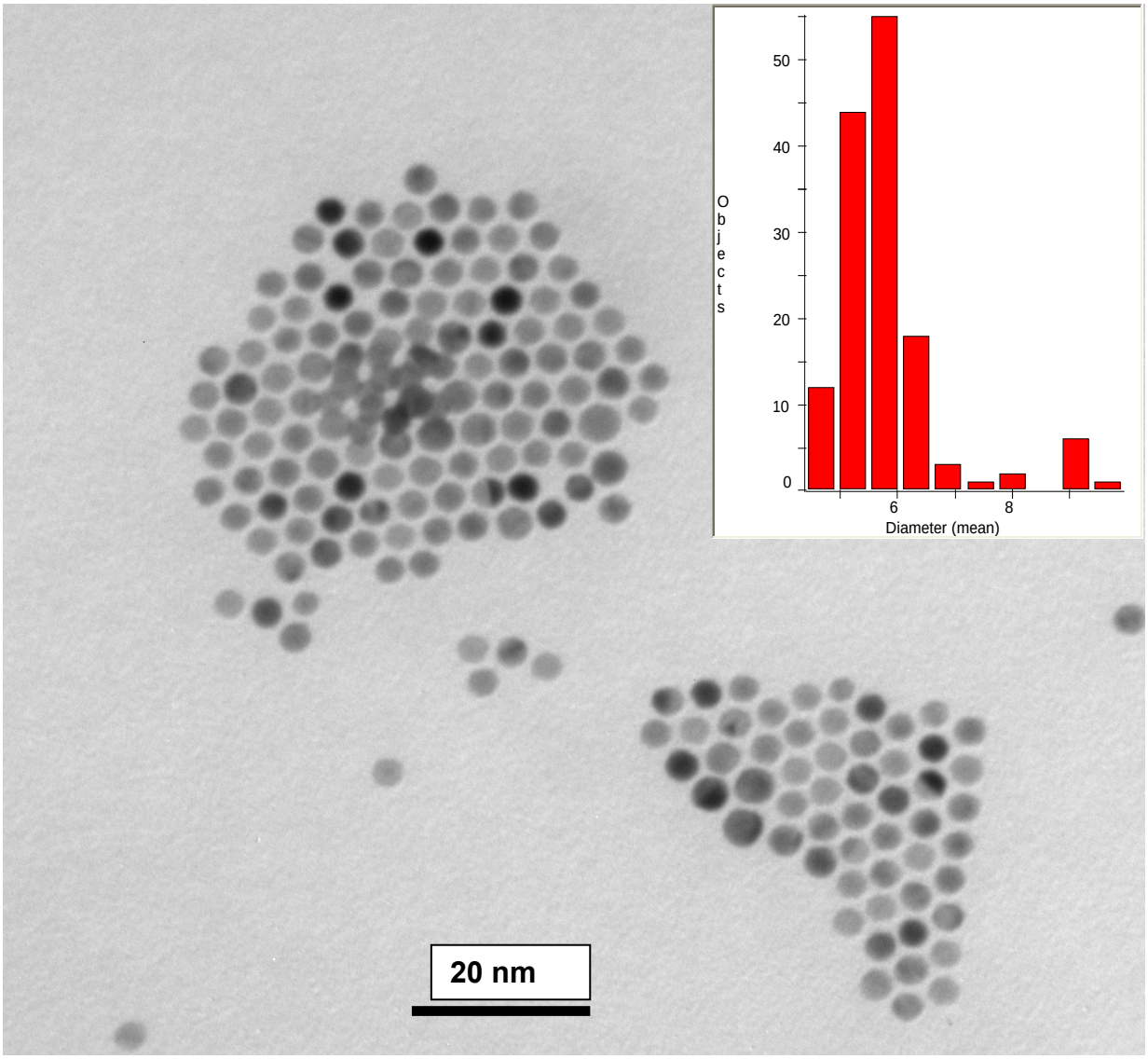

Figure 1.16 Gold-dodecanethiol stabilized nanoparticles after 30 minutes of digestive ripening in toluene. Insert is particle histogram.

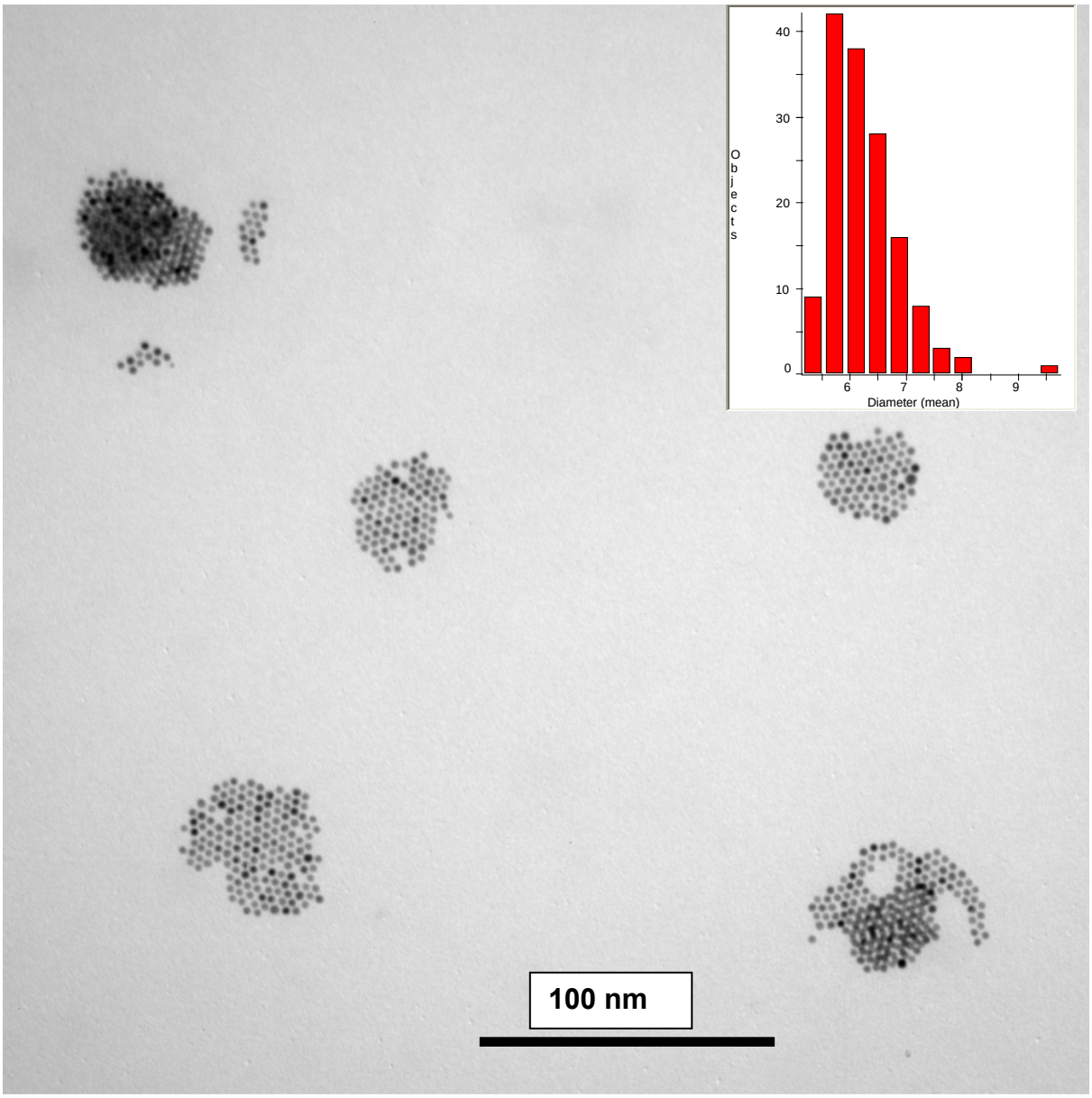

Figure 1.17 Gold-dodecanethiol stabilized nanoparticles after 60 minutes of digestive ripening in toluene, particles tend to form superlattice structure upon slow evaporation. Insert is particle histogram.

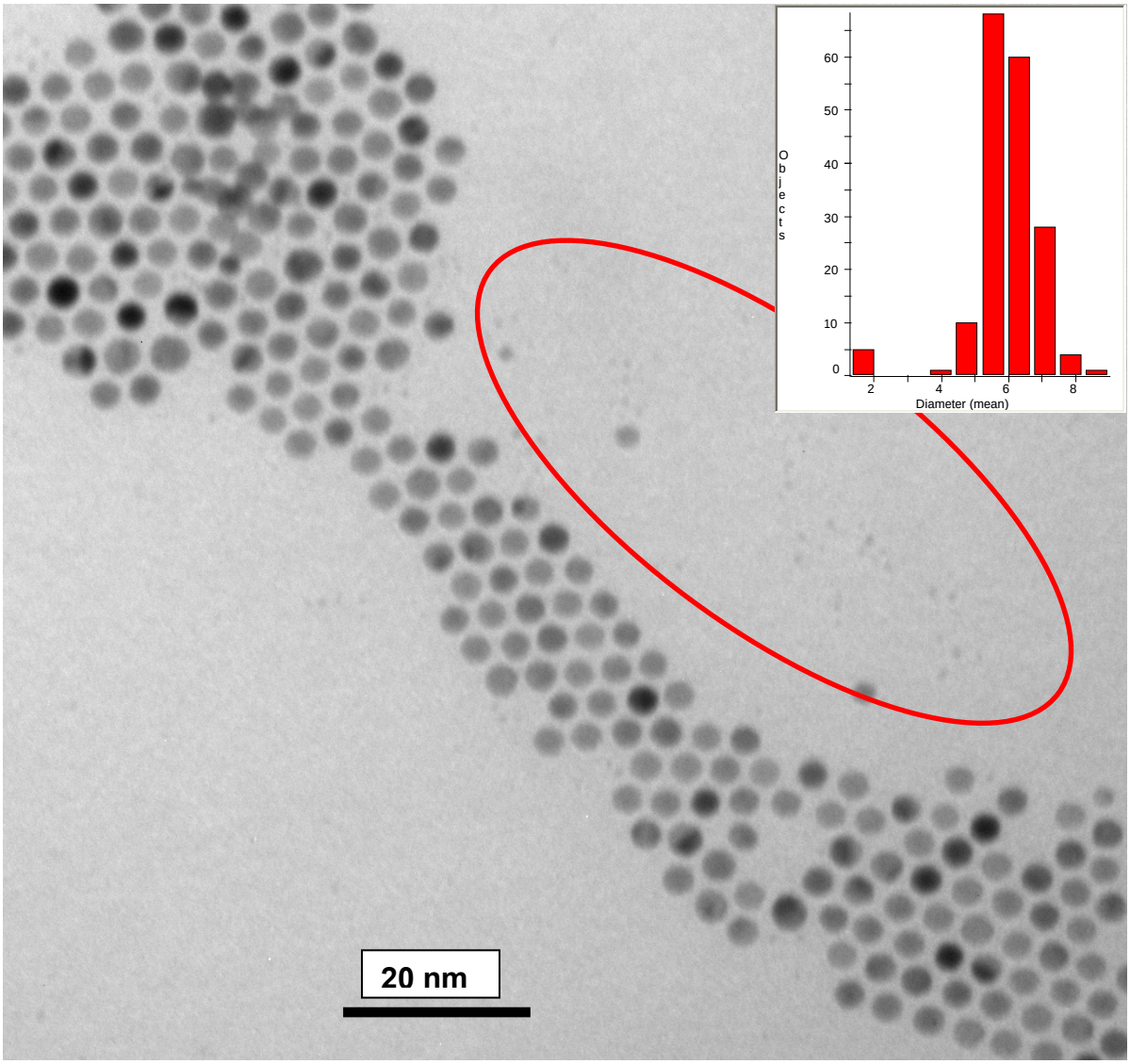

Figure 1.18 Gold-dodecanethiol stabilized nanoparticles after 90 minutes of digestive ripening in toluene. Insert is particle histogram. Re-appearance of ~ 2nm particles might be due to transformation of cluster of gold particle during digestive ripening?

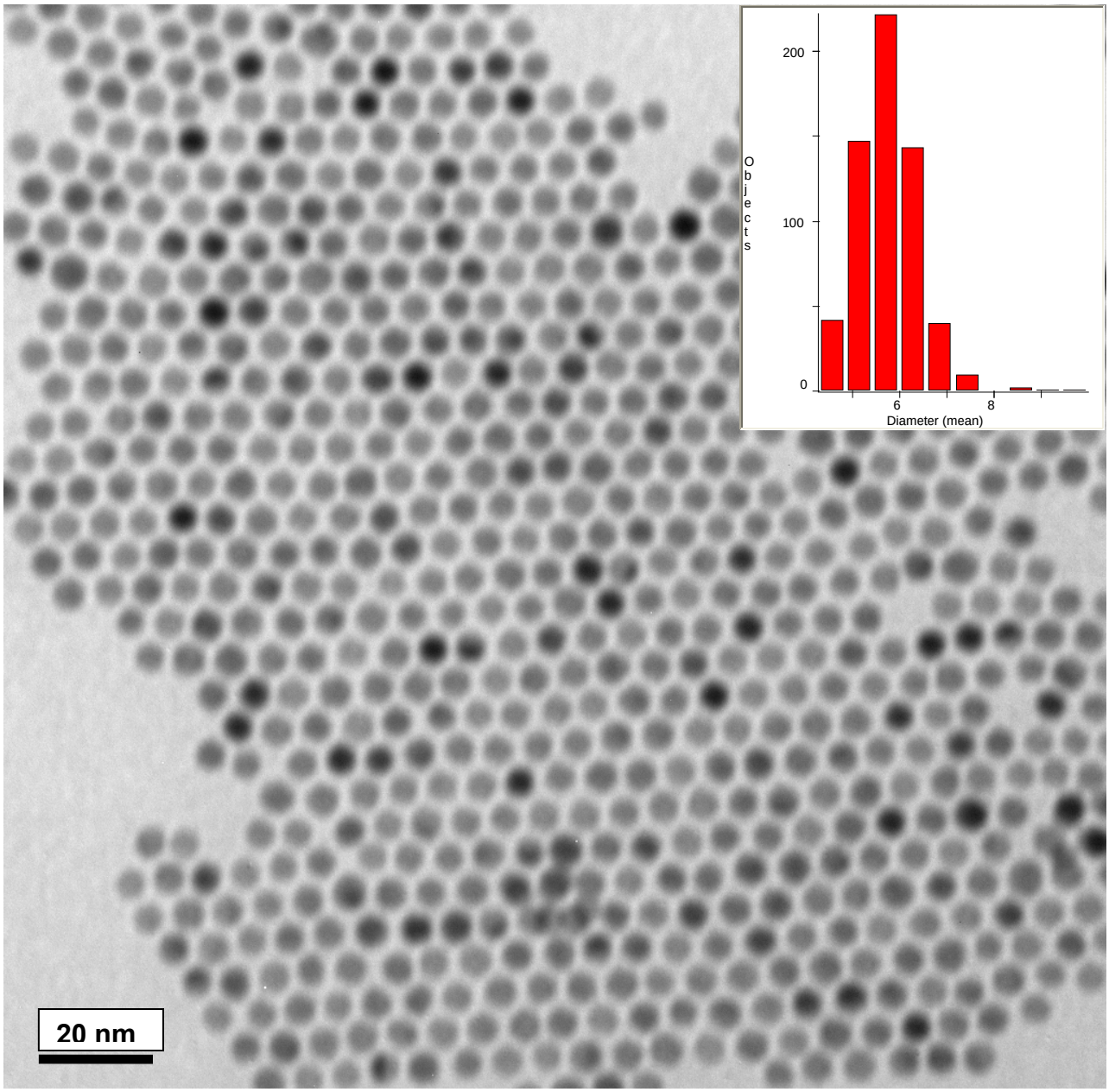

Figure 1.19 Gold-dodecanethiol stabilized nanoparticles after 120 minutes of digestive ripening in toluene. Insert is particle histogram.

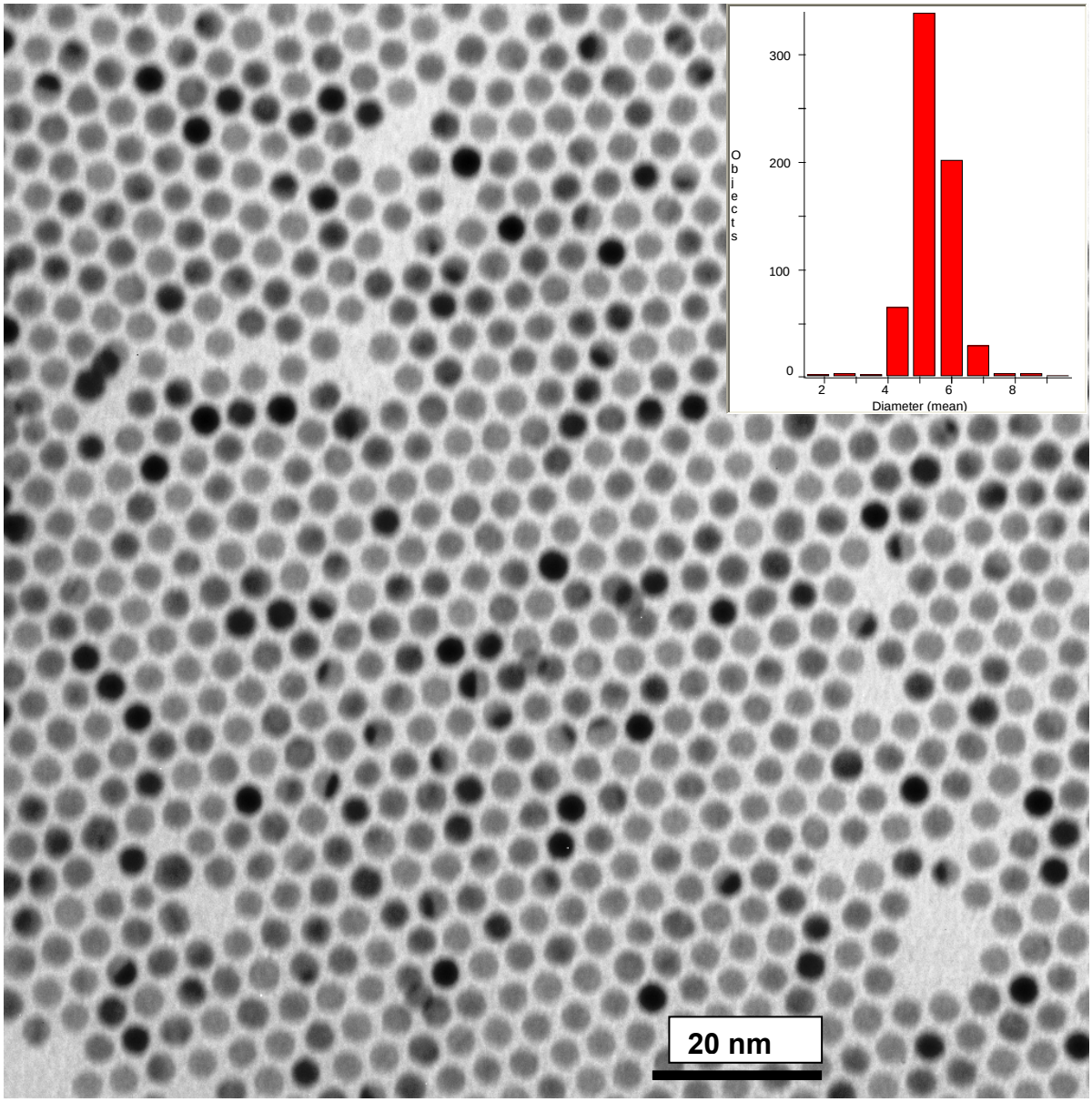

Figure 1.20 Gold-dodecanethiol stabilized nanoparticles after 24 hours of digestive ripening in toluene. Insert is particle histogram with an average particle size of ~ 5 nm.

CHAPTER 2 - Synthesis of Indium nanoparticles: A study of Digestive Ripening and Stabilizing Ligands

* A part of this work has been submitted to the *Nanoscale journal* 2010*21*, 1248–1252.

2.1 Introduction

In recent years, metal nanoparticles have received significant attention due to their unique properties such as melting point, conductivity, magnetism, specific heat, surface plasmon resonance (SPR), color.[1] These nanoparticles are used in diverse fields including catalysis,[2] magnetic recording media,[3,4] microelectronics,[5,6] sensing, clinical diagnostics, surface-enhanced Raman scattering (SERS), and energy conversion.[7,8] Hence, synthesizing metal nanoparticles with narrow size distribution, uniform shape, and good crystalline nature represents a significant challenge. There are many reports and reviews on the synthesis of noble and transition metal nanoparticles, but not on indium nanoparticles synthesis. Indium is widely used in the field of electronics including single electron transistor,[9] in nanoelectro-mechanical resonators,[10] electronic switchs,[11] as a component in low melting solders,[12] solid-state lubricants,[13] detection of DNA and protein,[14-16] and as printing nanoparticle building blocks in nanoxerography.[17] Silica-encapsulated indium nanoparticles were used as a phase-change material for enhancing heat capacity [18] and as a growth promoter for the III-V semiconductor rods.[19-21] Indium acts as a catalyst in various organic reactions as well.[22-25]

In general, indium nanoparticles have been synthesized by physical and chemical methods. Physical methods involve dispersion of molten metal in paraffin oil,[26] ultrasound irradiation,[13] laser ablation,[27] thermal evaporation followed by aerosol

formation,[28] emulsification by top-down and bottom- up approaches,[29,30] and oleylamine-driven phase transfer synthesis. [31] Unfortunately these methods offer little control over particle size.[13,26] Chemical methods involve reduction of metal salts by strong reducing agents like sodium metal, [32] sodium borohydride in ionic liquids,[33] zinc powder,[34,35] alkalides and electrides,[36] and decomposition of organometallic complexes.[37-40] More recently, it has been reported that the morphology of indium nanoparticles can be kinetically controlled by borohydride reduction at room temperature.[41] There are a few other reports on controlling the morphology of indium nanoparticles, which involves synthesis of hollow spheres and nanotubes,[34,42] nanowires, [43] and protein cavities as the reaction chamber for the fabrication.[44] In general, to control the particle size and size distribution, a variety of protecting agents have been investigated, which includes thiols,[45] phosphines,[46] amines,[47] alkanecyanides, [48] and thioethers. [49]

This chapter describes synthesis of indium nanoparticles by metal evaporation / condensation “SMAD” technique. Toluene and methylene chloride were tested as a digestive ripening solvents and to control the particle size; amines, phosphines and mixed ligand systems were investigated.

2.2 Experimental Section

2.2.1 Chemicals

Indium shot (99.9 %, Strem Chemicals Inc), Hexadecylamine (98%), oleylamine 98%, Trioctylphosphine oxide (Reagent Plus 99%), and trioctylphosphine were purchased

from Sigma-Aldrich and used without further purification. Toluene, methylene chloride, acetone, and methanol (Fisher Scientific) were used for the synthesis of nanoparticles. Toluene, acetone and methylene chlorides solvents were distilled and degassed four times by the standard freeze-thaw procedure prior to use.

2.2.2 Preparation Procedures

Typically, indium shot (0.3 g) was placed in a C9 boron nitride crucible (R.D. Mathis # C9-BN) resting in a metal basket (R. D. Mathis # B8B # x.030 w), which was in turn connected to water cooled copper electrodes and then the SMAD reaction chamber was charged with ligand (we chose 1:30 metal to ligand ratio based on previous work [50]) and vacuum sealed. After complete evacuation, a liquid N_2 Dewar was placed around the sealed SMAD reactor. Once the vacuum reached 4 X 10^{-3} torr, 50 mL of distilled and degassed either acetone or methylene chloride solvent was evaporated through the solvent shower head. The evaporated solvent was condensed on the wall of the SMAD reactor by external liquid N_2 cooling, which formed a uniform solvent matrix. Then the metal was heated gradually using water cooled electrodes. The vaporized metal was co-condensed with the continuous flow of co-condensing solvent vapor and this co-condensing restricts vaporized atoms from aggregation. The temperature required for the metal vaporization is ~ 900°C, and it took nearly 2-3 hrs based on the amount of starting material and a total of 100-125 mL of solvent. [Note about safety and cleanliness; before starting this procedure, the SMAD reactor was cleaned with aqua regia, base bath, acid bath and finally with copious amount of water, followed by drying. Special personal protection is necessary while working with a vacuum line, which

includes eye protection. Also acids and bases used for cleaning can cause severe burns, so proper acid proof gloves and clothing protection is necessary]. Once all the metal was vaporized, the liquid N_2 Dewar was removed. The solvent matrix along with the condensed metal appeared black in color and the matrix was allowed to melt and warm to room temperature, and the molten matrix along with the co-condensed metal slowly reaches the bottom of the SMAD reactor and mixes with the ligand. A homogeneous single phase as-prepared colloid was obtained after vigorous stirring for 30 minutes with a magnetic stirrer. Later, the as-prepared colloid was siphoned into a Schlenk glass tube under the protection of argon. This as-prepared SMAD product was then subjected to digestive ripening under the protection of argon.

2.2.3 Sample prepared in two- solvent system

In two-solvent system, acetone was used as a co-condensing solvent for condensing the evaporated indium metal and toluene as a digestive ripening solvent. After siphoning Indium –ligand- acetone- toluene SMAD product into a Schlenk glass tube; acetone was removed under dynamic vacuum leaving indium-ligand -toluene colloid, which was then digestively ripened in toluene at 110 °C.

2.2.4 Samples prepared in single solvent system

In this system, methylene chloride was used as a single solvent, which served as co-condensing solvent as well as digestive ripening solvent and digestive ripening was carried at the boiling point (38° C) of the solvent.

2.2.5 Digestive Ripening

Two solvents were used to determine the influence of the solvent boiling point on the indium nanoparticles and three colloids were produced by carrying digestive ripening in toluene (BP, 110 °C) and methylene chloride (BP, 38°C).

2.3 Characterization

Analyses of the particles were carried before and after the digestive ripening. UV-Vis absorption spectra were recorded using an in situ UV-Vis optical fiber, assisted by a DH-2000 UV-Vis optical spectrophotometer instrument (Ocean Optics Inc). The powder X-ray diffraction (PXRD) samples were prepared by the evaporation of solvent from the Indium/ toluene or indium/ methylene chloride dispersion loaded on XRD glass plates and PXRD patterns were recorded by a Bruker D8 X-ray diffractometer with CuKα radiation. The samples were scanned from $20 < 2\theta < 70^{\circ}$ at an increment of 0.02°/ min and the total acquisition time period was more than 2 hrs. A drop of washed and re-dispersed colloid was suspended on a transmission electron microscopy (TEM) carbon coated grid and allowed to dry under vacuum. TEM and selective- area electron diffraction (SAED) were performed on a Philips CM100 operating at 100kV. The yields were calculated based on a previously reported method for gold-dodecanethiol SMAD digestive ripening system,[50] and were 80 ± 5 % .

2.4 Results and Discussion

2.4.1 Trioctyl Phosphine Protected Particles - Digestive Ripening in *toluene*

Most metal nanoparticles are stabilized by the trioctyl phosphine ligand because the phosphorous head group binds strongly with the nanoparticles and the three octyl units of carbon chains acts as an insulating material, which not only protects nanoparticles from aggregation but also aids solubility in organic solvents.

The as-prepared SAMD colloid produced with trioctyl phosphine stabilized particles appeared black in color but upon digestive ripening in toluene, the color of the sample was slightly changed from black to light brown. Addition of ethanol caused precipitation and these precipitate was easily re-dissolved in toluene and chloroform. The UV-Vis absorption spectrum of the as-prepared SMAD product was broad and after digestive ripening the peak was narrowed considerable (Figure 2. 1) but unfortunately, due to interference of the UV-Vis of toluene, the expected surface Plasmon peak of indium nanoparticles could not be observed. The as-prepared indium nanoparticles are polydispersed (Figure 2. 2A) and upon digestive ripening in toluene, the particle size was narrowed but digestive ripening did not yield monodispersity as can be seen in Figure 2.2B. The XRD data in Figure 2.3a shows all the characteristic peak of indium and it matches with the literature data.[26]

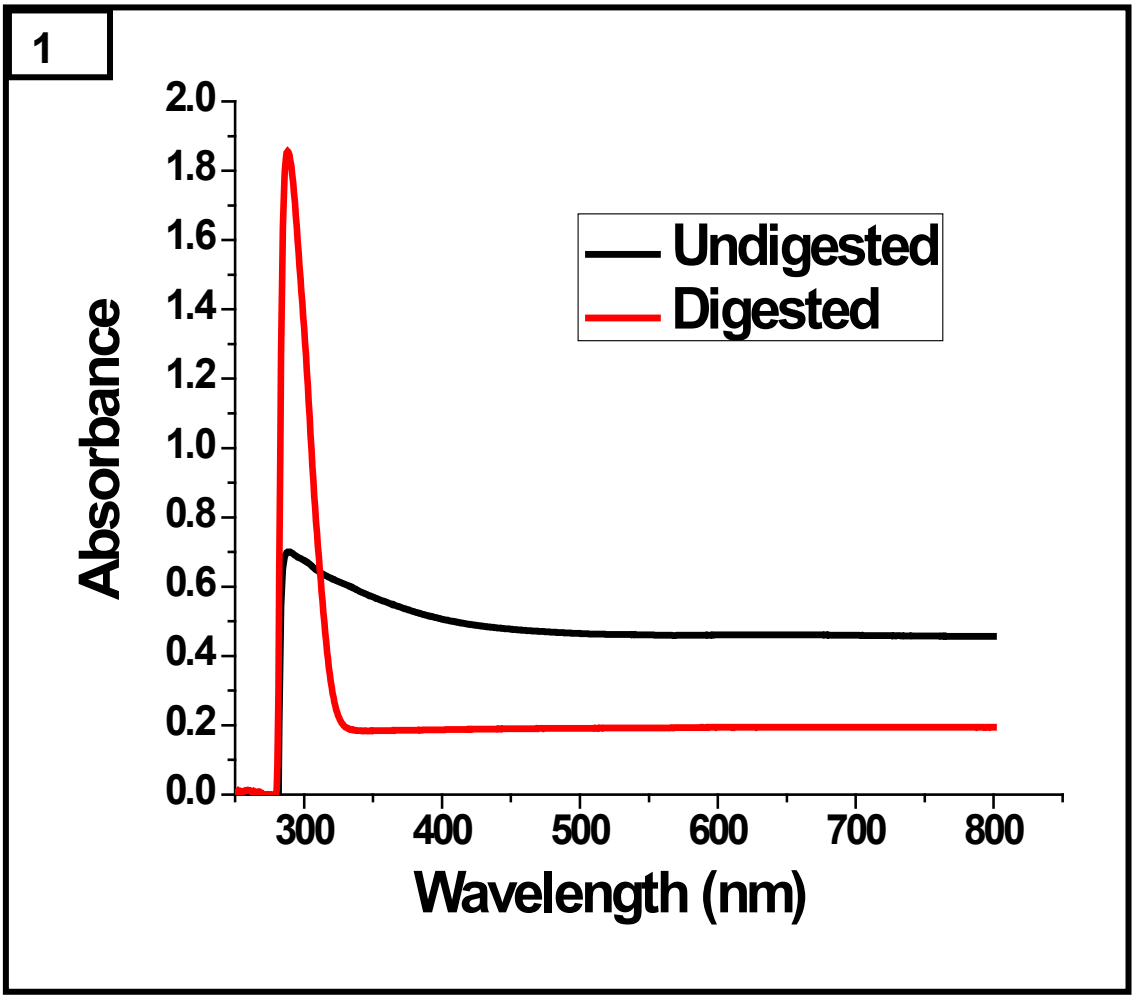

Figure 2.1 Surface Plasmon absorbance resonance peak for trioctyl phosphine indium nanoparticles. The Black line represents the as-prepared SMAD colloid and the red line represents particles after digestive ripening.

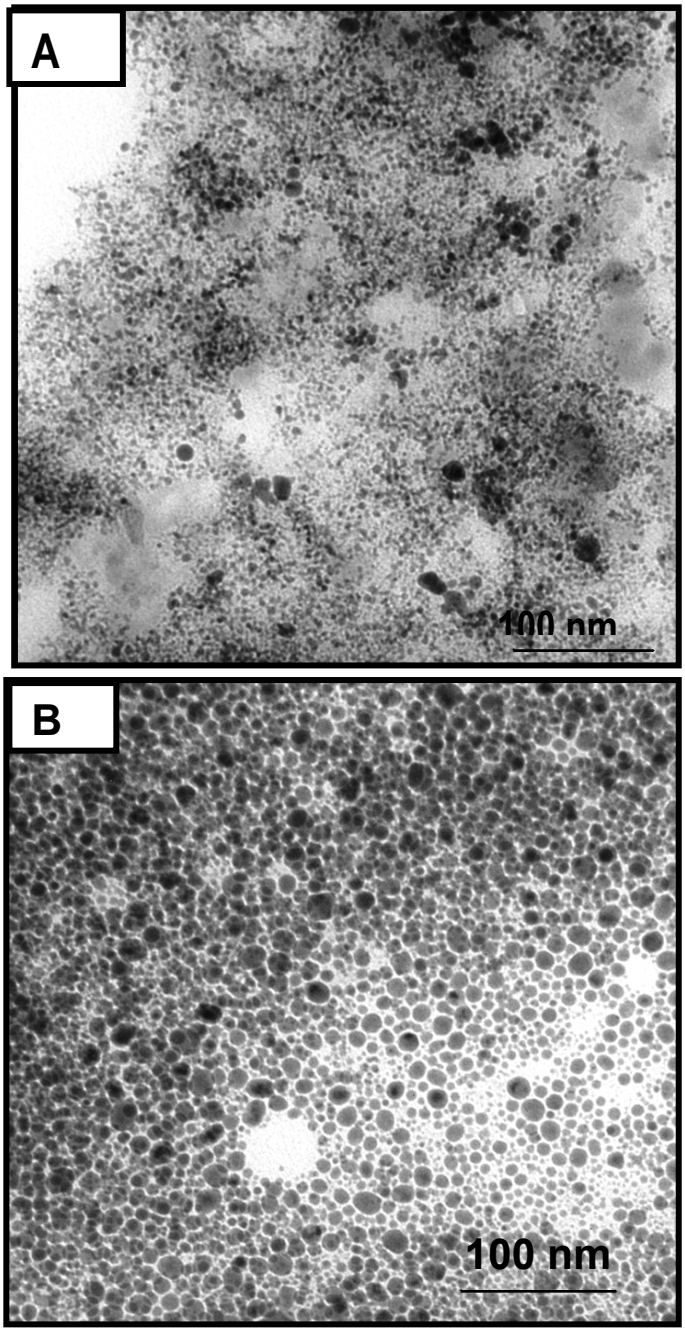

Figure 2.2 TEM images of Trioctyl phosphine coated indium nanoparticles (A) before digestive ripening and (B) after digestive ripening.

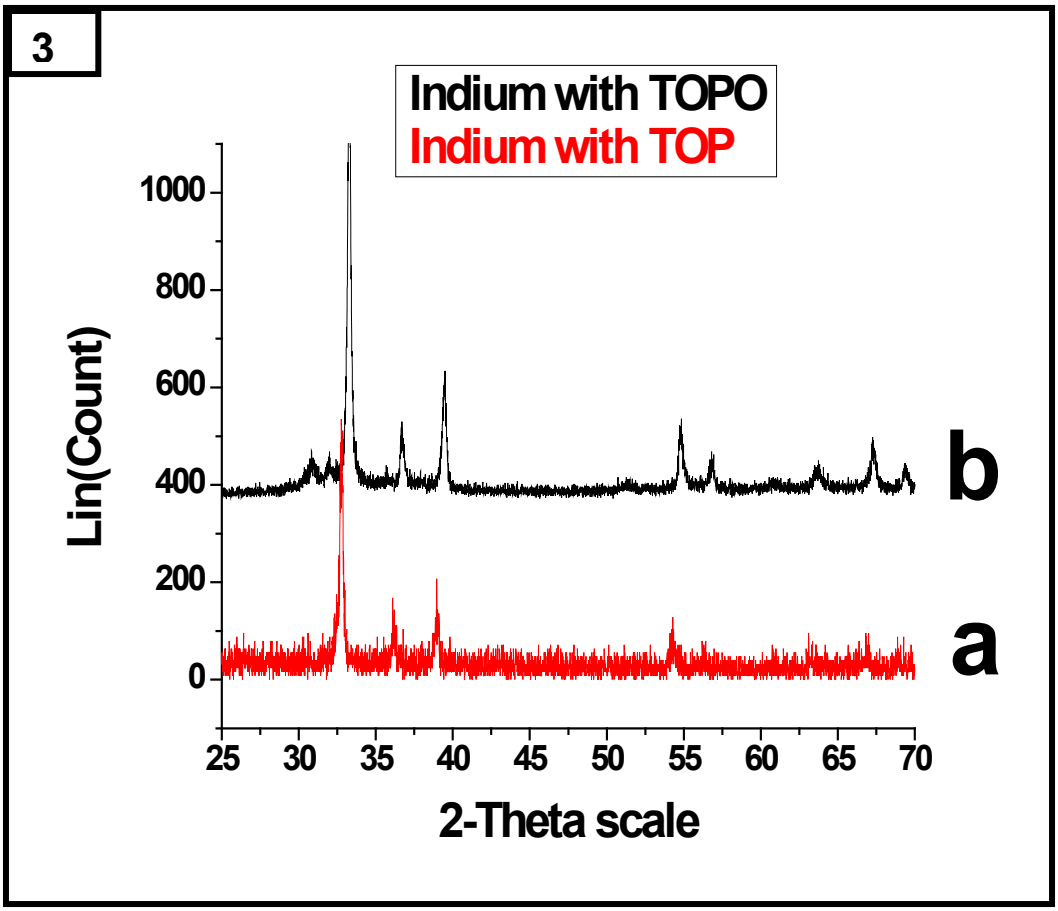

Figure 2.3 XRD of indium nanoparticles (a) stabilized with trioctyl phosphine and (b) with trioctyl phosphine oxide. There is no evidence of indium oxide formation.

2.4.2 Trioctyl Phosphine Oxide Protected Particles - Digestive Ripening in toluene

The as- prepared SMAD Indium nanoparticles protected with trioctyl phosphine oxide ligands exhibited a broad UV-Vis absorption peak but upon digestive ripening in toluene, the UV-Vis absorption peak was narrowed (Figure 2. 4) and the particle size was reduced after digestive ripening. Figure 2.5a shows the TEM images of undigested

as-prepared indium nanoparticles and Figure 2.5b after digestive ripening. Compared to trioctyl phosphine stabilized particles, trioctyl phosphine oxide stabilized nanoparticles yield more spherical particles. The XRD data (Figure 2.3b) reveals that the formed particles are indium and there were no signs of indium oxide.

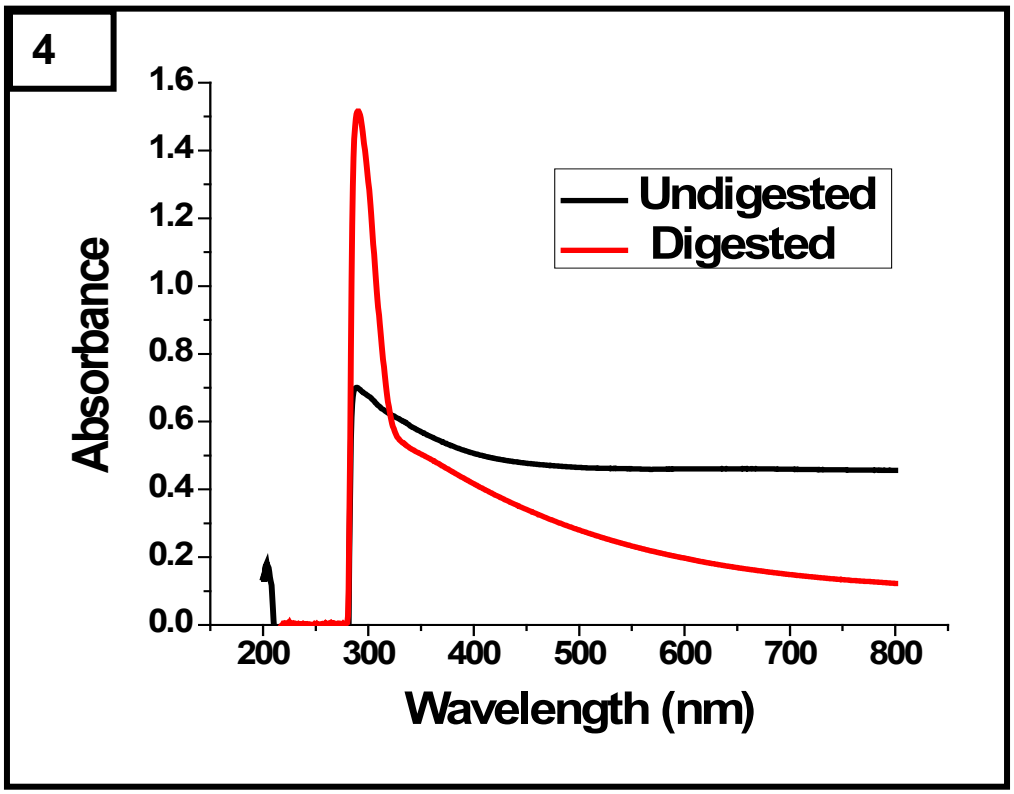

Figure 2.4 Surface Plasmon absorbance resonance peak for trioctyl phosphine oxide coated indium nanoparticles (Black) before digestive ripening and (Red) after digestive ripening.

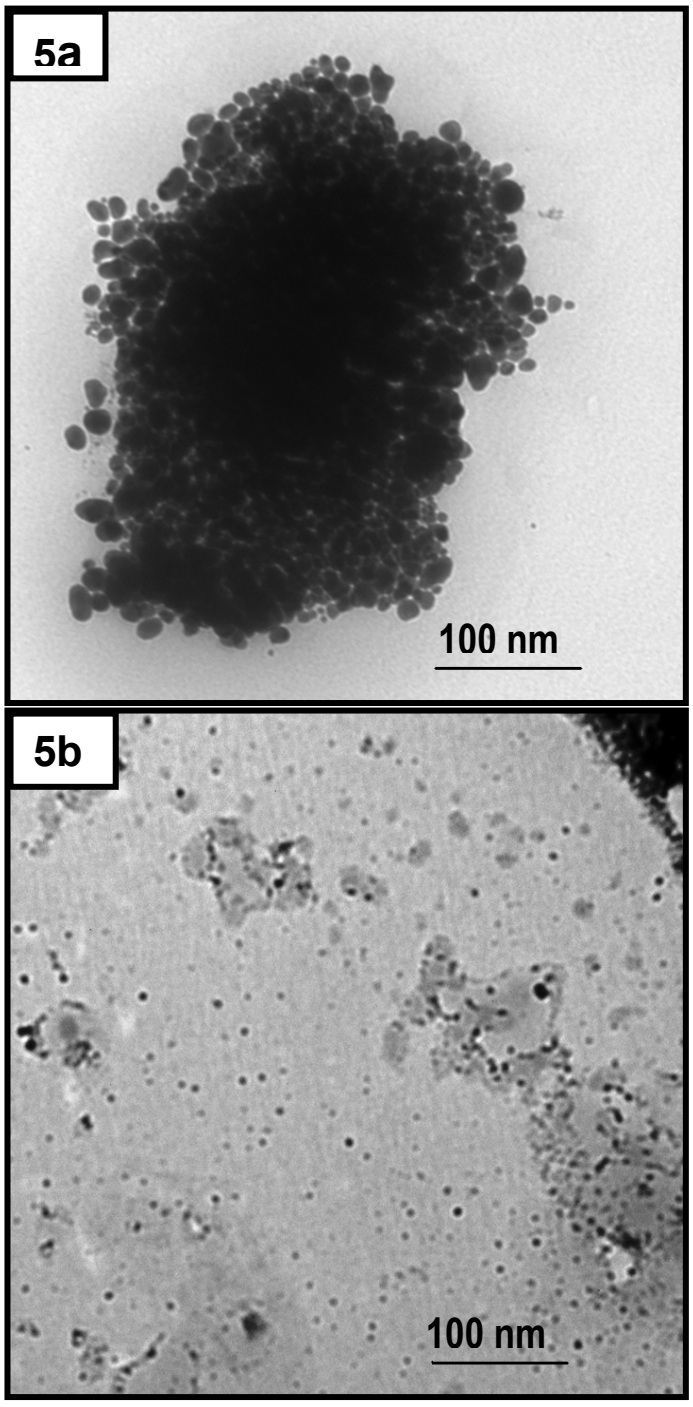

Figure 2.5 TEM images of Trioctyl phosphine oxide coated indium nanoparticles (a) before digestive ripening and (b) after digestive ripening in toluene solvent.

2.4.3 Oleyl amine Protected Particles - Digestive Ripening in *toluene*

The UV-Vis absorption spectrum of oleyl amine stabilized indium nanoparticles before digestive ripening is broad (Figure 2.6) but after digestive ripening the peak become narrow and from the TEM images the particles look amorphous but after digestive ripening the particles appear more crystalline (Figure 2.7a and 2.7b), but the particles did not yield special particles and the XRD data (Figure 2.8) shows all characteristic futures of tetragonal crystalline indium.

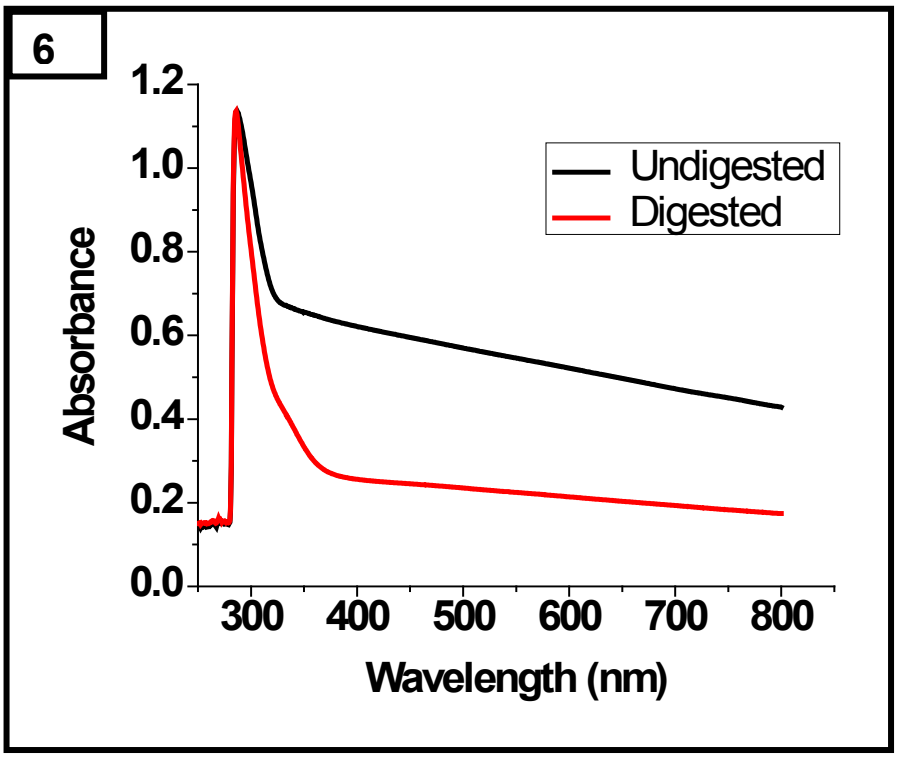

Figure 2.6 Surface Plasmon absorbance resonance peak for oleyl amine protected indium nanoparticles. The Black line represents the as-prepared SMAD colloid and the red line represents particles after digestive ripening.

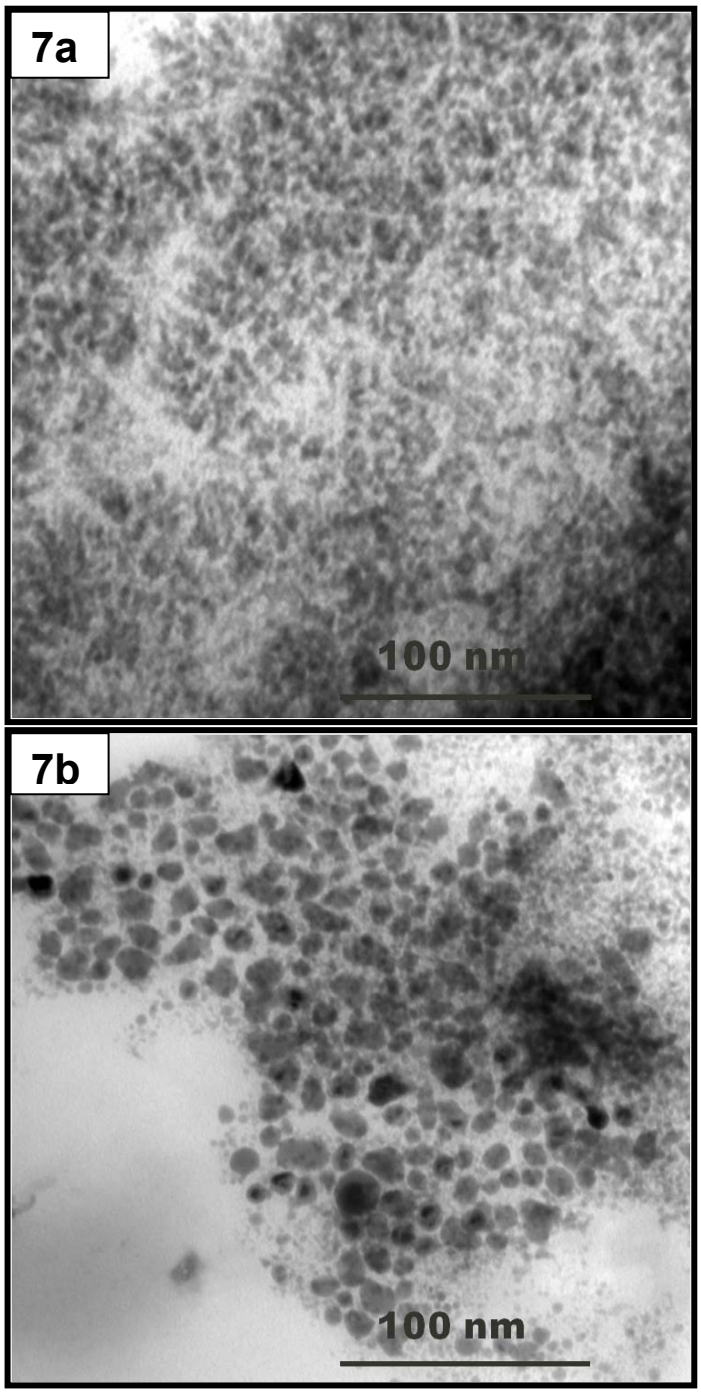

Figure 2.7 TEM images of Oleyl amine coated indium nanoparticles (a) before digestive ripening and (b) after digestive ripening in toluene solvent.

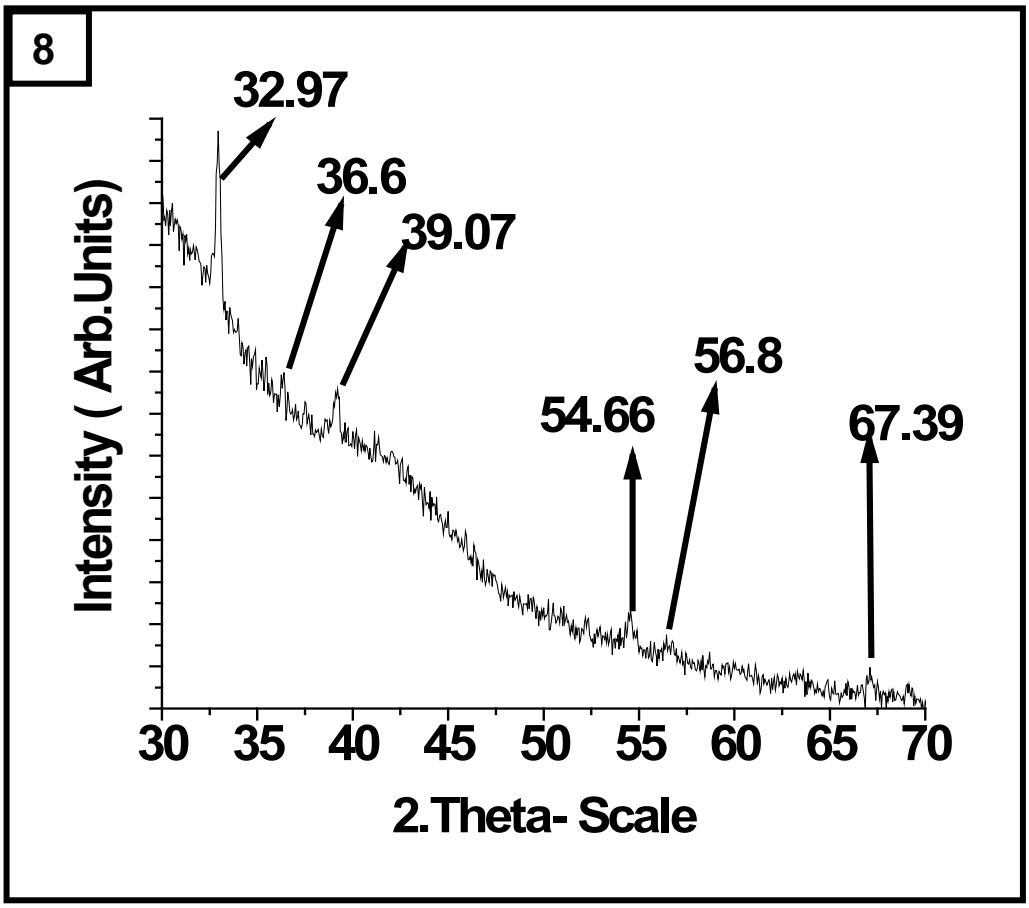

Figure 2.8 Powder XRD data of indium nanoparticles stabilized with oleyl amine ligand after digestive ripening in toluene was recorded without any beam slits. These patterns represent the tetragonal crystalline diffraction patterns from indium nanoparticles.

2.4.4 Trioctyl Phosphine Oxide Protected Particles - Digestive Ripening in *methylene chloride*

In general, in the SMAD technique two solvents were employed where one solvent was used for solvation of vaporized particles and another solvent for digestive ripening. [49-51] However, in the current synthesis methylene chloride worked well for both purposes. The SMAD technique allows the synthesis of polydispersed colloidal particles by vaporization and co-condensation.[2,49-53] As discussed in an early chapter, a polydispersed colloidal solution were made monodispersed by a unique process known as "Digestive ripening".[54] Digestive ripening is a post preparative process which involves heating of polydispersed colloid particles at the boiling point of solvent in the presence of excess surface active ligands.[49-52] Previously, it was reported that highly monodispersed magnesium nanoparticles were achieved by digestive ripening at room temperature.[55] Hence, controlling of particle size can be achieved even at room temperature by digestive ripening under appropriate conditions.

Figure 2.9 shows the UV-Vis absorption spectrum of indium nanoparticles stabilized by TOPO. The as- prepared SMAD particles exhibit a little hump around 280 nm in the absorption spectrum, but during digestive ripening a new peak appeared around 400 nm, and this peak gradually vanished but reappeared at 280 nm after 24 hrs of digestive ripening. This sharp stable absorption peak after 24 hrs of digestive ripening indicates that the particles attained an equilibrium size distribution. The temporal evolution of particles was shown in Figure 2.10 (a- d).

The estimated particle sizes deduced from the TEM are in the range of ~ 5 nm ± 0.6 (Figure 2.11(a - b)), and the selective area electron diffraction shows evidence of crystalline nature (Insert in Figure 2.10 d). The appearance of the new peak around 400 nm might be due to either dissolving or breaking down of bigger particles in the initial digestive ripening time. Indeed, digestive ripening causes bigger particles to break down into very small particles and these smaller particles tend to grow and finally the system reaches to an equilibrium size regime.[49] Further, the absorption phenomenon in indium nanoparticles due to SPR is found to be both solvent and morphology dependent and hence its absorption shifts in-between 240-370 nm.[26,32,33,40] The little hump of the as- prepared sample can be explained by the fact that the initial particles are polydispersed (25- 50 nm in diameter) according to TEM images (Figure 2.10 a). The XRD patterns (Figure 2.12) of all three indium colloids (TOPO, HDA, and TOPO/ HAD stabilized indium nanoparticles) exhibit prominent peaks at scattering angles (2Θ) of 32.96, 36.31, 39.17, 54.48, 56.58, 63.21, 67.04 and 69.10, which are assigned to scattering from the 101, 002, 110, 112, 200, 103, 211 and 202 crystal planes, and all these peaks can be indexed to the body-centered tetragonal indium phase of indium. These XRD peaks were verified from the XRD data file (SS-NNN 85-1409) and match with the published literature.[34]

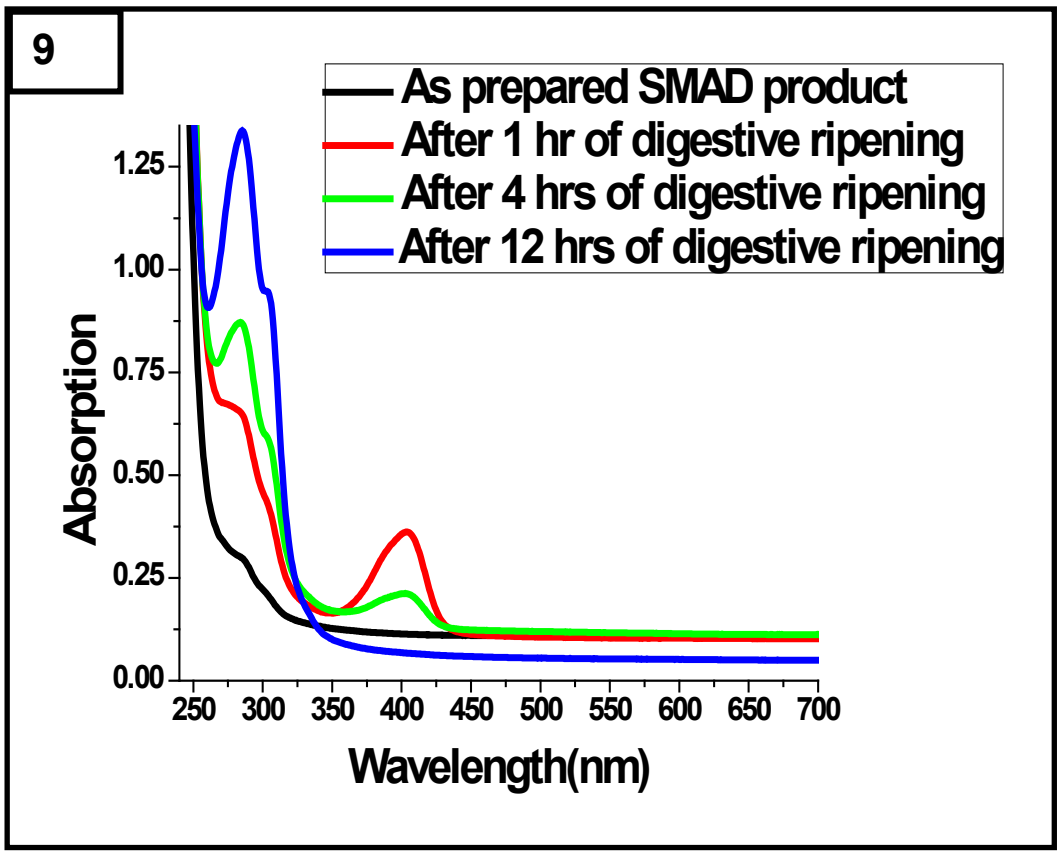

Figure 2.9 Temporal evolution of surface Plasmon absorbance resonance peak for trioctylphosphine oxide protected indium nanoparticles. The Black line represents the as-prepared SMAD colloid and the red line represents sample after 1 hr of digestive ripening, green line after 4 hrs, and blue line represents the surface Plasmon of indium after 12 hrs of digestive ripening in methylene chloride.

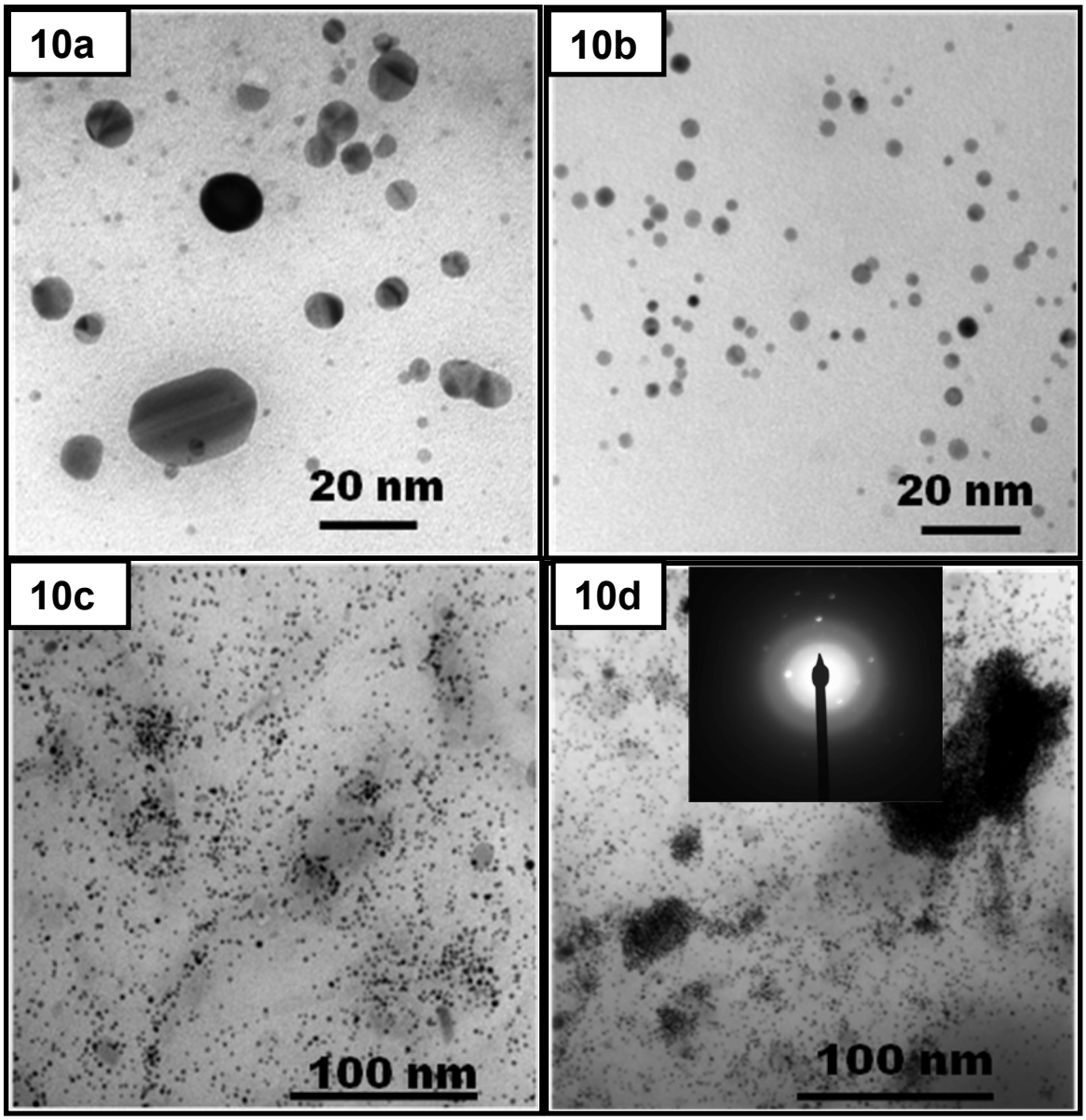

Figure 2.10 (a) TEM image of as-prepared polydispersed SMAD product of trioctyl phosphine oxide stabilized particles (b) after 1 hr of digestive ripening (c) after 12 hrs of digestive ripening and (d) after 24 hrs of digestive ripening in methylene chloride solvent.

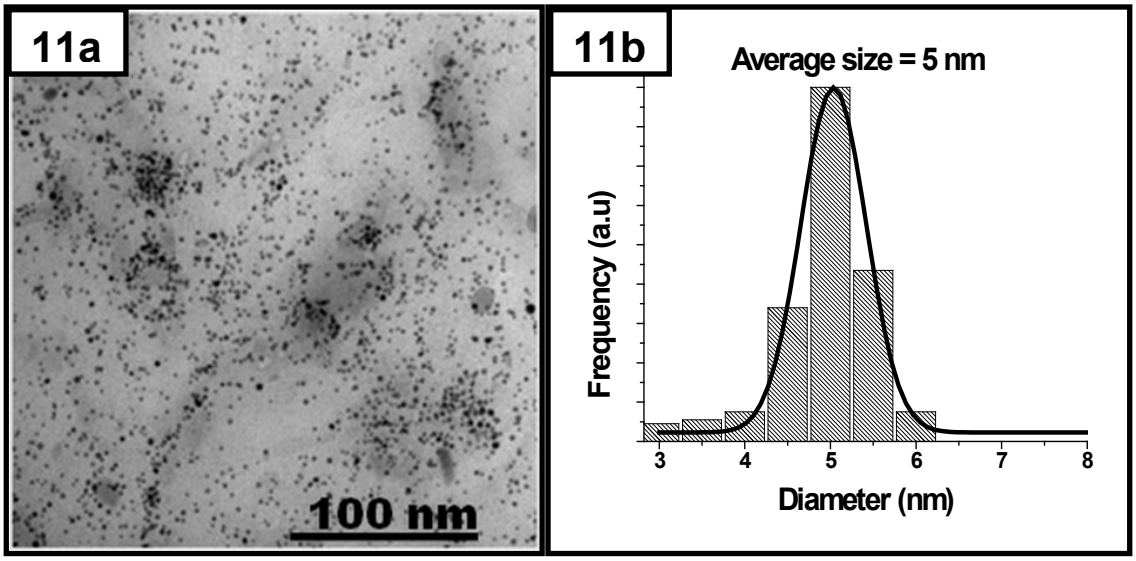

Figure 2.11 TEM image after 12 hrs of digestive ripening and corresponding histogram of particle size (~ 5 nm in diameter).

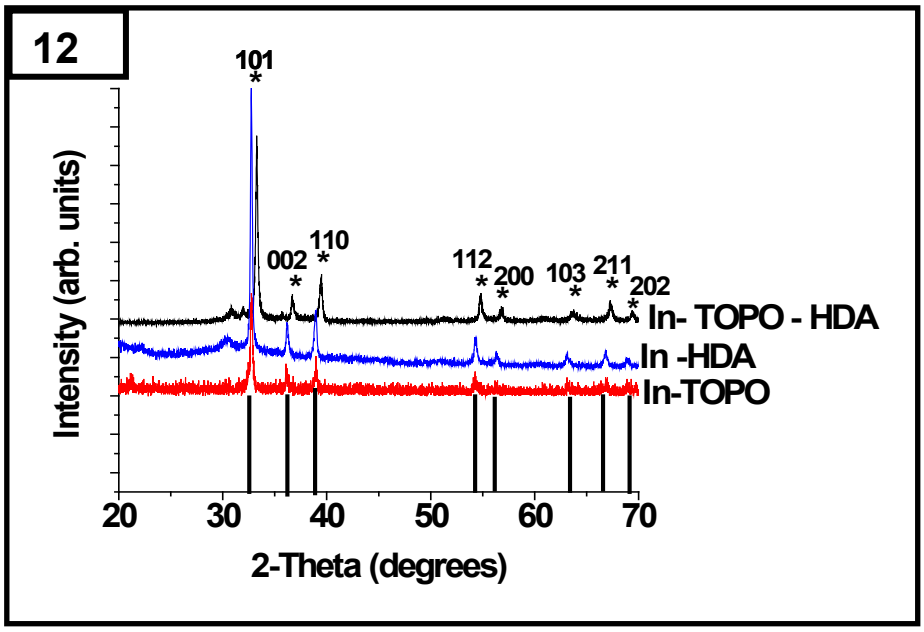

Figure 2.12 The XRD patterns of all three indium colloids exhibit prominent peaks at scattering angles (2Θ) of 32.96, 36.31, 39.17, 54.48, 56.58, 63.21, 67.04 and 69.10, which are assigned to scattering from the 101, 002, 110, 112, 200, 103, 211 and 202 crystal planes, and all these peaks can be indexed to the body-centered tetragonal indium phase of indium.

2.4.5 Hexadecyl amine stabilized indium nanoparticles: Digestive ripening in *methylene chloride.*

The UV-Vis absorption spectrum of as-prepared hexadecyl amine stabilized indium particles is broad but upon digestive ripening the UV-Vis peak becomes much sharper (Figure 2.13) at 290 nm wavelength.

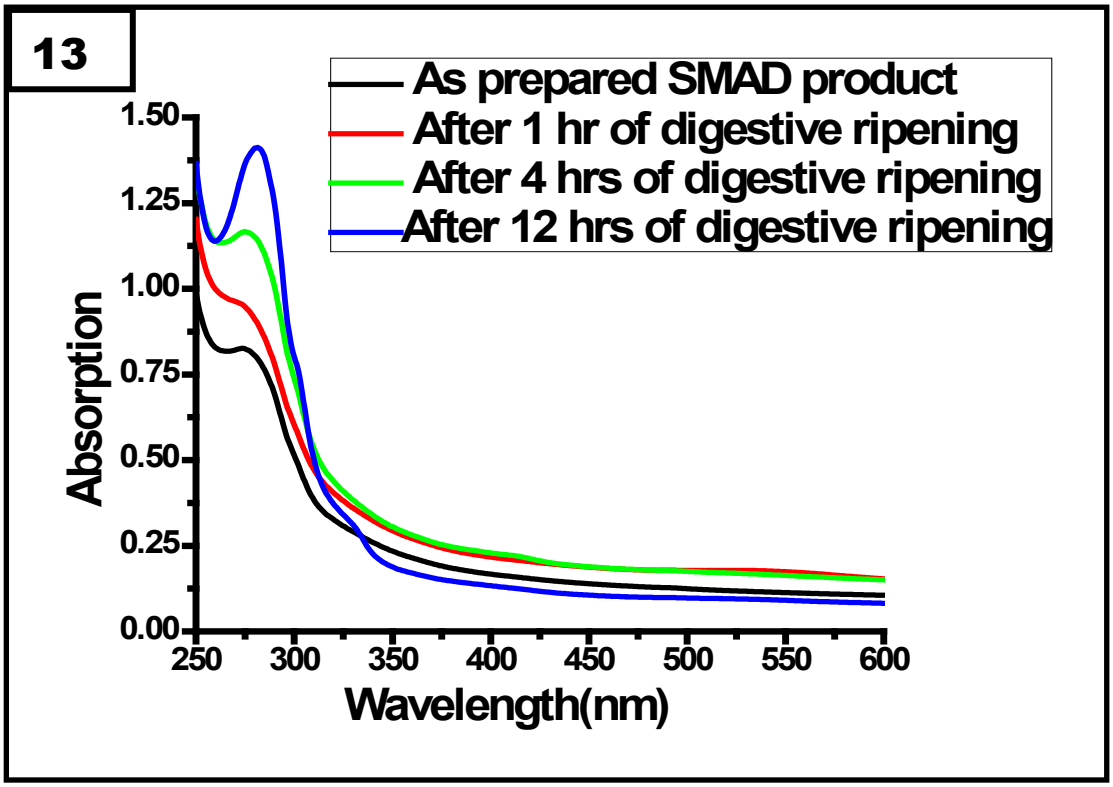

Figure 2.13 Temporal evolution of surface Plasmon absorbance resonance peak for hexadecyl amine protected indium nanoparticles. The Black line represents the as-prepared SMAD colloid and the red line represents sample after 1 hr of digestive ripening, green line after 4 hrs, and blue line represents the surface Plasmon of indium after 12 hrs of digestive ripening in methylene chloride.

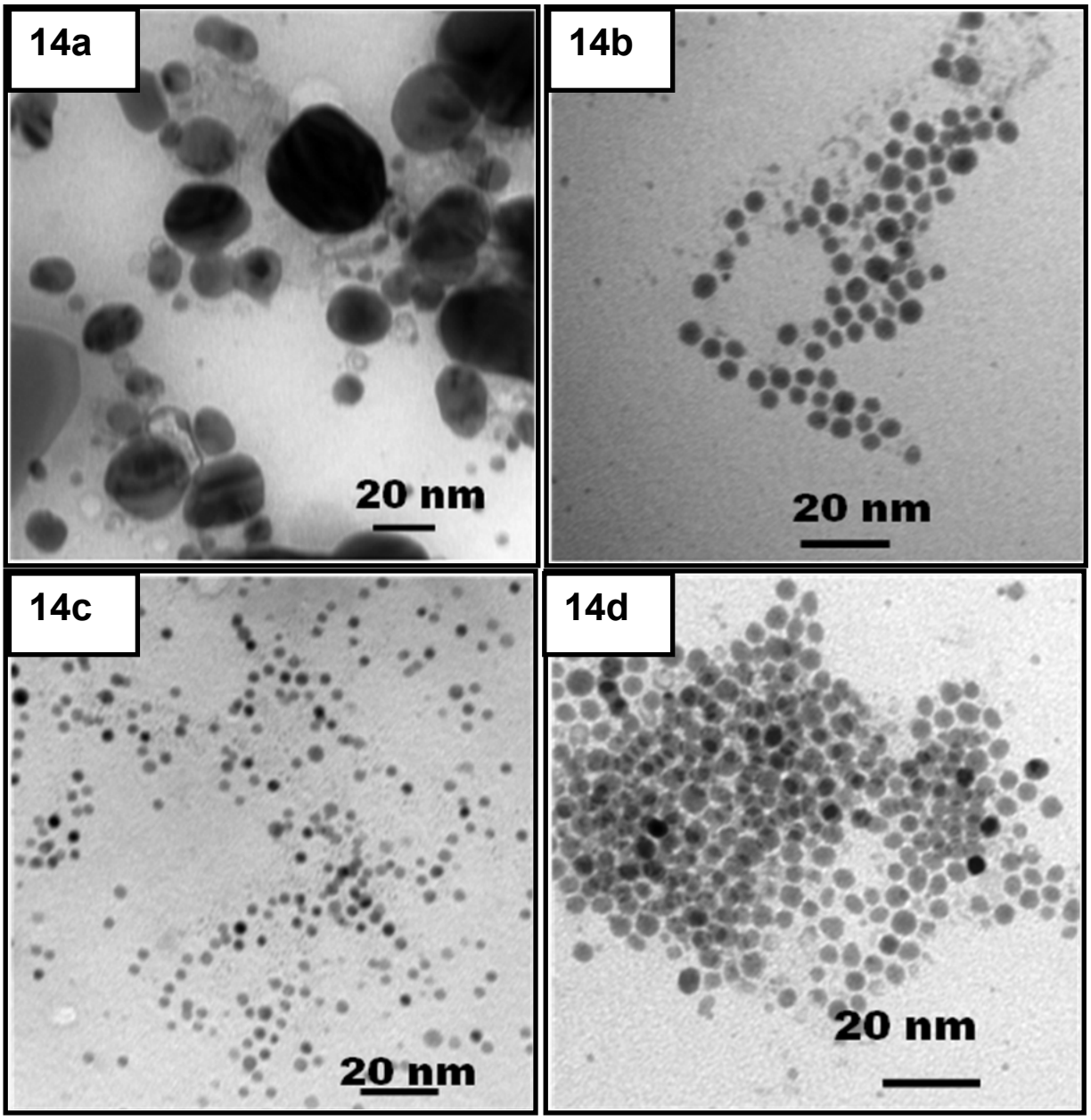

Figure 2.14 TEM image of (a) as -prepared polydispersed indium nanoparticles stabilized with hexadecyl amine ligand (b) after 1 hr of digestive ripening (c) after 12 hrs of digestive ripening and (d) after 24 hrs of digestive ripening in methylene chloride.

The particles attained an equilibrium size regime within 24 hrs of digestive ripening (Figure 2.14 (a-d)) and the particle mean size measured on the TEM images lie in the range of ~ 9 nm ± 0.5 nm, histogram of particles after 24 hrs of digestive ripening is shown in Figure 2.15 a a -b; whereas TOPO stabilized particle mean size measured from TEM is ~ 5 nm± 0.6 % (histogram of TOPO stabilized particle mean size distribution (Figure 2.11 b) and the XRD data of HDA stabilized particles is free from indium oxide (Figure 2. 12).

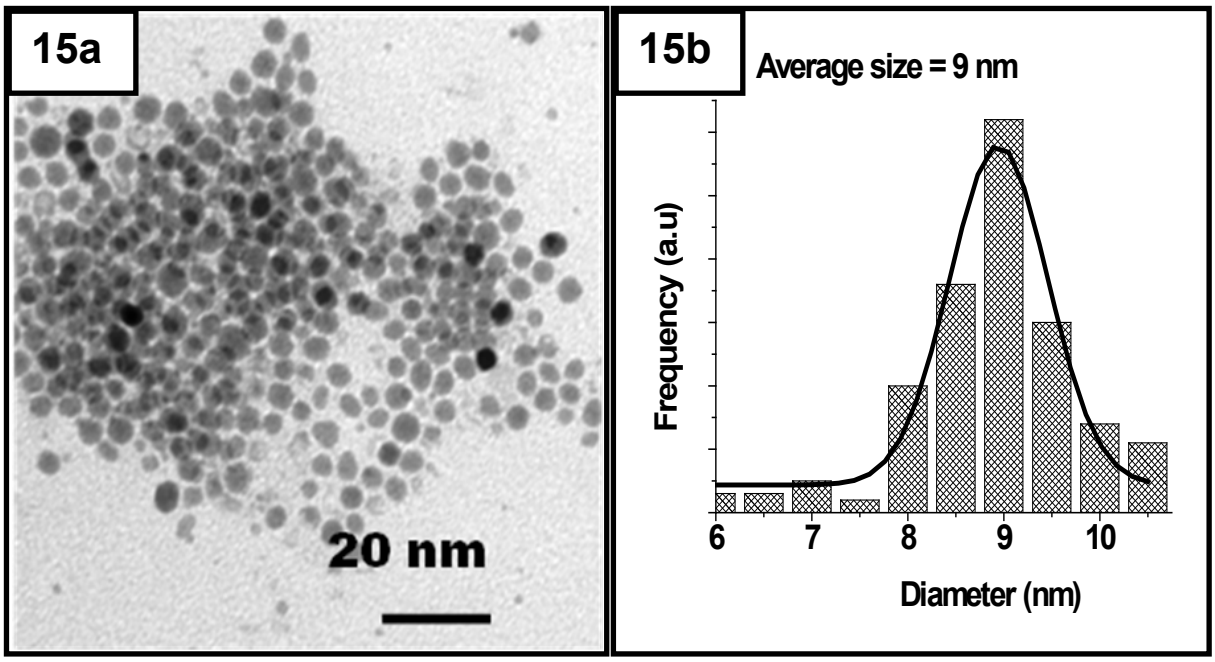

Figure 2.15 TEM image of hexadecyl amine stabilized indium colloid after 24hrs of digestive ripening in methylene chloride and (b) histogram of corresponding sample.

2.4.6 Trioctyl phosphine oxide / Hexadecyl amine (20:10) mixed ligand stabilized indium nanoparticles: Digestive ripening in methylene chloride.

Compared to neat ligands (Either TOPO or HDA), the mixed ligand system has a strong UV-Vis absorption peak even before digestive ripening, but after digestive ripening the peak further strengthens (Figure2.16) and stabilizes at 280 nm. Further comparison on as- prepared SMAD particles of TOPO or HDA stabilized particles, the mixed ligand particles are relatively more soluble and quasi-monodispersed size distribution was achieved at relatively shorter time (4 to 6 hrs). Figure 2.17 (a-d) shows the TEM images of particles with the progress of digestive ripening. The mean size measured from TEM is ~ 5 nm, histogram of TOPO and HDA mixed ligand stabilized particle mean size distribution is shown in Figure 2.18a-b. This indicates that the mixed ligand system works best for the digestive ripening of indium nanoparticles and the XRD shows all the characteristic features of indium as could be seen in Figure 2.12.

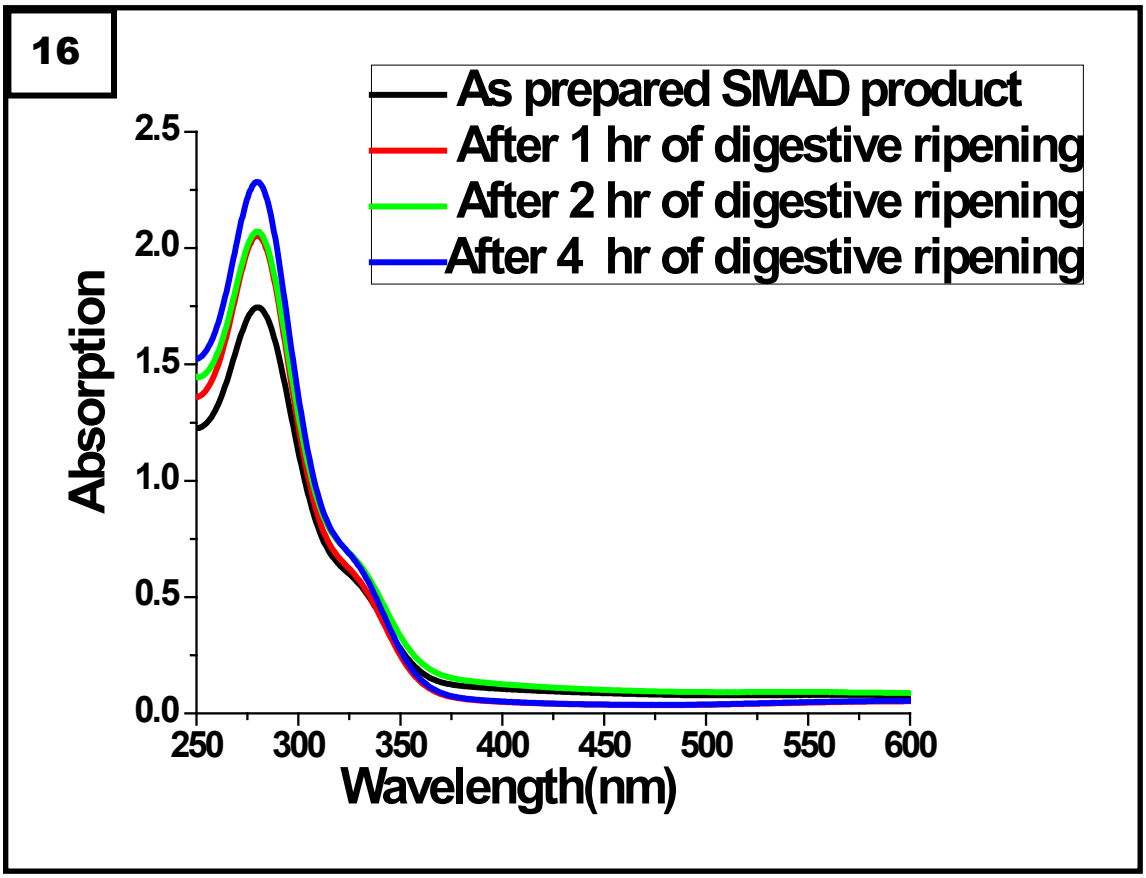

Figure 2.16 Temporal evolution of surface Plasmon absorbance resonance peak indium nanoparticles stabilized with mixed ligands (Trioctyl phosphine oxide and hexadecyl amine in 20: 10 ratio). The Black line represents the as-prepared SMAD colloid and the red line represents sample after 1 hr of digestive ripening, green line after 2 hrs, and blue line represents the surface Plasmon of indium after 4 hrs of digestive ripening in methylene chloride

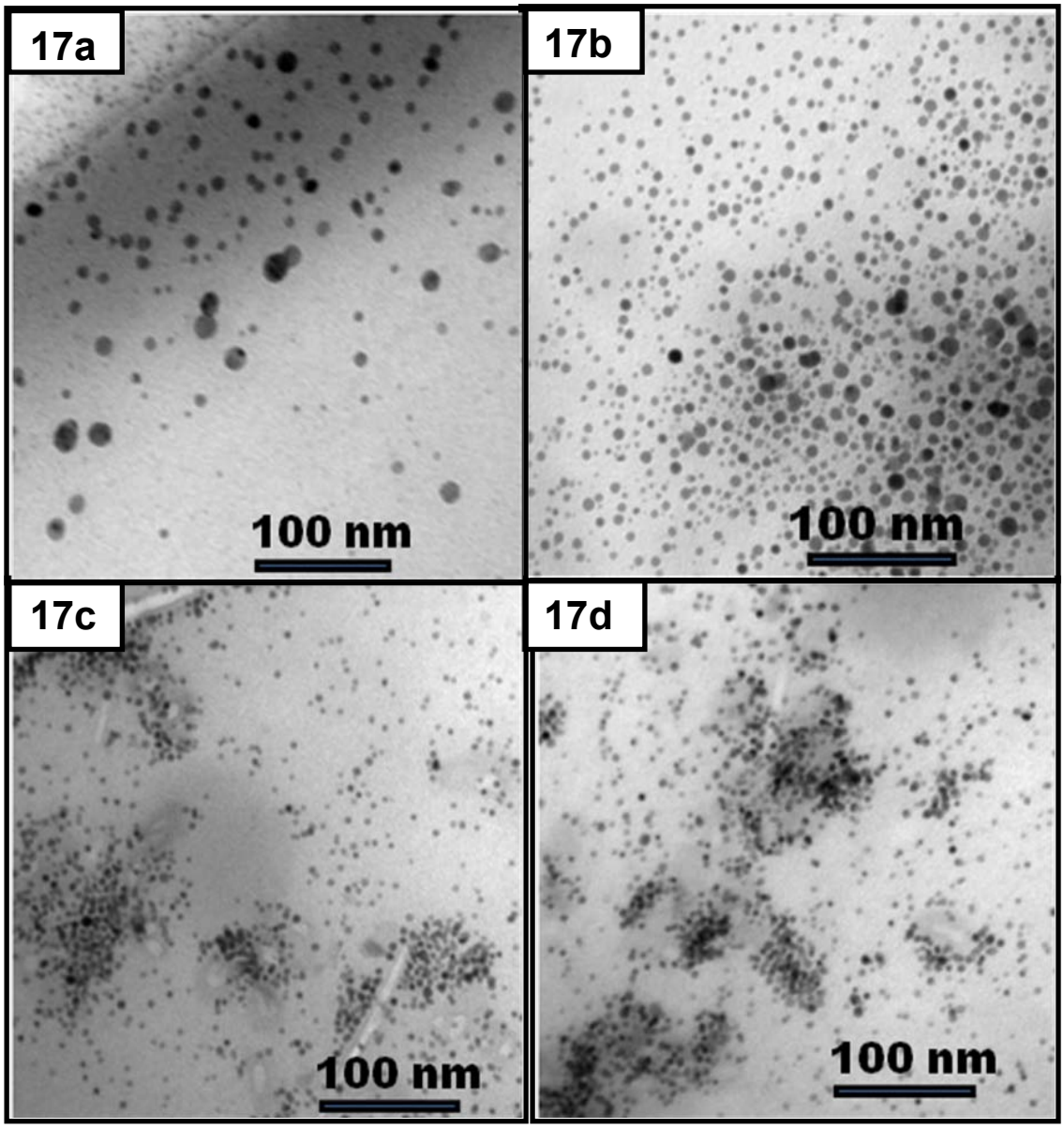

Figure 2.17 TEM image of (a) as -prepared polydispersed indium nanoparticles stabilized with trioctyl phosphine oxide and hexadecyl amine ligand (b) after 1 hr of digestive ripening (c) after 2 hrs of digestive ripening and (d) after 4 hrs of digestive ripening in methylene chloride.

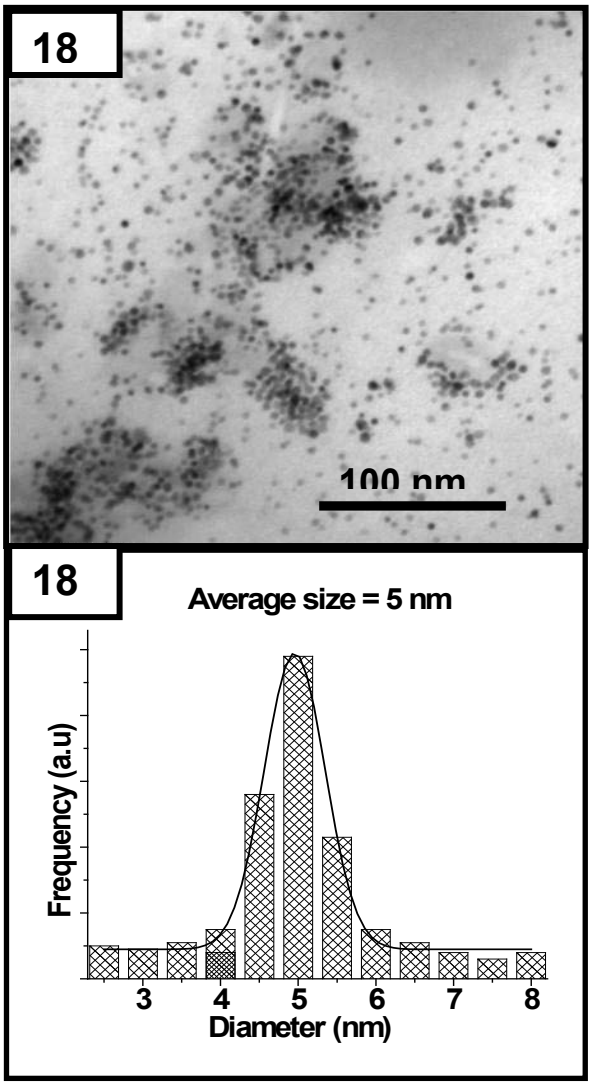

Figure 2.18 Histogram of mixed ligand stabilized indium colloid after 24hrs of digestive ripening in methylene chloride.

2.5 Control Experiment

Surprised with the controlling phenomenon by ligands at this low temperature, a control experiment was carried out to understand the effect of ligands on bulk metal. In this control experiment all reaction parameters were kept constant (metal to ligand ratio,

amount of solvent, and digestive ripening time) and the process was carried under the protection of argon but with bulk indium pieces. Even after 3 days of digestive ripening there was no evidence of nanoparticles formation (Figure 2.19). So, this suggests that the metal vaporization is necessary and this vaporization under dynamic vacuum leads to the formation of small crystallites or aggregates of small crystallites, and that these small particles are much more reactive than bulk indium. Along with other factors, formations of these crystallites are crucial in attaining narrow size distribution of particles.

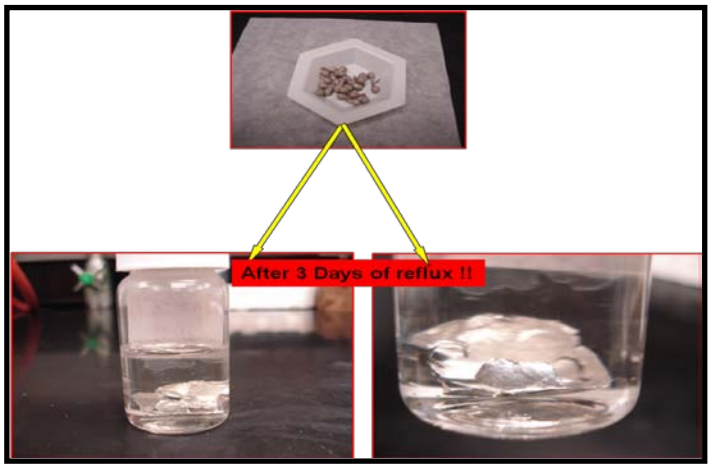

Figure 2.19 In controlled experiment all the reaction parameters were kept constant but with bulk indium pieces. Even after 3 days of digestive ripening in methylene chloride, there was no evidence of formation of indium nanoparticles.

2.6 Summary

Gram scale synthesis of indium nanoparticles from bulk metal has been achieved, and size adjusted by Digestive Ripening. Added ligands stabilize and solubilize the nanosized material.

Three new features have been uncovered: (1) Digestive ripening of indium can be carried out using very low boiling point solvent. (2) In fact, higher boiling solvent (toluene), where the indium nanoparticles at reflux temperature are probable molten, do not allow the best result, and less monodispersity is achieved; (3) Nanoparticle size can be varied by choice of stabilizing ligand; with TOPO in methylene chloride, 5 nm, but with hexadecylamine (HDA), 9 nm (See Figure 2.1, and 2. 15). Obviously, ligand choice and solvent choice are important and help control this thermodynamic phenomenon.

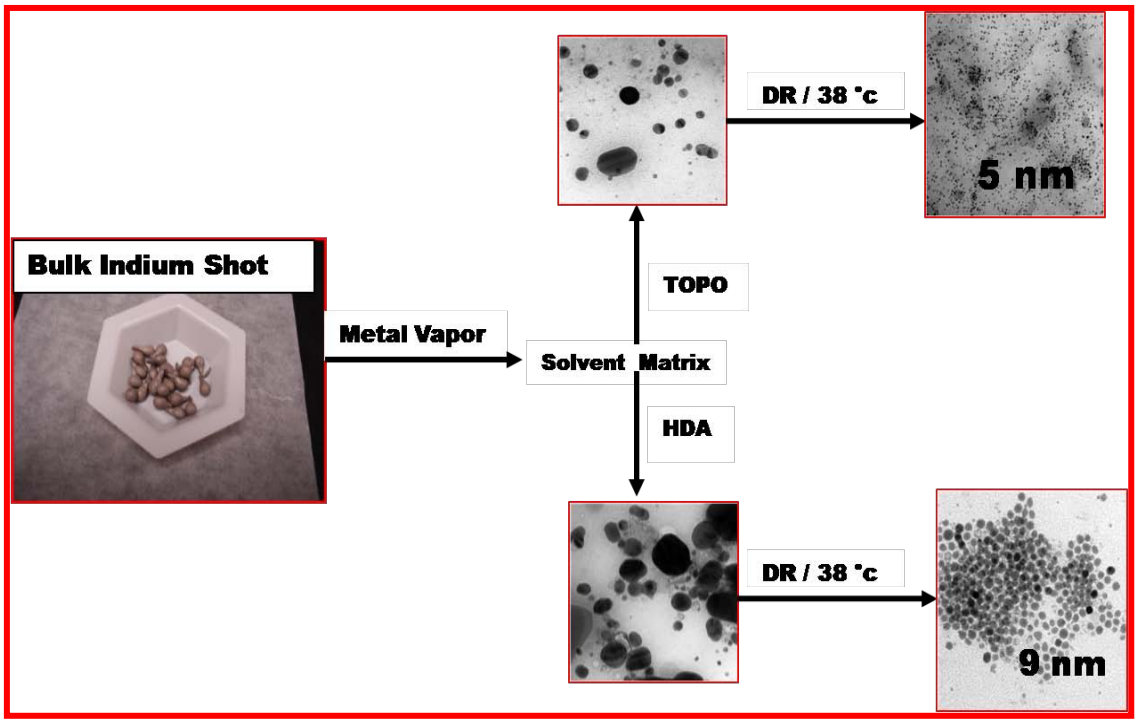

Figure 2.20 Schematic Representation of Overall Synthesis of Indium Nanoparticles

2.7 References

(1) Sau, T. K.; Rogach, A. L.; Jackel, F.; Klar, T. A.; Feldmann, J. *Advanced Materials*, *22*, **2010**, 1805-1825.

(2) Ponce, A. A.; Klabunde, K. J. *J. Mol. Catal. A: Chem.* **2005,** *225*, 1-6.

(3) Majetich, S. A.; Jin, Y. *Science* **1999,** *284*, 470-473.

(4) Black, C. T.; Murray, C. B.; Sandstrom, R. L.; Sun, S. H. *Science* **2000,** *290*, 1131-1134.

(5) Simon, U.; Flesch, R.; Wiggers, H.; Schon, G.; Schmid, G. *J. Mater. Chem.* **1998,** *8*, 517-518.

(6) Tang, M. L.; Reichardt, A. D.; Miyaki, N.; Stoltenberg, R. M.; Bao, Z. *J. Am. Chem. Soc.* **2008,** *130*, 6064-

(7) Novak, J. P.; Brousseau, L. C.; Vance, F. W.; Johnson, R. C.; Lemon, B. I.; Hupp, J. T.; Feldheim, D. L. *J. Am. Chem. Soc.* **2000,** *122*, 12029-12030.

(8) Kim, J. Y.; Yoon, S. B.; Yu, J. S. *Chemical Communications* **2003,** 790-791.

(9) Junno, T.; Magnusson, M. H.; Carlsson, S. B.; Deppert, K.; Malm, J. O.; Montelius, L.; Samuelson, L. *Microelectronic Engineering* **1999,** *47*, 179-183.

(10) Kim, K.; Jensen, K.; Zettl, A. *Nano Letters* **2009**, *9*, 3209-3213.

(11) Gittins, D. I.; Bethell, D.; Schiffrin, D. J.; Nichols, R. J. *Nature* **2000,** *408*, 67-69.

(12) Abtew, M.; Selvaduray, G. *Mater. Sci. Eng.* **2000**, *27*, 95.

(13) Li, Z.; Tao, X.; Cheng, Y.; Wu, Z.; Zhang, Z.; Dang, H. *Mater. Sci. Eng., A* **2005,** *407*, 7.

(14) Wang, J.; Liu, G. D.; Zhu, Q. Y. *Analytical Chemistry* **2003,** *75*, 6218-6222.

(15) Wang, C.; Ma, L.; Chen, L.-M.; Chai, K. X.; Su, M. *Analytical Chemistry*, **2010,** *82*, 1838- 1843.

(16) Ma, L.; Wang, C.; Hong, Y.; Zhang, M.; Su, M. *Analytical Chemistry*, **2010***, 82*, 1186- 1190.

(17) Barry, C. R.; Lwin, N. Z.; Zheng, W.; Jacobs, H. O. *Applied Physics Letters* **2003,** *83*, 5527-5529.

(18) Hong, Y.; Ding, S.; Wu, W.; Hu, J.; Voevodin, A. A.; Gschwender, L.; Snyder, E.; Chow, L.; Su, M. *ACS Applied Materials & Interfaces*, *2*, **2002** 3685-1691.

(19) NedeljkoviÄ‡, J. M.; MiÄ‡iÄ‡, O. I.; Ahrenkiel, S. P.; Miedaner, A.; Nozik, A. J. *J. Am.Chem. Soc.* **2004,** *126*, 2632-2639.

(20) Li, B.; Xie, Y.; Huang, J. X.; Liu, Y.; Qian, Y. T. *Ultrasonics Sonochemistry* **2001**, *8*, 331- 334.

(21) Kan, S. H.; Aharoni, A.; Mokari, T.; Banin, U. *Faraday Discussions* **2004,** *125*, 23-38.

(22) Bang, K.; Lee, K.; Park, Y. K.; Lee, P. H. *Bulletin of the Korean Chemical Society* **2002,** *23*, 1272- 1276.

(23) Takai, K.; Ikawa, Y. *Organic Letters* **2002**, *4*, 1727-1729.

(24) Lee, K.; Kim, H.; Miura, T.; Kiyota, K.; Kusama, H.; Kim, S.; Iwasawa, N.; Lee, P. H. *J. Am. Chem. Soc.* **2003,** *125*, 9682-9688.

(25) Schneider, U.; Ueno, M.; Kobayashi, S. *J. Am. Chem. Soc.* **2008,** *130*, 13824-13825.

(26) Zhao, Y.; Zhang, Z.; Dang, H. *J. Phys. Chem. B* **2003,** *107*, 7574.

(27) Ganeev, R. A.; Ryasnyanskiy, A. I.; Chakravarty, U.; Naik, P. A.; Srivastava, H.; Tiwari, M. K.; Gupta, P. D. *Appl. Phys. B: Laser Opt.* **2007**, *86*, 337.

(28) Balamurugan, B.; Kruis, F. E.; Shivaprasad, S. M.; Dmitrieva, O.; Zahres, H. *Applied Physics Letters* **2005,** *86*.

(29) Wang, Y.; Xia, Y. *Nano Letters* **2004,** *4*, 2047-2050.

(30) Han, Z. H.; Cao, F. Y.; Yang, B. *Applied Physics Letters* 2008, *92*.

(31) Hammarberg, E.; Feldmann, C. *Chemistry of Materials* **2009,** *21*, 771-774.

(32) Khanna, P. K.; Jun, K. W.; Hong, K. B.; Baeg, J. O.; Chikate, R. C.; Das, B. K. *Mater. Lett.* **2005,** *59*, 032.

(33) Singh, P.; Kumar, S.; Katyal, A.; Kalra, R.; Chandra, R. *Materials Letters* **2008,** *62*, 4164- 4166.

(34) Zhang, Y.; Li, G.; Zhang, L. *Inorg. Chem. Commun.* **2004,** *7*, 344.

(35) Wang, J.; Yang, Q.; Zhang, Z. *Crystal Growth & Design* **2009**, *9*, 3036-3043.

(36) Tsai, K. L.; Dye, J. L. *J. Am. Chem. Soc.* **1991,** *113*, 1650.

(37) Nedeljkovic, J. M.; Micic, O. I.; Ahrenkiel, S. P.; Meidaner, A.; Nozik, A. J. *J. Am. Chem.Soc.* **2004,***126*, 2632.

(38) Soulantica, K.; Maisonnat, A.; Fromen, M. C.; Casanove, M. J.; Lecante, P.; Chaudret, B. *Angew. Chem., Int. Ed.* **2001,** *40*, 448--451.

(39) Yu, H.; Gibbons, P. C.; Kelton, K. F.; Buhro, W. E. *J. Am. Chem. Soc.* **2001,** *123*, 9198.

(40) Soulantica, K.; Erades, L.; Sauvan, M.; Senocq, F.; Maisonnat, A.; Chaudret, B. *Adv. Funct. Mater.* **2003,** *13*, 553.

(41) Chou, N. H.; Ke, X. L.; Schiffer, P.; Schaak, R. E. *J. Am. Chem. Soc.* **2008**, *130*, 8140

(42) Kar, S.; Santra, S.; Chaudhuri, S. *Crystal Growth & Design* **2008**, *8*, 344-346.

(43) Soulantica, K.; Maisonnat, A.; Senocq, F.; Fromen, M. C.; Casanove, M. J.; Chaudret, B. *Angewandte Chemie-International Edition* **2001**, *40*, 2984-2986.

(44) Okuda, M.; Kobayashi, Y.; Suzuki, K.; Sonoda, K.; Kondoh, T.; Wagawa, A.; Kondo, A.;Yoshimura, H. *Nano Letters* **2005,** *5*, 991-993.

(45) Prasad, B. L. V.; Stoeva, S. I.; Sorensen, C. M.; Klabunde, K. J. *Langmuir* **2002,** *18*, 7515-7520.

(46) Son, S. U.; Jang, Y.; Yoon, K. Y.; Kang, E.; Hyeon, T. *Nano Letters* **2004**, *4*, 1147-1151.

(47) Prasad, B. L. V.; Stoeva, S. I.; Sorensen, C. M.; Klabunde, K. J. *Chemistry of Materials,* **2003,** *15*, 935-942.

(48) Horinouchi, S.; Yamanoi, Y.; Yonezawa, T.; Mouri, T.; Nishihara, H. *Langmuir* **2006**, *22*, 1880-1884.

(49) Ganesan, M.; Freemantle, R. G.; Obare, S. O. *Chemistry of Materials* **2007**, *19*, 3464- 3471.

(50) Stoeva, S.; Klabunde, K. J.; Sorensen, C. M.; Dragieva, I. *J. Am. Chem. Soc.* **2002**, *124*, 2305-2311.

(51) Smetana, A. B.; Klabunde, K. J.; Sorensen, C. M. *J. Colloid Interface Sci.* **2005,** *284*,521-526.

(52) Cingarapu, S.; Yang, Z.; Sorensen, C. M.; Klabunde, K. J. *Chem. Mater.* **2009,** *21*, 1248-1252.

(53) Stoeva, S. I.; Smetana, A. B.; Sorensen, C. M.; Klabunde, K. J. *J. Colloid Interface Sci.* **2007**, *309*, 94-98.

(54) Heroux, D.; Ponce, A.; Cingarapu, S.; Klabunde, K. J. *Adv. Funct. Mater.* **2007,** *17*, 3562-3568.

(55) Lin, X. M.; Sorensen, C. M.; Klabunde, K. J. *J. Nanopart. Res.* **2000,** *2*, 157-164.

(56) Kalidindi, S. B.; Jagirdar, B. R. *Inorg. Chem.* **2009**, *48*, 4524-4529.

CHAPTER 3 - Transformation of Indium Nanoparticles to *β*-Indium Sulphide: Digestive Ripening and Visible Light-Induced Photocatalytic Properties

3.1 Introduction

The properties of nanomaterial depend not only on their structure, shape, size, size distribution but also on the chemical composition of the material. Indium sulfide is a III – VI group semiconductor and it has two composite forms, InS and In_2S_3, with band gaps of 2.44 eV[1] and 2.0-2.2 eV [2] respectively. At atmospheric pressure, In_2S_3 is found to crystallize into three different structural forms. Among them, defective cubic structure, α-In_2S_3; a defective spinel structure, β-In_2S_3; and a layered hexagonal structure, γ - In_2S_3. However, among these three forms β-In_2S_3 has gained much attention because of its unique electronic, [3] optical,[4] optoelectronic, [5] and semiconductor sensitization [6] properties. Perhaps this may be due to its defective spinel structure. β-In_2S_3 has inspired its applications in the preparation of green and red phosphors for color televisions displays units,[7] as a buffer layer in solar cells, [8] as a heterojunction for use in photovoltaic electric generators, [9] as a photocatalytic material for hydrogen evolution,[10-13] as a biological imaging sensor, [14] and as photocatalytic material for degradation of dyes. [15,16]

There are several ways of synthesizing β-In_2S_3, one direct way is by high temperature treatment of sulfur and indium elements in a quartz vessel.[17] Other ways are by heat treating In_2O_3 by H_2S gas, [18] sonochemical,[19] solvent reduction,[20] thermal

decomposition of a single-source precursor,[21] hydrothermal,[22] and by laser induced synthesis. [23] And usually the sulfur is provided either by sulfides, (for example Li_2S,[24] Na_2S_3,[25] NaHS,[26] H_2S[27]) or sulfur powder,[9] sodium thiosulfate,[20] dimethyl sulfoxide, [28] thioacetamide,[19] thioglycolic acid,[7] sulfonate,[29] CS_2,[30] thiourea,[31] L-cystine,[32] sulfur-oleylamine complex, [33] and thiols. [34]

In recent years, metal alkanethiolates are used as precursor molecules for the synthesis of metals and metal sulfides by thermal decomposition at moderately low temperature (120 -200° C) either in solvents or solventless conditions. For example, Carotenuto et al reported a general method to synthesize metal or metal sulfide clusters embedded in polymer matrices.[35] Korgel et al reported the solventless synthesis of nickel sulfide and copper sulfide by decomposing corresponding thiolate precursors in the presence of octanoate,[36,37] and Nakamoto et al reported the synthesis of gold nanoparticles by thermal decomposition of gold tholate precursors [38,39]

In current work, a novel way of synthesizing indium sulfide is reported. The as-prepared dodecanethiol stabilized indium nanoparticles were transformed into β-indium sulfide (In_2S_3) upon a post-preparative digestive ripening treatment with high boiling point (190° C) t-butyl toluene under the protection of argon, and its visible light photcatalytic properties were investigated with methylene blue and Rhodamine B dye degradation.

3.2 Experimental

3.2.1 Materials required

Indium shot (99.9 %, Strem Chemicals Inc), Dodecanethiol ≥98% (Sigma –Aldrich), t-butyltoluene (TBT) 99% (Alfa Aesar), methylene chloride, Acetone (Fisher Scientific) and Ethanol (Absolute, 200 Proof, Aaper Alcohol and Chemical Co.), were used as received without further purification but, TBT was purged with argon for 2 hrs prior to use and methylene chloride was distilled and degassed four times by the standard freeze – thaw procedure prior to the reaction.

3.2.2 Synthesis of as- prepared Indium Nanoparticles by Evaporation and Co-condensation SMAD technique

In a typical synthesis, a stationary reactor was used as described in reference([40]). 0 .3 g of indium shot was charged into a C9 boron nitride crucible (R.D. Mathis # C9-BN) resting in a metal basket (R. D. Mathis # B8B # x.030 w) and the entire setup was then covered with insulating packing material (Zircar product, Inc.) to dissipate the heat generated during the metal evaporation. This crucible was then connected to water cooled copper electrodes. The SMAD reactor was then charged with dodecanethiol ligand (1:30 metal to ligand ratio) and 60 mL of *t*-butyl toluene. The entire setup was then vacuum sealed. A liquid N_2 Dewar was placed around the sealed SMAD reactor and once the vacuum attains 4 X 10^{-3} torr, 50 mL of distilled and degassed methylene chloride (Fisher chemicals) was evaporated through a solvent shower head, which was inserted into the reactor. The evaporated solvent was condensed on the wall of SMAD

reactor by external liquid nitrogen cooling. The metal was heated resistively by gradual increase of heat and the temperature required for the metal vaporization is ~ 900°C, and it took nearly 2 hrs of time for complete vaporization, this vaporized metal was co-condensed along with the solvent, (a total of 100 mL of methylene chloride solvent was used) which restricts particles form aggregation. The matrix was then allowed to melt room temperature and by vigorous stirring, the molten matrix and the vaporized indium was mixed with dodecanethiol stabilized ligand. The as-prepared indium colloid appears black in color. The as-prepared SMAD product was then siphoned into a Schlenk tube under argon and the solvent methylene chloride was vacuum evaporated leaving indium-dodecanethiol-TBT colloid.

3.2.3 Digestive Ripening:

The as-prepared indium-dodecanethiol-TBT was then subjected to digestive ripening at the boiling point of the solvent (190 °C) under the protection of argon for 4 hrs. Digestive ripening is a post preparative treatment used to make monodispersed particles from polydispersed colloidal particles in the presence of excess ligands, upon heating the colloid near or at the boiling point of the solvent. In current work, we adopted the same technique for the transformation of as-prepared polydispersed indium nanoparticles to highly monodispersed indium sulfide semiconductor.

3.2.4 Visible light Photocatalytic activity: Degradation of Methylene blue (Me B) and Rhodamine B (RhB) dye.

In order to investigate the visible light photocatalytic activity of β-In_2S_3, Methylene blue and Rhodamine dyes were chosen as probe molecules, photocatalytic experiments

were performed in a cylindrical glass reactor (capacity of the glass cylinder is 300 mL) as shown in Figure 3. 1 with a quartz window was used. The light source was an Oriel 1000-W high-pressure Hg arc lamp. The combination of a vis-NIR long-pass filter (400 nm) and colored glass filter (>420 nm) was used to eliminate ultraviolet radiation. At first, 0.39 mg of β-In_2S_3 was placed at the bottom of the glass reactor. Then, 100 mL of 2 X 10^{-5} M ethanol solution of Methylene blue dye was added to the catalytic present in the cylinder glass reactor. Before shining visible light, the catalyst and methylene blue dye solution was stirred vigorously, 3 mL of sample was collected periodically (every 10 minutes) to monitor the absorption and deabsorption of dye by the catalyst material and, the absorbance was monitored by Cary 500 UV- Vis-NRI spectrometer. After reaching equilibrium (It took 120 minutes), then the light source was turned on. The reactor was cooled by water circulation, and the experiments were performed at 25°C. After each UV-vis analysis, the sample was returned to the reactor.

After completion of the experiment, 0.29 mg of catalyst was recovered by filtration (Note 0.039 mg of catalyst was used). Then, the recovered catalyst was vacuum dried and re-used for the degradation of Rhodamine B (Rh B) dye (100 mL of 2 X 10^{-5} M ethanol solution of Rh B dye was used) and the same procedure was adopted.

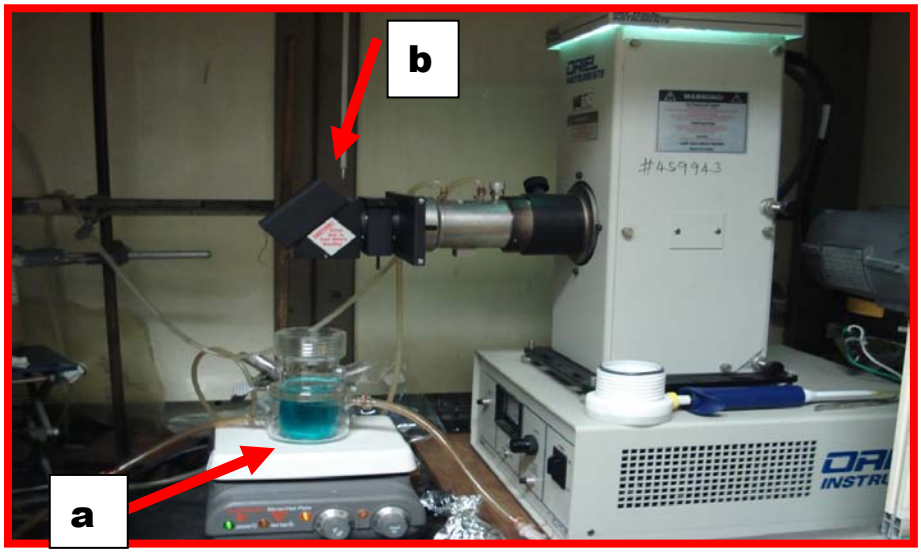

Figure 3.1 Visible light photocatalytic dye degradation experimental set up. (a) Methylene blue dye and (b) glass filter (>420 nm) used to eliminate ultraviolet radiation during visible light experiments

3.3 Characterization

3.3.1 UV – Vis Spectroscopy

UV-vis absorption spectra were obtained using a Cary 500 Scan UV–vis–NIR spectrophotometer. All samples were washed with absolute ethanol, acetone, and were dried under vacuum. The dried samples were then re-dissolved in toluene for analysis.

3.3.2 Transmission Electron Microscopy (TEM)

TEM studies were performed on a Philips CM100 operating at 100kV. The TEM samples were prepared by placing a few micro liters of precipitated, washed, vacuum dried and re-dissolved sample in toluene onto a carbon-coated Formvar copper grid and the grids were allowed to dry overnight. The facilities were provided by the Microscopy and Analytical Imaging Laboratory at Department of Biology, Kansas State University.

3.3.3 Powder X-ray diffraction (PXRD)

Powder X-ray diffraction patterns were recorded by a Bruker D8 X-ray diffractometer with CuKα radiation. PXRD samples were prepared by the evaporation of toluene from the sample / toluene dispersion loaded on XRD glass plates. The samples were scanned from 10< 2θ < 70° at an increment of 0.01°/ min and the total acquisition time period was more than 6 hrs.

3.3.4 Scanning Electron Microscope (SEM) with Energy-Dispersive X-Ray (EDX) analyzing system.

SEM analysis was performed using a Scanning Electron Microscope-S3500N, Hitachi Science System, Ltd. at the Entomology Department of Kansas State University, and were used to measure the EDX spectrum to determine the surface composition of the samples under conditions of 20 keV.

3.3.5 X-ray photoelectron spectroscopy (XPS)

XPS data were recorded using a Perkin–Elmer PHI 5400 electron spectrometer using acrochromatic Al Kα radiation (1486.6 eV) with Ar+ sputtering to remove the surface layer of the sample. Analysis was carried under vacuum (2.0×10^{-9} Torr). The XPS binding energies were measured with precision of 0.1 eV. The analyzer pass energy was set to 17.9 eV, and the contact time was 50 ms. The spectrometer was calibrated by setting the binding energies of Au 4f7/2 and Cu 2p3/2 to 84.0 and 932.7 eV, respectively. The facility was provided by Prof. Keith Hohn of Department of Chemical Engineering at Kansas State University.

3.4 Results and Discussion

The as-prepared SMAD product is black in color and turns lighter dark, then to yellow; dark yellow with digestive ripening and finally a dark brown precipitate (Figure 3.2) was obtained after 4 hrs of digestive ripening. At room temperature, these samples appear like gel, upon addition of ethanol, the precipitated sample appears like a polymer fiber (Figure 3.2 (insert figure)), and they easily re-dissolved in toluene.

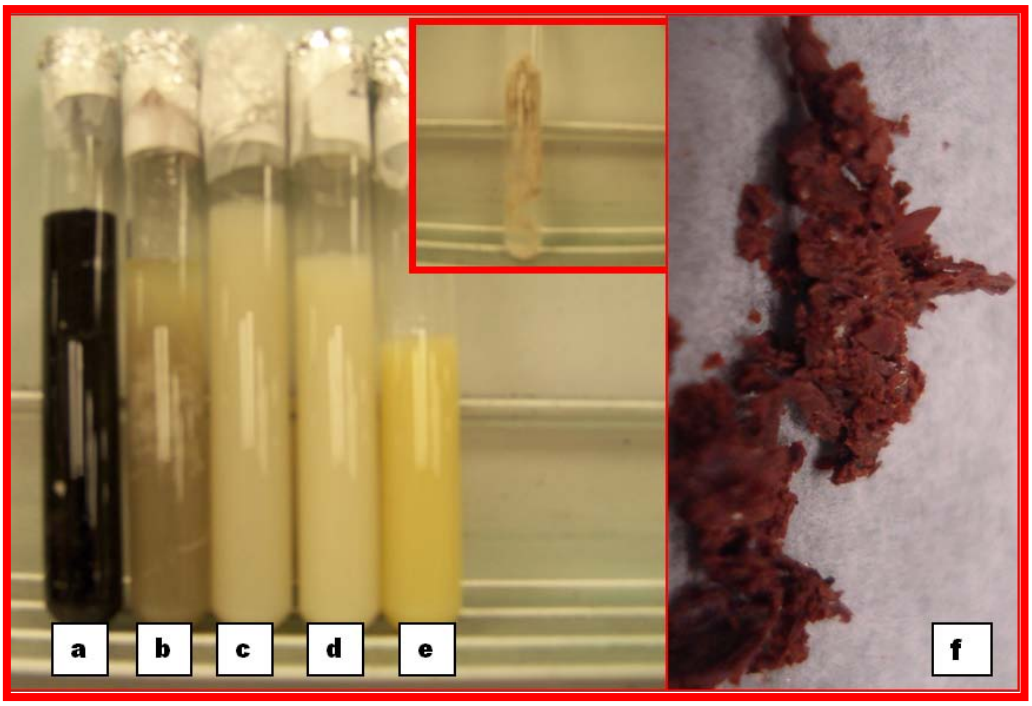

Figure 3.2 Transformation of as-prepared indium-dodecanethiol sample color from black to dark yellow. (a) as-prepared SMAD product, (b) after 30 min, (c) 60 min, (d) 120 min, (e) after 180 minutes, and after 4 hrs of digestive ripening in t-butyl toluene. Note, the final product (f) is brown color precipitate. Insert picture is the polymer like fiber obtained upon addition of ethanol to sample (c). Same kind of material was obtained for (d) and (e) samples too.

Figure 3.3 shows the absorption spectrum of the samples in toluene. The as-prepared SMAD indium-dodecanethiol-TBT has a broad UV-Vis absorption peak ranging from 550 to 610 nm but, within 15 minutes of digestive ripening the UV-Vis peak shifts to 375nm and stabilizes at the same wavelength. This spectral shift indicates a strong quantum confinement of the excitonic transmission expected for the In_2S_3 nanoparticles.[41] The position (375 nm) of the absorption band correlate well with the UV-vis characteristic of In_2S_3 nanoparticles prepared by other groups. [14]

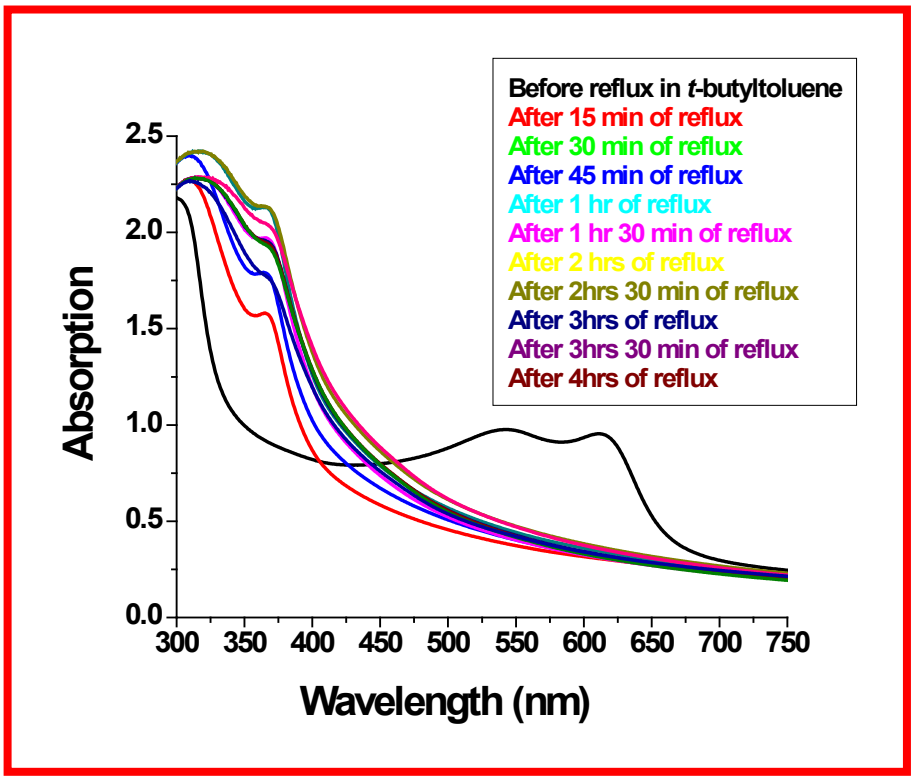

Figure 3.3 UV-Vis absorption peaks before digestive ripening appears at 550 and 610 nm but upon digestive ripening the peak stabilizes at 375 nm. The samples were measured in toluene solvent.

The TEM images shown in Figure 3.4 (a), the as-prepared SMAD-Indium-dodecanethiol sample before digestive ripening is polydispersed, Figure 3.4 (b –c) are the polymer like fibers (Note: Polymer like fiber shown in figure 3.2 (Insert) after precipitation with ethanol) obtained after precipitation with ethanol, vacuum dry, and re-dispersion in toluene. The intermediate samples are amorphous (Figure 3. 4d) But, upon prolonged digestive ripening (4 hrs), the final product (Brown precipitate in Figure 3.2 f) formed superlattice structure (Figure 3.4 e), which are crystalline in nature (Figure 3.4f). The XRD patterns of the final brown product shown in Figure 3.5 revealed the formation of $In_2 S_3$.

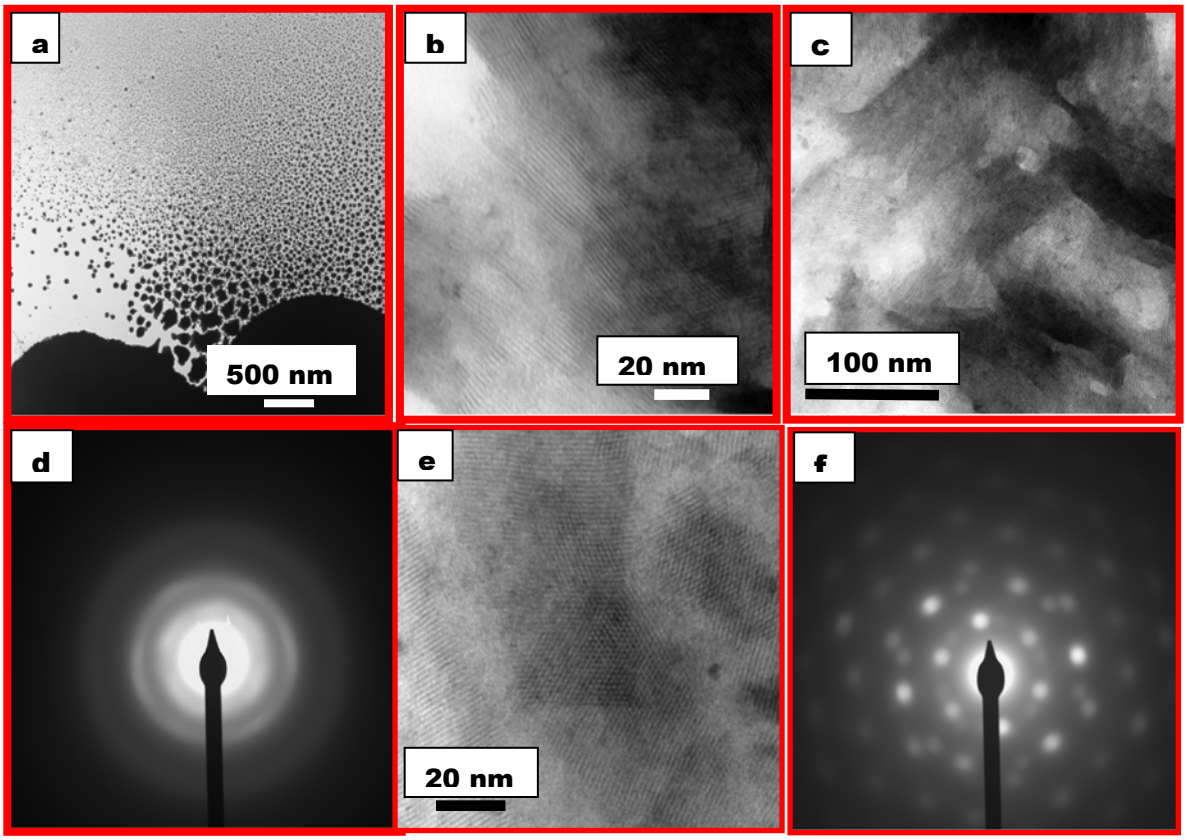

Figure 3.4 (a) As-prepared SMAD indium-dodecanethiol, (b) intermediates obtained after 30 minutes of digestive ripening, (c) intermediates obtained after 1 hr of digestive ripening,(d) corresponding electron diffraction showing amorphous nature of the intermediate, (e) after 4 hrs of digestive ripening and, (f) corresponding ED of the final product.

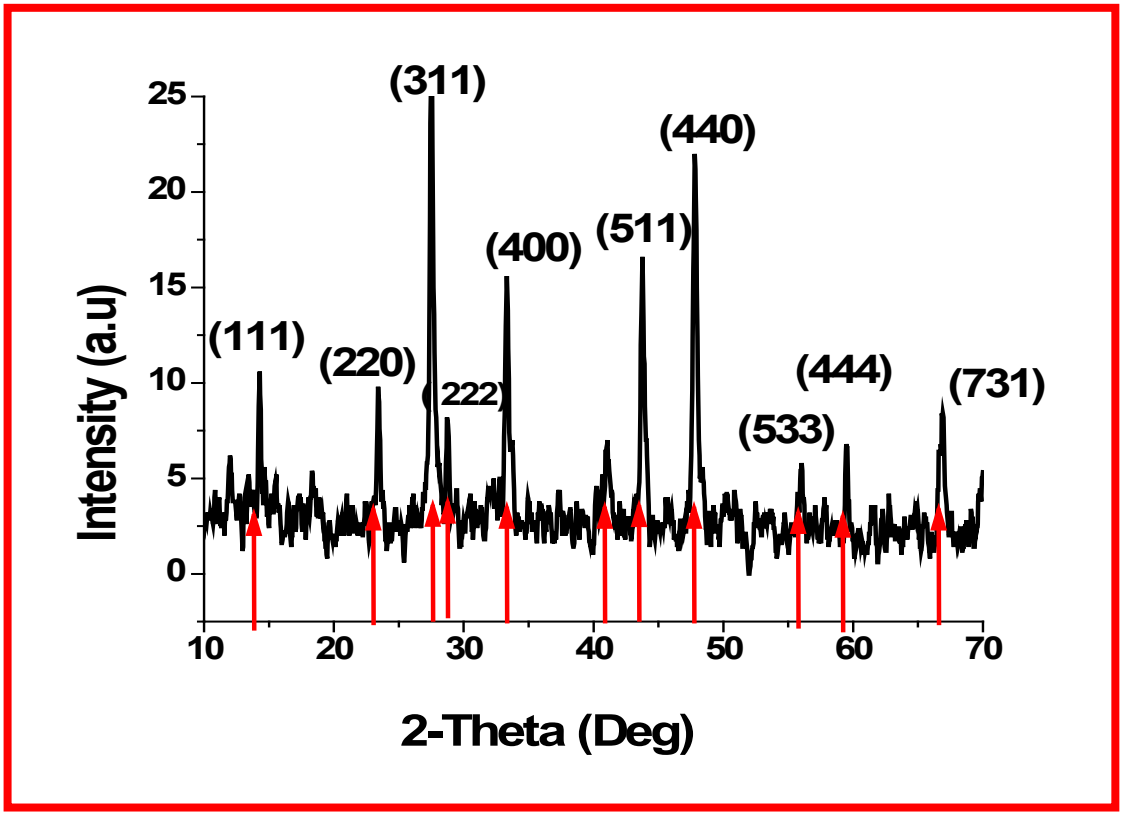

Figure 3.5 The XRD patterns of the final product. All the diffraction peaks can be indexed to the cubic β- In_2S_3 with a= 10. 77°A (JCPDS 65-0459)

The XRD diffraction peaks obtained from final product can be indexed to the cubic-In_2S_3 with a = 10. 77°A (JCPDS 65-0459). In order to further demonstrate the transformation of In_2S_3, SEM images of samples collected at different intervals of digestive ripening time are presented in Figure 3.5 and Figure 3.6 are the results of EDX analysis of corresponding samples.

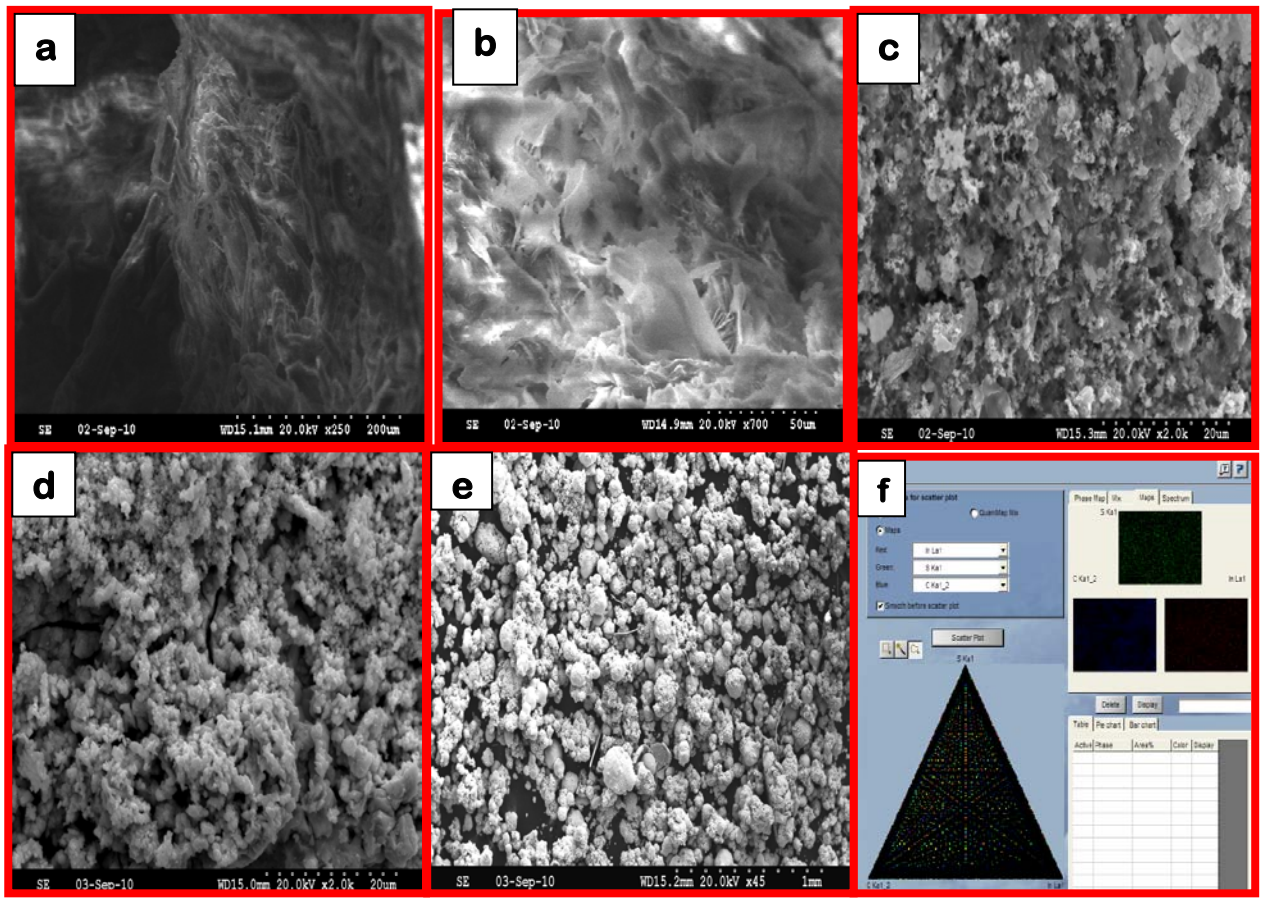

Figure 3.6 Figure 3.6 SEM image of samples obtained during the digestive ripening of polydispersed indium-dodecanethiol. (a) Intermediate obtained after 30 minutes of digestive ripening, (b) intermediate obtained after 1 hour of digestive ripening, (c) after 2 hrs of digestive ripening, (d) after 3 hrs of digestive ripening and, (e) the final product obtained after 4 hrs of digestive ripening. (f) Phase map of the intermediate showing the elemental arrangement within the intermediate (Red-In, Green-S, and Blue- C)

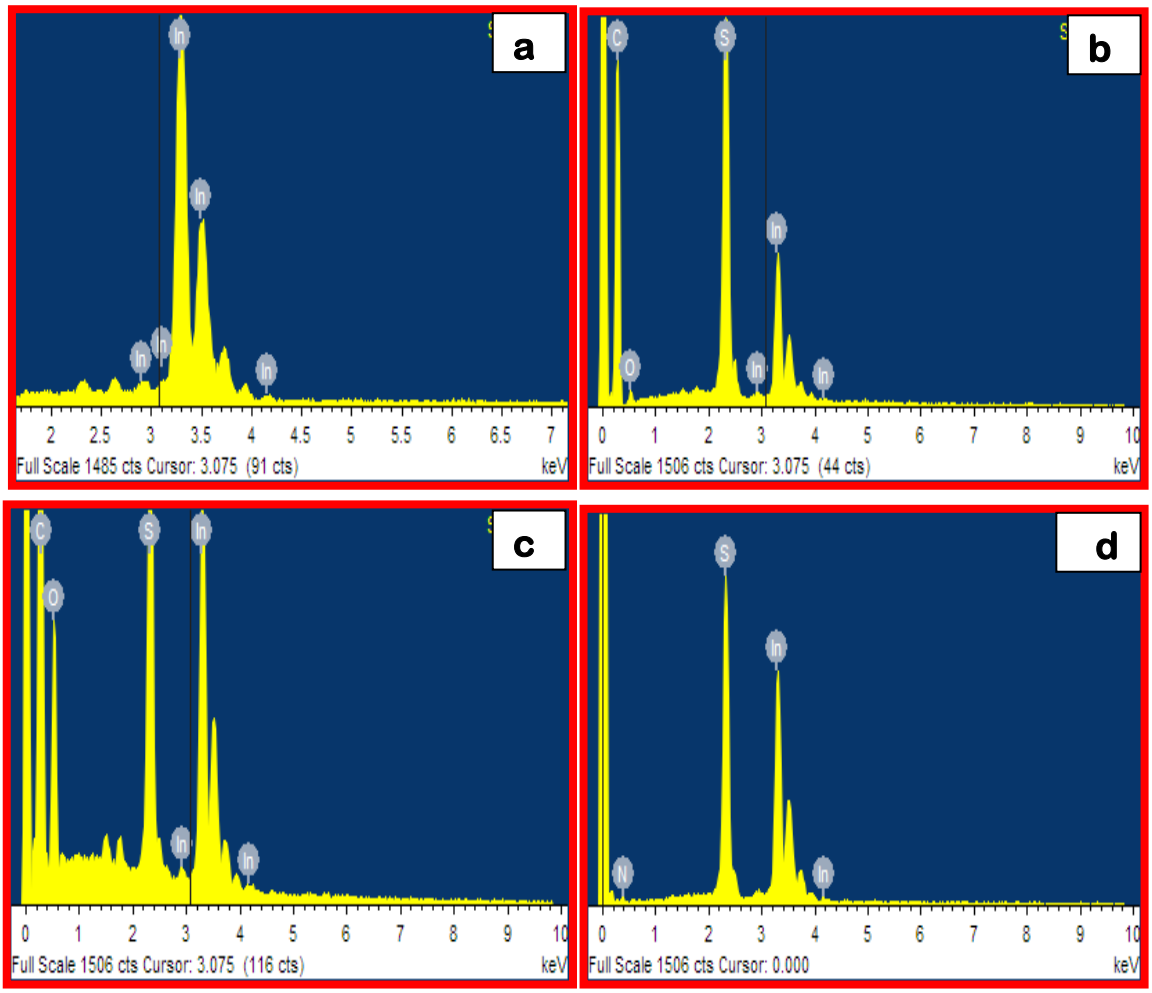

Figure 3.7(a) as- prepared indium-dodecanethiol showing mainly indium metal, (b) intermediate cmpound obtained after 30 minutes of digestive ripening, (c) after 1 hr of digestive ripening (Note- Appearance of carbon and sulfur peaks) and, (d) final product showing both sulfur and indium.

The energy dispersive X-ray analysis (Figure 3.7 (a-d)) results suggest that the as-prepared SMAD product mainly consist of Indium. After 30 minutes of digestive ripening, appearance of sulfur along with carbon indicate the formation of an intermediate and after 1 hr of digestive ripening, carbon is found to be more predominant and true to predominance of carbon, during the SEM image analysis

samples (Figure 3.6 (b-c)) acquired more charge. The final product was composed of sulfur and indium, and the ratios of sulfur to indium atoms were 1: 1.58 and this value is close to the theoretical values of 1.5 expected for In_2S_3. Further, this value matches with group 12 sulfides formed by thermal decomposition of metal-complexes in high-boiling point solvents. [42-44]

To further investigate the surface composition and chemical state of the as-prepared SMAD product, intermediate(s), and In_2S_3, XPS measurements were carried out. Figure 3.8 shows the observed binding energy spectrum for the In d electron and Figure 3. 9 show the S2p electron of as-prepared SMAD indium-dodecanethiol product, intermediate(s) and the final product (In_2S_3). The observed binding energy of 443.5 eV and 452.1 eV were related to In $3d_{5/2}$ and In $3d_{3/2}$ of the as-prepared indium-dodecanethiol product, while there was no evidence (Figure 3.9) of binding energy of sulfur. Indeed, the starting material has only indium metal stabilized with thiol (Note-the EDX data (Figure 3.7a) of as-prepared indium-dodecanethiol consist of mainly indium, there was no evidence of sulfur presence in starting material). The standard binding energy of pure metal was found to be 443.49 and 451.18 eV [45], however, Balamurgan et.al have found an increase in binding energy of core electrons of indium with a decrease in the particle size. [46] The observed binding energy of In $3d_{5/2}$ and In $3d_{3/2}$ for intermediates are slightly higher in energy compared to In $3d_{5/2}$ and In $3d_{3/2}$ of the as-prepared indium-dodecanethiol product, Further, the S $2p_{3/2}$ binding energy value for intermediate compounds is at 162.3 eV, which is typical for metal thiolate bonds [47] and this value matched with the reported literature for indium thiolates. [48] Hence, the formed

intermediates are most likely indium thiolates. The binding energy values at 445 and 452.5 eV of In $3d_{5/2}$ and In $3d_{3/2}$ and 162.5 eV to S 2p agreed well with the reported data for In_2S_3. [22,49-51]

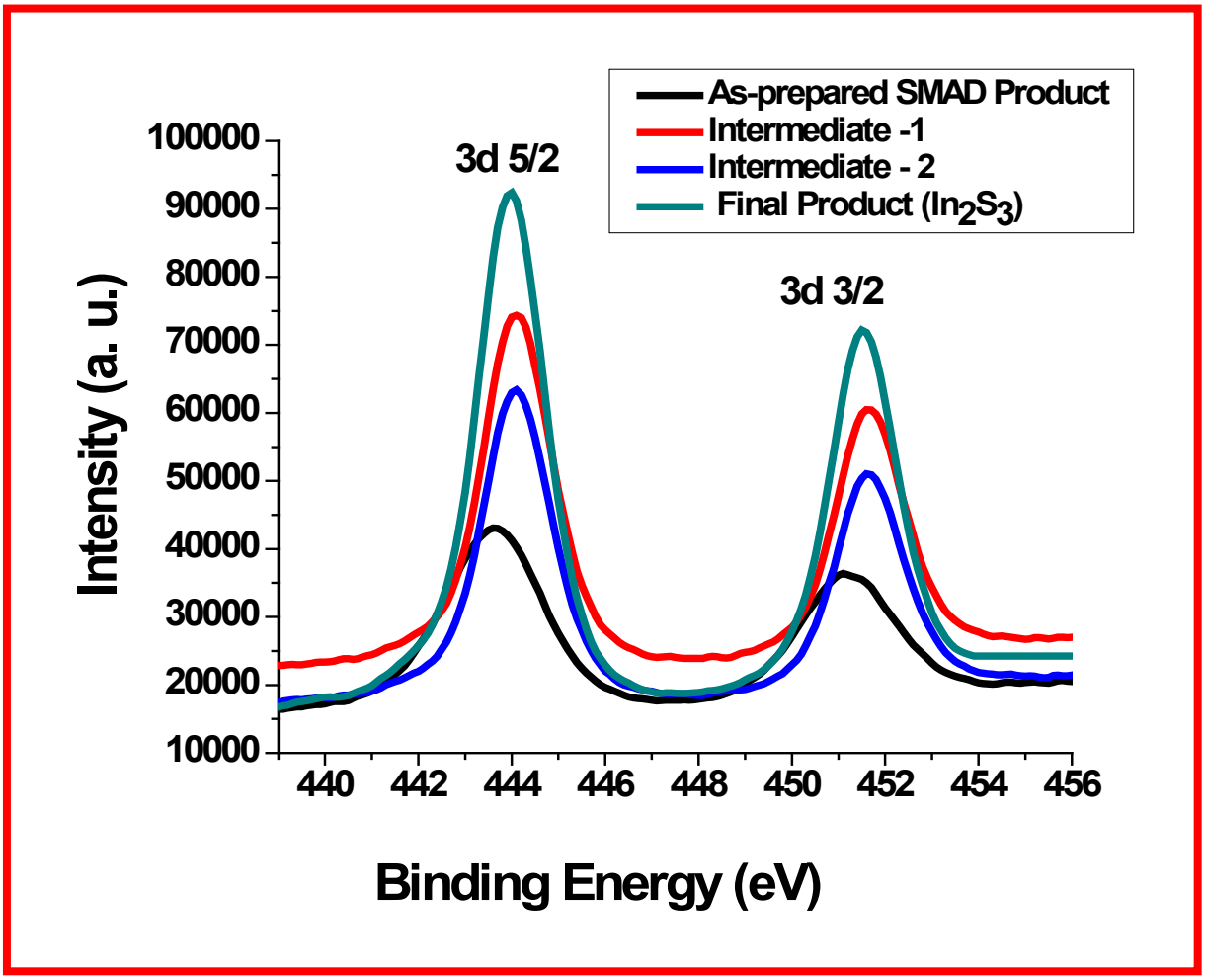

Figure 3.8 Binding energy spectrum of as-prepared indium-dodecanethiol (before digestive ripening), intermediate compounds (Obtained during the digestive ripening 30, 60 minutes) and, final product (In_2S_3). (a) In3d $_{5/2}$ and In3d $_{3/2}$, and S 2p.

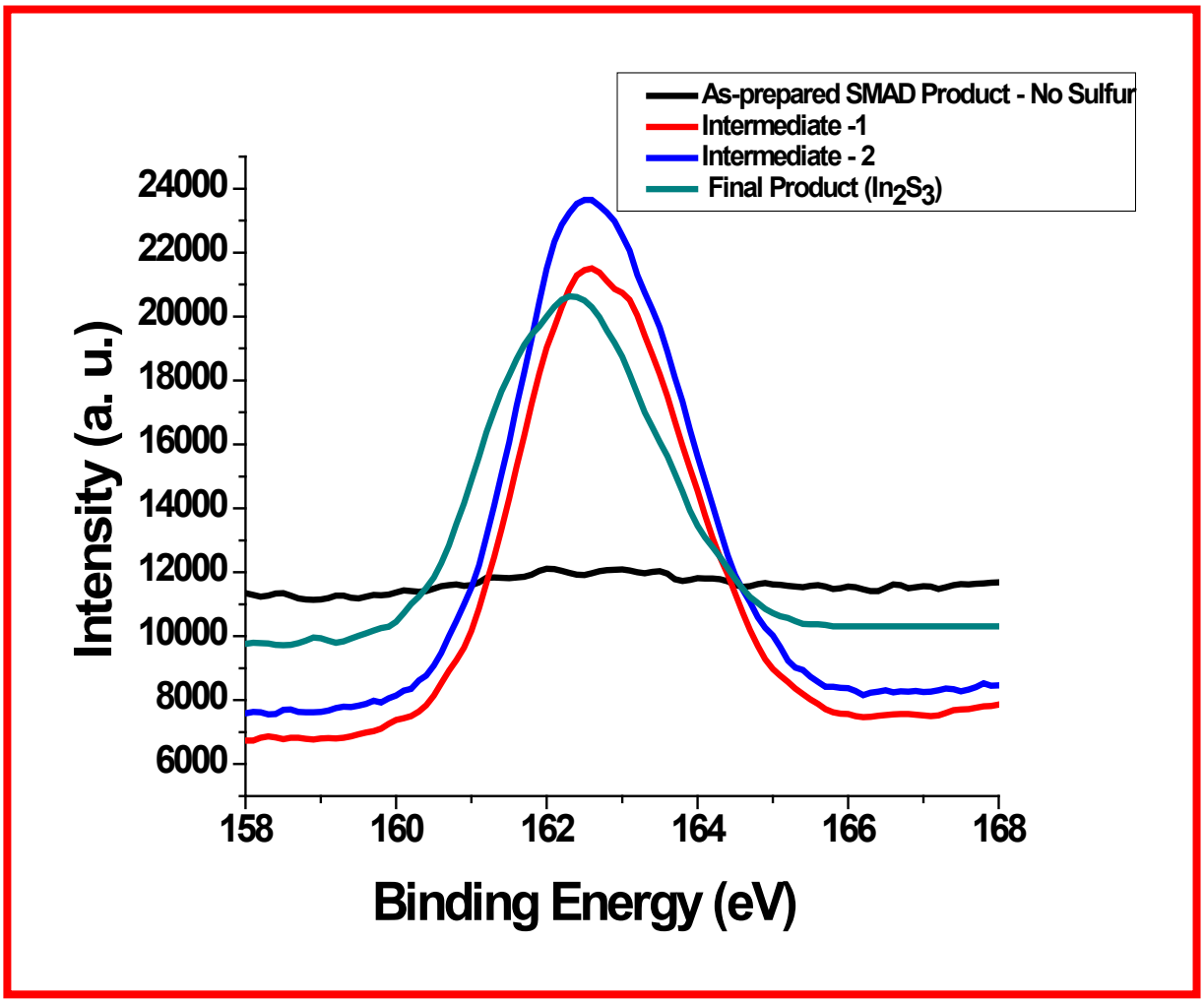

Figure 3.9 Binding energy spectrum of as-prepared indium-dodecanethiol (before digestive ripening), intermediate compounds (Obtained during the digestive ripening 30, 60 minutes) and, final product (In_2S_3) of S 2p.

The overall picture that emerges is that, owing to the high reactivity of indium, it reacts with the dodecanethiol ligand and spontaneously transforms into an intermediate thiolate and eventually into In_2S_3 via thermally activated digestive ripening and indium-catalyzed interfacial C-S cleavage reactivities. Based on the solubility, the formed intermediate might be a cyclic (tiara) alkanethiolate compound because metal alkanethiolates, which are found to be insoluble in organic solvents have been found to

have layered structures (for example, Ag ,[52-54] Pb, [55,56] Cu[57]) and those, which are soluble in organic solvents have cyclic structures. [58-61] Efforts to grown crystals from these intermediates were not successful, and only amorphous structures were obtained (Figure 3.2 (d)).

A possible reaction sequence for the transformation of indium to In_2S_3 is as follows.

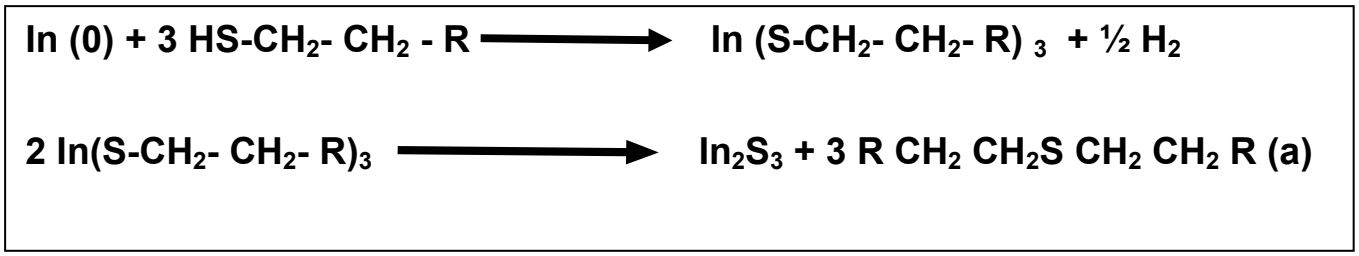

3.4.1 Visible light photodegradation of organic dyes

Methylene blue (MeB) is a organic dye, and often is used as a model pollutant to study the photocatalytic activity.[43,62] We chose MeB as a probe molecule to investigate photocatalytic degradation property of the final product (In_2S_3) with the help of UV-vis absorption spectrum. The maximal absorption energy of MeB is at 655 nm, the decrease in the absorbance at 655 nm reflects the degradation of MeB, which can therefore be used as an indicator of the photocatalytic activity. Figure 3.10 demonstrates the absorbance spectral change of MeB in the presence of In_2S_3. Based on other research group findings with the MeB degradation, it is possible that upon photoexciment, electrons injection from MeB molecule to β- In_2S_3 lead to reduction of molecular oxygen and thereby oxidation decomposition of the electron deficient Me B.

[62,63] It took 120 minutes for the complete degradation of 100 mL of 2 X 10^{-5} M ethanol solution of Methylene blue dye under visible light.

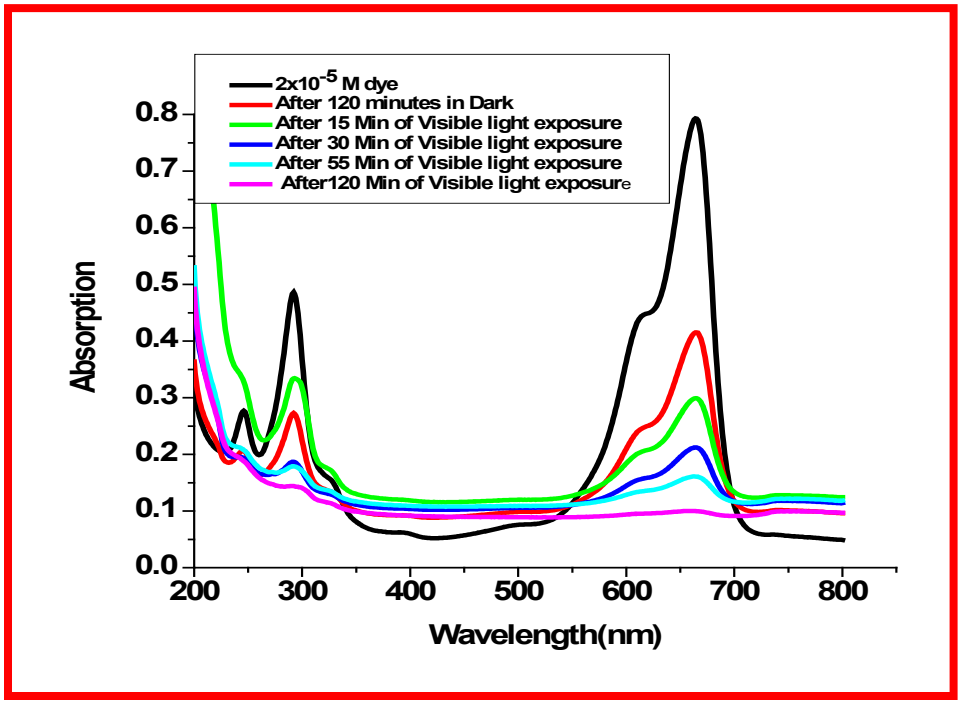

Figure 3.10 3.9 Room-temperature UV-Vis absorption spectrum of methylene blue in *β*- In_2S_3 (Black line the pure dye) suspensions irradiated for different times.

Further to investigate the visible light photocatalytic activity of *β*- In_2S_3, the recovered (0.029 mg) catalyst was re-used for photodegradation of Rhodamine B (RhB). Many research groups have used RhB as a model pollutant because it exhibits absorbance maxima at 552 nm and the decrease in the absorbance at 552 nm reflects the dye degradation. However, Zhao et al [64,65]have reported that RhB de-ethylation (300 nm) is mainly a surface reaction, whereas RhB chromophore ring degradation (552 nm) is mainly due to a solution bulk process. [64,65] Hence, the fast de-ethylation of RhB indicates the photodegradation of dye molecule by the catalytic material as shown in

Figure 3.11,after being illuminated under visible light for 60 minutes, the RhB decreases by 96%.

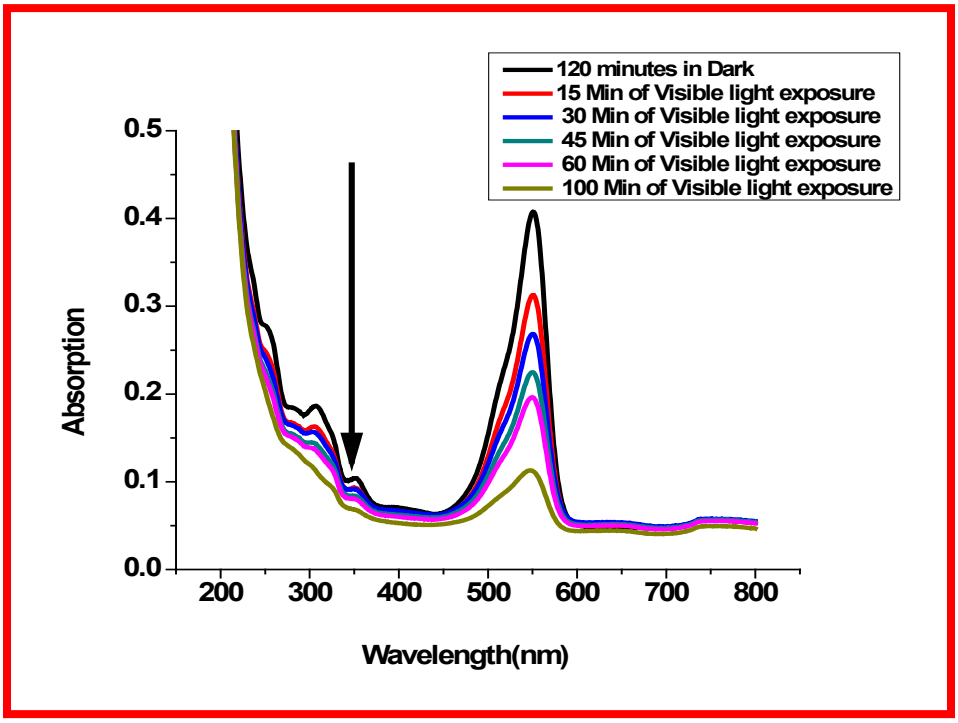

Figure 3.11 shows the spectral change of RhB / In2S3 dispersion under visible light irradiation

These results revealed that the final product obtained was indeed In_2S_3 and it has good photocatalytic activity for both methylene blue and Rhodamine B dye degradation. However, the intermediate(s) obtained were not clealyr understood. More in depth analysis is needed.

3.5 SUMMARY

1. Synthesis of highly monodispersed *β*-IndiumSulphide (In_2S_3) by evaporation/ condensation of indium shots using the solvated metal atom dispersion (SMAD)

technique, followed by digestive ripening in high boiling point *t*-butyltoluene (190° C) solvent was achieved.

2. The as-prepared polydispersed indium nanoparticles were stabilized by dodecanethiol and the sample looks black in color but upon digestive ripening the color of the sample changed from black to cream; pale yellow to yellow and finally to brown in color, suggesting the transformation of indium to β -In_2S_3.

3. The crystallite size distribution of the transformed product was obtained from the XRD diffraction profile and particle size measurement on the transmission electron microscopy (TEM) grid is found to be ~ 5nm. Further these particles organize in to 2D and 3D super lattices.

4. The optical absorbance of as-prepared sample showed an absorption peak around 538 and 613 nm but upon digestive ripening, these two peaks disappears and stabilized at 366 nm. This is further for the transformation to In_2S_3, and is also evidence of strong quantum confinement of excitons transmission expected for the In_2S_3 nanoparticles

5. The visible light-induced photo -catalytic activity of In_2S_3 was performed on Rhodamine B (RhB) and methyleneblue dye, in which 95% of both dyes were photodegraded after 60 min.

6. This is a unique work, where thermally activated digestive ripened indium clusters might catalyze the C- S bond cleavage to convert indium nanoclusters towards

the formation of In_2S_3 semiconductor. This post preparative digestive ripening is highly effective for tuning size, and composition.

3.6 References

(1) Nishino, T.; Hamakawa, Y. *Japanese Journal of Applied Physics* **1977**, *16*, 1291-1300.

(2) Timoumi, A.; Bouzouita, H.; Kanzari, M.; Rezig, B. *Thin Solid Films* **2005**, *480*, 124-128.

(3) Kamoun, N.; Belgacem, S.; Amlouk, M.; Bennaceur, R.; Bonnet, J.; Touhari, F.; Nouaoura, M.; Lassabatere, L. *Journal of Applied Physics* **2001**, *89*, 2766-2771.

(4) Choe, S.-H.; Bang, T.-H.; Kim, N.-O.; Kim, H.-G.; Lee, C.-I.; Jin, M.-S.; Oh, S.-K.; Kim, W.-T. *Semiconductor Science and Technology* **2001**, *16*, 98-102.

(5) Kim, W. T.; Kim, C. D. *Journal of Applied Physics* **1986**, *60*, 2631-3.

(6) Yasaki, Y.; Sonoyama, N.; Sakata, T. *Journal of Electroanalytical Chemistry* **1999**, *469*, 116-122.

(7) Chen, W.; Bovin, J.-O.; Joly, A. G.; Wang, S.; Su, F.; Li, G. *Journal of Physical Chemistry B* **2004**, *108*, 11927-11934.

(8) Dalas, E.; Sakkopoulos, S.; Vitoratos, E.; Maroulis, G.; Kobotiatis, L. *Journal of Materials Science* **1993**, *28*, 5456-60.

(9) Dalas, E.; Kobotiatis, L. *Journal of Materials Science* **1993**, *28*, 6595-6597.

(10) Osterloh, F. E. *Chemistry of Materials* **2008**, *20*, 35-54.

(11) Naik, S. D.; Jagadale, T. C.; Apte, S. K.; Sonawane, S.; Kulkarni, M. V.; Patil, S. I.; Ogale, S. B.; Kale, B. B. *Chemical Physics Letters* **2008**, *452*, 301-305.

(12) Kudo, A.; Nagane, A.; Tsuji, I.; Kato, H. *Chemistry Letters* **2002**, 882-883.

(13) Fu, X. L.; Wang, X. X.; Chen, Z. X.; Zhang, Z. Z.; Li, Z. H.; Leung, D. Y. C.; Wu, L.; Fu, X. Z. *Applied Catalysis B-Environmental*, ***2010****, 95*, 393-399.

(14) Nagesha, D. K.; Liang, X.; Mamedov, A. A.; Gainer, G.; Eastman, M. A.; Giersig, M.; Song, J.-J.; Ni, T.; Kotov, N. A. *The Journal of Physical Chemistry B* **2001**, *105*, 7490-7498.

(15) Du, W. M.; Zhu, J.; Li, S. X.; Qian, X. F. *Crystal Growth & Design* **2008**, *8*, 2130-2136.

(16) He, Y. H.; Li, D. Z.; Xiao, G. C.; Chen, W.; Chen, Y. B.; Sun, M.; Huang, H. J.; Fu, X. Z. *Journal of Physical Chemistry C* **2009**, *113*, 5254-5262.

(17) Kaito, C.; Saito, Y.; Fujita, K. *Journal of Crystal Growth* **1989**, *94*, 967-77.

(18) Bube, R. H.; McCarroll, W. H. *Journal of Physics and Chemistry of Solids* **1959**, *10*, 333-335.

(19) Avivi, S.; Palchik, O.; Palchik, V.; Slifkin, M. A.; Weiss, A. M.; Gedanken, A. *Chemistry of Materials* **2001**, *13*, 2195-2200.

(20) Xiong, Y.; Xie, Y.; Du, G.; Tian, X. *Journal of Materials Chemistry* **2002**, *12*, 98-102.

(21) Afzaal, M.; Malik, M. A.; O'Brien, P. *Chemical Communications (Cambridge, United Kingdom)* **2004**, 334-335.

(22) Vigneashwari, B.; Dash, S.; Tyagi, A. K.; Parameswaran, P.; Ravichandran, V.; Sunthathiraraj, S. A. *Journal of Nanoscience and Nanotechnology* **2007**, *7*, 2087-2091.

(23) Asikainen, T.; Ritala, M.; Leskelae, M. *Applied Surface Science* **1994**, *82/83*, 122-5.

(24) Richard, H. B. a. W. M. *J. Phys. Chem. Solids* **1959**, *10*, 333.

(25) Nosaka, Y.; Ohta, N.; Miyama, H. *Journal of Physical Chemistry* **1990**, *94*, 3752-5.

(26) Kumta, P. N.; Phule, P. P.; Risbud, S. H. *Materials Letters* **1987**, *5*, 401-4.

(27) Kamat, P. V.; Dimitrijevic, N. M.; Fessenden, R. W. *Journal of Physical Chemistry* **1988**, *92*, 2324-9.

(28) Gao, P.; Xie, Y.; Chen, S.; Zhou, M. *Nanotechnology* **2006**, *17*, 320-324.

(29) Dutta, D. P.; Sharma, G.; Ghoshal, S.; Kushwah, N. P.; Jain, V. K. *Journal of Nanoscience and Nanotechnology* **2006**, *6*, 235-240.

(30) Xiong, Y.; Xie, Y.; Du, G.; Tian, X.; Qian, Y. *Journal of Solid State Chemistry* **2002**, *166*, 336-340.

(31) Zhu, X.; Ma, J.; Wang, Y.; Tao, J.; Zhou, J.; Zhao, Z.; Xie, L.; Tian, H. *Materials Research Bulletin* **2006**, *41*, 1584-1588.

(32) Chen, L.-Y.; Zhang, Z.-D.; Wang, W.-Z. *The Journal of Physical Chemistry C* **2008**, *112*, 4117-4123.

(33) Kim, Y. H.; Lee, J. H.; Shin, D. W.; Park, S. M.; Moon, J. S.; Nam, J. G.; Yoo, B. *Chemical Communications*, *46*, 2292-2294.

(34) Dutta, D. P.; Sharma, G.; Tyagi, A. K.; Kulshreshtha, S. K. *Materials Science & Engineering, B: Solid-State Materials for Advanced Technology* **2007**, *138*, 60-64.

(35) Carotenuto, G.; Martorana, B.; Perlo, P.; Nicolais, L. *J. Mater. Chem.* **2003**, *13*, 2927.

(36) Larsen, T. H.; Sigman, M. B.; Ghezelbash, A.; Doty, R. C.; Korgel, B. A. *J. Am. Chem. Soc.* **2003**, *125*, 5638.

(37) Ghezelbash, A.; Sigman, M. B.; Jr, n. *Nano Lett.* **2004**, *4*, 537.

(38) Nakamoto, M.; Kashiwagi, Y.; Yamamoto, M. *Inorg. Chim. Acta* **2005**, *358*, 4229.

(39) Nakamoto, M.; Yamamoto, M.; Fukusumi, M. *J. Chem. Soc. Chem. Commun.* **2002**, 1622.

(40) Klabunde, K. J. T., P. L.; Skell, P. S.; Ittel, S. Inorg. Synth. 1979, 19, 59-86, Shriver, D.; Ed.

(41) Lavrent'ev, A.; Safontseva, N.; Dubeiko, V.; Gabrel'yan, B.; Nikiforov, I. *Physics of the Solid State* **2000**, *42*, 2047-2053.

(42) Malik, M. A.; Revaprasadu, N.; O'Brien, P. *Chemistry of Materials* **2001**, *13*, 913-920.

(43) Du, W.; Zhu, J.; Li, S.; Qian, X. *Crystal Growth & Design* **2008**, *8*, 2130-2136.

(44) Trindade, T.; O'Brien, P.; Zhang, X.-m. *Chemistry of Materials* **1997**, *9*, 523-530.

(45) Laine, E.; Tamminen, M.; Mäkelä, R.; Pessa, M. *Journal of Materials Science* **1983**, *18*, 295-298.

(46) Balamurugan, B.; Kruis, F. E.; Shivaprasad, S. M.; Dmitrieva, O.; Zahres, H. *Applied Physics Letters* **2005**, *86*, 3.

(47) Bensebaa, F.; Zhou, Y.; Deslandes, Y.; Kruus, E.; Ellis, T. H. *Surface Science* **1998**, *405*, L472-L476.

(48) Zerulla, D.; Chasse, T. *Langmuir* **1999**, *15*, 5285-5294.

(49) Fu, X. L.; Wang, X. X.; Chen, Z. X.; Zhang, Z. Z.; Li, Z. H.; Leung, D. Y. C.; Wu, L.; Fu, X. Z. *Applied Catalysis B-Environmental*, *95*, 393-399.

(50) Wu, Z.; Ma, D. K.; Zhen, H.; Tang, Q.; Xie, O.; Qian, Y. T. *Journal of Nanoscience and Nanotechnology* **2005**, *5*, 776-780.

(51) Yu, S. H.; Shu, L.; Wu, Y. S.; Yang, J.; Xie, Y.; Qian, Y. T. *Journal of the American Ceramic Society* **1999**, *82*, 457-460.

(52) Baena, M. J.; Espinet, P.; Lequerica, M. C.; Levelut, A. M. *J. Am. Chem. Soc.* **1992**, *114*, 4182.

(53) Bensebaa, F.; Ellis, T. H.; Hruus, E.; Voicu, R.; Zhou, Y. *Langmuir* **1998**, *14*, 6579.

(54) Dance, I. G.; Fisher, K. J.; Herath Banda, R. M.; Scudder, M. L. *Inorg. Chem.* **1991**, *30*, 183.

(55) Shaw, R. A.; Woods, M. *J. Chem. Soc. A* **1971**, *10*, 1569.

(56) Tiers, G. V. D.; Brostrom, M. L. *J. Appl. Cryst.* **2000**, *33*, 915.

(57) Sandhyarani, N.; Predeep, T. *J. Mater. Chem.* **2001**, *11*, 1294.

(58) Gould, R. O.; Harding, M. M. *J. Chem. Soc. A* **1970**, 875.

(59) Ivanov, S. A.; Kozee, M. A.; Merrill, W. A.; Agarwal, S.; Dahl, L. F. *J. Chem. Soc. Dalton Trans.* **2002**, 4105.

(60) Kunchur, N. R. *Acta Crystallogr.* **1968**, *B24*, 1623.

(61) Woodward, P.; Dahl, L. F.; Abel, E. W.; Crosse, B. C. *J. Am. Chem. Soc.* **1965**, *87*, 5251.

(62) Mills, A.; Wang, J. *Journal of Photochemistry and Photobiology A: Chemistry* **1999**, *127*, 123-134.

(63) Chatterjee, D.; Mahata, A. *Journal of Photochemistry and Photobiology A: Chemistry* **2002**, *153*, 199-204.

(64) Zhao, J.; Wu, T.; Wu, K.; Oikawa, K.; Hidaka, H.; Serpone, N. *Environmental Science and Technology* **1998**, *32*, 2394-2400.

(65) Wu, T.; Liu, G.; Zhao, J.; Hidaka, H.; Serpone, N. *Journal of Physical Chemistry B* **1998**, *102*, 5845-5851.

CHAPTER 4 - Synthesis and Characterization of Cadmium Selenide Quantum Dots by Evaporation of Bulk Cadmium Selenide using the Solvated Metal Atom Dispersion Technique and Digestive Ripening

*This work has been published in *Chemistry of Materials* **2009**, *21*, 1248–1252.

4.1 Introduction

Semiconductor quantum dots of groups II - VI have been intensively studied due to their size-tunable optical properties and their applications, primarily involving CdSe NCs in photostable luminescent biomedical labeling,[1,2] solar cells,[3,4] and light emitting devices (LEDs).[5-7] Over the past few years, several synthetic routes have been established to synthesize CdSe NCs and one such synthetic route is the use of $(CH_3)_2Cd$ as a source of Cd , SeTOP as a source of Se, trioctylphosphine (TOP) and trioctylphosphine oxide (TOPO) as capping agents.[8] An alternate method was established by Peng et al., where they used CdO with hexylphosphonic acid or tetradecylphosphonic acids and SeTOP to synthesize high-quality CdSe NCs.[9] A single source precursor composed of both Cd and Se has also been employed for the synthesis of CdSe NCs.[10,11] Porous CdSe aerogels have also been synthesized,[12] where thiolated-capped CdSe nanoparticles were transformed into aerogels by CO_2 supercritical drying,[12,13]. In many of these procedures there is an effect of ligand choice, ligand amount, solvent chosen and temperature.[14,15] that allows the control of particle size and resultant optical properties. Besides TOP and TOPO, hexadecylamine (HDA) has also been used as a third coordinating ligand for surface passivation, and for aid in particle size adjustment. [16]

This chapter focuses on the synthesis of cadmium selenide quantum dots by evaporation of bulk CdSe using the solvated metal atom dispersion (SMAD) technique. For the very first time, a two-ligand strategy has been employed as coordinating ligands, which facilitated the "digestive ripening" of CdSe QDs in toluene (B.P 110 °C) and in *t*-butyltoluene (B.P 190 °C) solvent.

4.2 Experimental Section

4.2.1 Chemicals

Bulk Cadmium Selenide (99.9 %, Strem Chemicals Inc), Hexadecylamine (98%), Trioctylphosphine oxide (Reagent Plus 99%), and trioctylphosphine were purchased from Sigma-Aldrich and used without further purification. Toluene, tetrahydrofuran, acetone, and methanol were purchased from Fisher Scientific. Toluene and tetrahydro-furan solvents were distilled and degassed four times by the standard freeze-thaw procedure prior to use. T-butyl toluene was purchased from ACROS Organic chemicals and it was purged with argon for 2 hrs prior to use.

4.2.2 Preparation of CdSe – THF –TOP – HDA -Toluene as-prepared SMAD Colloid

A stationary reactor described in detail in ref.[17] was used for the synthesis of CdSe – THF – Toluene – TOP – HDA colloid. Typically, 0.3 g of bulk CdSe powder was evaporated using a C9 boron nitride crucible (R.D. Mathis # C9-BN) resting in a tungsten wire basket (R. D. Mathis # B8B # x. 030 w), which was in turn connected to water – cooled copper electrodes. CdSe is carcinogenic, while handling this chemical a

protective gloves are necessary. During the vaporization process, heat transfer from the hot crucible to the walls of the SMAD reactor was minimized by covering the crucible and the basket with a fibrous alumina ceramic insulator (Zircar product, Inc.). A solvent shower head was inserted into the reaction vessel for THF solvent vapor delivery. Coordination ligands (TOP and HDA in 60:40 molar ratios) were dissolved in 60 mL of toluene and were placed at the bottom of a 3 L reactor vessel along with a stirring bar. The above crucible connected to electrodes was then vacuum sealed within the reactor vessel using a vacuum line with a liquid nitrogen trap and diffusion pump. The reactor vessel was then surrounded by a liquid nitrogen Dewar and cooled to 77K. When the vacuum reached 4 X 10^{-3} torr, 50 mL of THF was initially condensed onto the reactor vessel, then the bulk CdSe was vaporized by gradually increasing the heating temperature approximately up to 900°C using the water-cooled electrodes.

During vaporization 50 mL of THF was allowed to co-condense with the evaporated CdSe. A total sum of 100 mL of THF was used for co-condensation. In this way the aggregation of evaporated CdSe was restricted. It took ~ 2 hrs for complete vaporization of CdSe. The frozen matrix had a deep brown color. The liq. N_2 Dewar was removed, and the matrix was warmed with a heat gun. Upon melting, the CdSe-THF matrix was allowed to mix with the coordination ligands in toluene by vigorous stirring for 45 min and the color became yellow-orange with a single phase. The as prepared SMAD product was then siphoned into a Schlenk tube under argon. *Caution:* While working with vacuum line, eye protection is necessary**.**

4.2.3 Preparation of CdSe– TOP – HDA – Toluene Colloid

The Schlenk tube containing the as-prepared SMAD product was connected to a vacuum and the THF was evaporated along with a small amount of toluene. The remaining product, now CdSe -TOP – HDA-Toluene colloid was deep yellow-orange in color.

4.2.4 Digestive Ripening

Digestive ripening [18] involves heating of the CdSe– TOP – HDA-Toluene solution under reflux at the boiling point of toluene (109°C) under argon. It is the key step for the formation of monodispersed and highly fluorescent QDs. Isolation of CdSe QDs was carried out by precipitation in anhydrous methanol, then washed with acetone and anhydrous methanol, this process was repeated three times to remove excess ligands, and then re-dispersion in toluene. No post-preparative size-selective precipitation process was carried out.

4.2.5 Preparation of CdSe – TOP – HDA – *t*- Butyltoluene (TBT) Colloid

In order to achieve a higher temperature for digestive ripening, instead of toluene, TBT was used while keeping all other parameters constant.

4.2.6 Yield Calculations

Based on a previous calculations on gold-dodecanthiol SMAD preparation system [19] (See reference 17 in that paper), the yield is about 78% based on CdSe.

Based on gold-dodecanthiol system, each QD have Cd_{3000}, Se_{3000}, $(TOP)_{325}$, and $(HDA)_{325}$. Based on this the empirical formula of QD is $(CdSe)(TOP)_{0.11}(HDA)_{0.11}$;

80% of CdSe (0.3g) weight is available during QD synthesis. So, CdSe used for QD is 0.24g.

Total number of CdSe molecules present in 0.24g = 0.24g X (6.023×10^{23} mol $^{-1}$) / (191.36 g mol^{-1}) = 7.554×10^{20}

Total number of TOP in the system = $7.554 \times 10^{20} \times 0.11 = 8.31 \times 10^{19}$

Total number of HDA in the system = $7.554 \times 10^{20} \times 0.11 = 8.31 \times 10^{19}$

Therefore, total number of ligands = 1.662×10^{20}

Converting the number of molecules into weight (grams), weight of CdSe = 0.24g

Weight of TOP = (8.31×10^{19}) X (370.65 g mol^{-1}) / (6.023×10^{23} mol^{-1}) = 0.0511 g

Weight of HDA = (8.31×10^{19}) X (241.46 g mol^{-1}) / (6.023×10^{23} mol^{-1}) = 0.0333g

Total weight of QDs (theoretical yield) = 0.24g + 0.0511 g + 0.0333 g = 0.3244 g

Experimental Yield = 0.2547 g

Percentage yield = (Experimental Yield) / (Theoretical Yield) X 100

= (0.2547g) / (0.3244g) X 100 = **78.5%**

4.3 Characterization

4.3.1 UV – Vis Spectroscopy

UV-Vis absorption spectra were obtained using an in situ UV-Vis optical fiber, assisted by a DH-2000 UV-Vis optical spectrophotometer instrument (Ocean Optics Inc).

4.3.2 Photoluminescence Spectroscopy

Fluorescence spectra were measured by using a Fluoro Max- 2 instrument from HORIBA Jobin Yvon Company. These samples were all excited at 400 nm. Photoluminescence quantum yields value (Φ_{em}) of CdSe were measured relative to Rhodamine 6G in methanol, assuming it's PL QYs as 95% by following the previous procedures[11,20] and were calculated by using equation 1.

$$\Phi_{em} = \Phi_S (I / I_S) (A_S / A) (n^2/n_S^2) \ldots\ldots\ldots\ldots\ldots\ldots \text{eq -1}$$

In equation 1, I (sample) and I_S (standard) are the integrated emission peak areas, up to 480 nm excitation. A (sample) and A_S (standard) are the absorption (<.1) at 480 nm; n (sample) and n_S (standard) are the refractive indices of the solvents; and the Φ_{em} and Φ_S are the PL QYs for the sample and the standard respectively.

4.3.3 Transmission Electron Microscopy

TEM studies were performed on a Philips CM100 operating at 100kV. The TEM samples were prepared by placing a few micro liters of precipitated, washed and re-dissolved sample in toluene onto a carbon-coated Formvar copper grid. The grids were allowed to dry under ambient conditions for 4-5 hrs.

4.3.4 Powder X-ray Diffraction (PXRD)

Powder X-ray diffraction patterns were recorded by a Bruker D8 X-ray diffractometer with CuKα radiation. PXRD samples were prepared by the evaporation of toluene from the CdSe/toluene dispersion loaded on XRD glass plates. The samples were scanned

from 20< 2θ < 80° at an increment of 0.02°/ min and the total acquisition time period was more than 2 hrs.

4.4 Results and Discussion

4.4.1 CdSe – TOPO - Toluene

Initial attempts to synthesize CdSe QDs by adopting our previous bulk material to ligand ratio (1:30),[19] were not satisfactory. A higher ligand ratio (1:40) produced particles in different shapes as shown in Figure 4.1(a-d), and this procedure lacked reproducibility. Such results were not uncommon especially when using TOPO.[21]

4.4.2 CdSe – TOP – HDA – Toluene

Hexadecyl amine as a coordination ligand in addition to TOP or TOPO worked best when the molar ratio was 60:40 for TOP: HDA. It is believed that HDA, being a weaker ligand than TOP/TOPO, helps in nanocrystal growth kinetics.[15,16] Figure 4.2A shows the UV-Vis absorption spectra of "as prepared CdSe– TOP – HDA – Toluene colloidal SMAD product", after 1 hr of reflux and 24 hrs of reflux in toluene and Figure 4.2B shows the corresponding emission data, all the samples being excited at 400 nm. . The as - prepared SMAD product is poly-dispersed in size and the narrow size distribution of these quantum confined particles was achieved by the digestive ripening. The as-prepared SMAD product has a broad fluorescence band, (Figure 4.2B (a)) but upon digestive ripening, the fluorescence narrowed significantly (Figure 4.2B (b, c)). The TEM (Figure 4.3 (a-c) images also support the formation of quasi monodispersed particles,

showing narrowing of the size distribution after digestive ripening, even after just one hour. The measured QY of these samples after reflux are 6 – 11%.

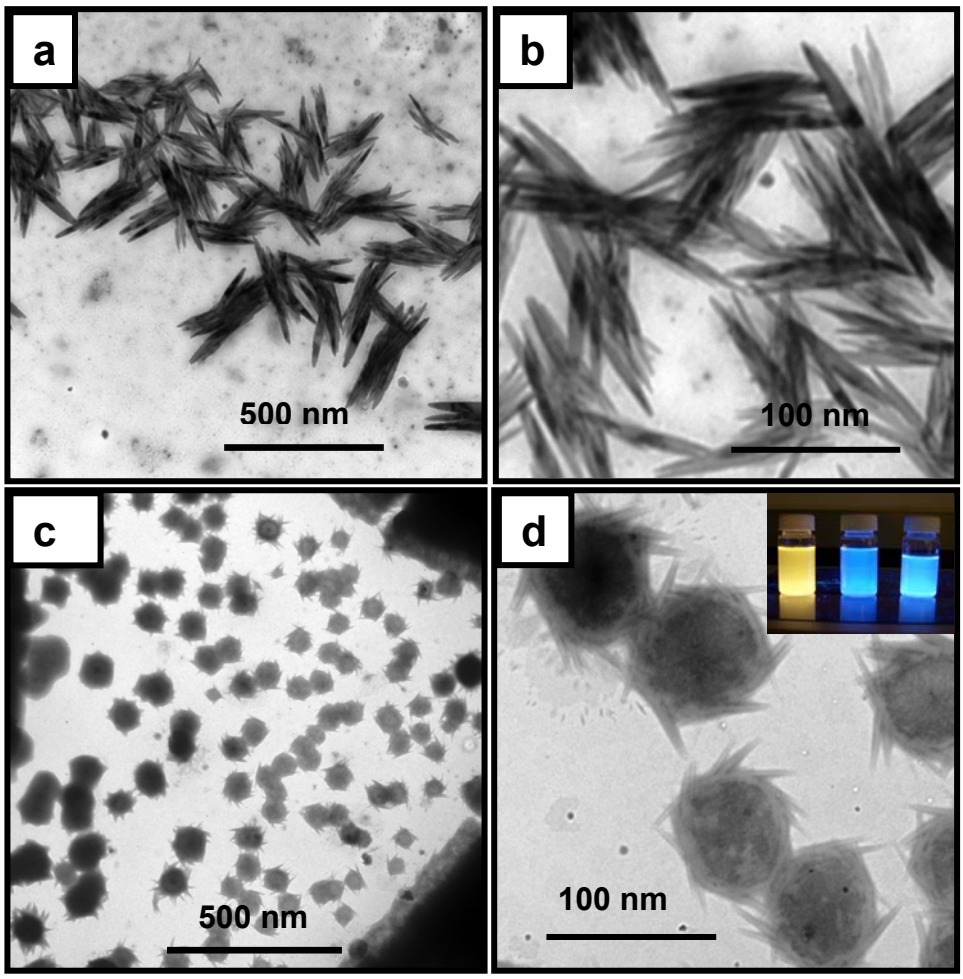

Figure 4.1(a-d) are the Transmission Electron Microscopy images of two different batches of CdSe QDs stabilized with TOPO in 1:40 ratio and insert picture shows the corresponding samples under UV-Vis illuminator. Large crystals are TOPO crystals and CdSe QDs can be seen as small dots in background.

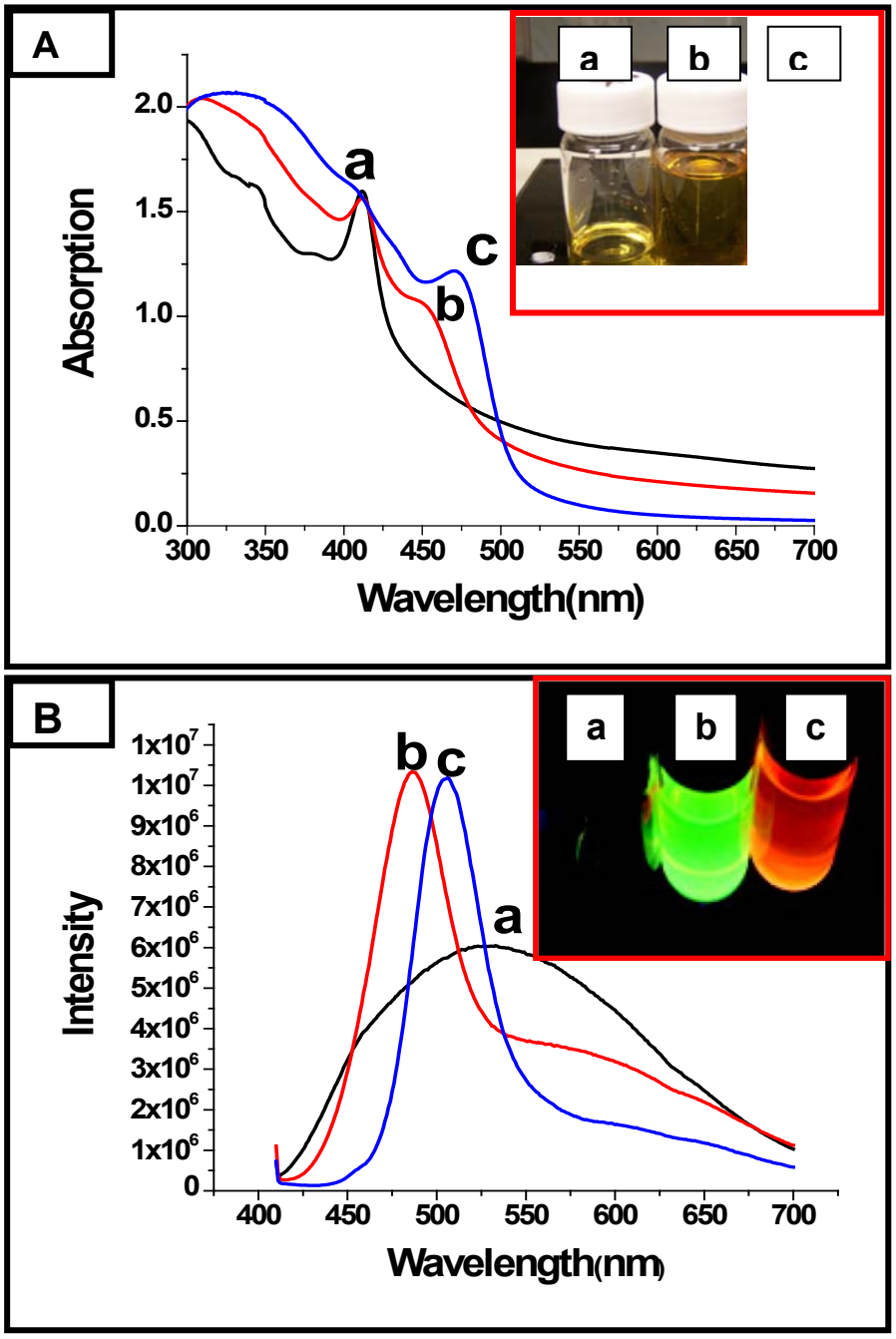

Figure 4.2(A) UV-Vis absorption spectra of CdSe with TOP and HDA in 60: 40 ratio (a) as prepared SMAD product, (b) after 1 hr of reflux and (c) after 24 hr of reflux in toluene and (B) shows the corresponding photoluminescence spectra. Insert are the corresponding samples without and with UV-Vis illuminator.

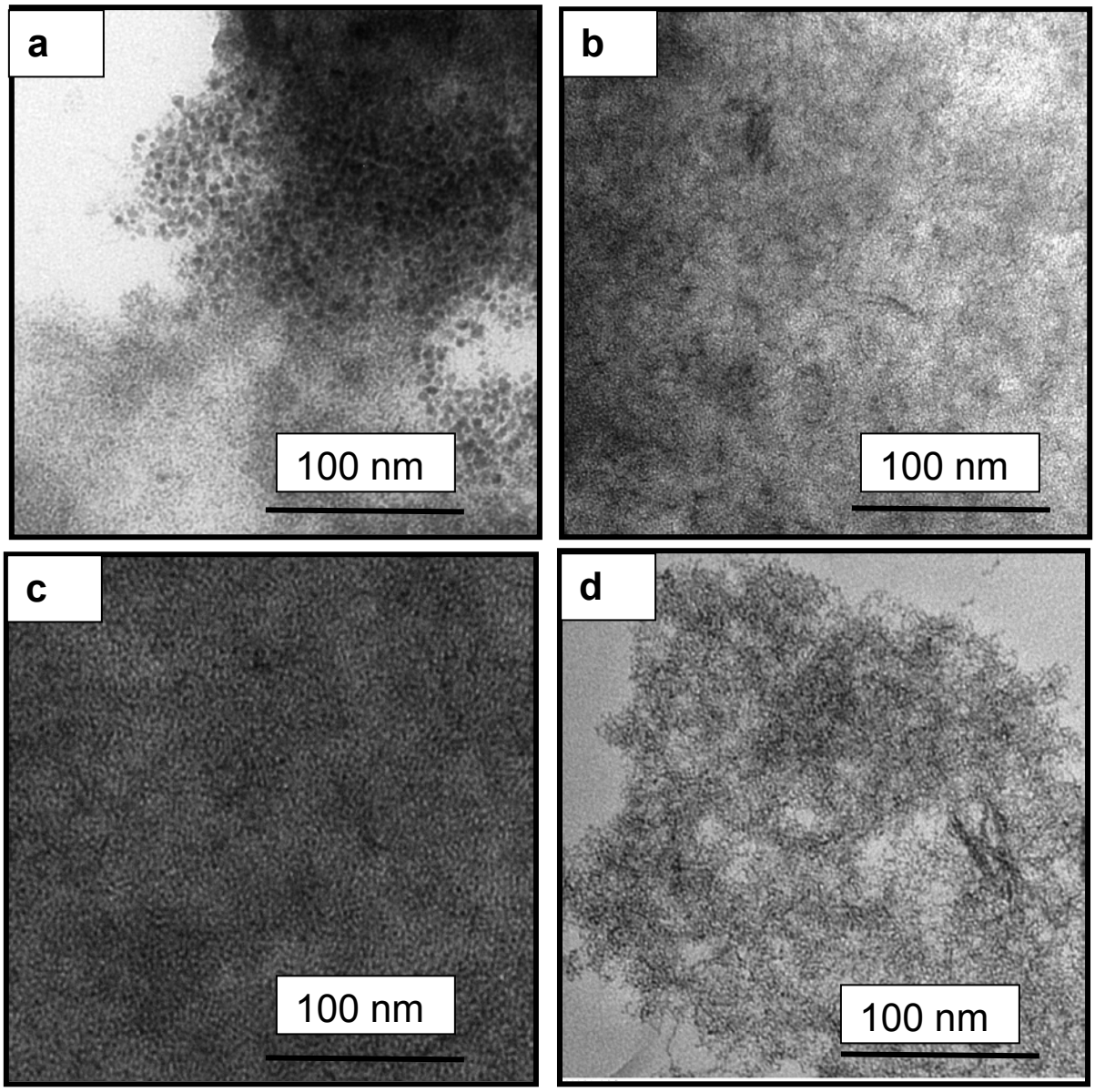

Figure 4.3 Transmission Electron Microscopy images of Cadmium Selenide stabilized with trioctylphosphine and hexadecyl amine (a) before reflux, (b) after 1 hr of reflux, (c) after 16 hr of reflux in toluene, and (d) after 24 hrs of reflux in toluene.

4.4.3 CdSe – TOP – HDA – *t* – Butyl toluene

In toluene (b.p 109°C), only smaller size particles were synthesized. A possible explanation for the smaller size of CdSe QDs in toluene is, when the boiling point is lower (109°C), lower kinetic motion for CdSe QDs and hence fewer collisions, thus slower particle size adjustment. So, we used TBT (b. p 190°C) to achieve higher temperature for reflux. Figure 4.4 (A) shows the UV-Vis and Figure 4.4 (B) shows the fluorescence spectra of the sample heated at 120°C for 6 hrs, heated at 150°C for 6hrs and after 6 hrs of reflux at 190°C in TBT. The measured QY of these samples are 16-28%. The increased QY can be attributed to the larger; more monodisperse particles with fever defects and surface traps than in smaller particles**.** The broad band from 650 nm to 700 nm in Figure 4.4 (B) might be due to the loss of some of the surface ligands during the washing process.[22] The TEM images (Figure 4. 5 (a- d)) shows narrowing of the particles size distribution after 16 hrs of reflux in TBT at 190°C. It took 16 hr to see a considerable increase in fluorescence intensity and to form quasi monodispersed QDs in toluene; in TBT it took 6 hrs. UV-Vis and PL spectral data in Table 4.1 show a red shift in absorption as well as in emission with raise in temperature.

6hrs of heating and reflux in TBT	UV-Vi absorption wavelength (λ max)	Emission spectra
Before reflux	410 nm	Broad band
120°C	446 nm	528 nm
150°C	488 nm	536 nm
After reflux at 190°C	518 nm	552 nm

Table 2 Comparison of UV-Vis absorption and emission spectra of CdSe with TOP and HDA in 60: 40 ratio at various temperatures in *t*-butyl toluene solvent.

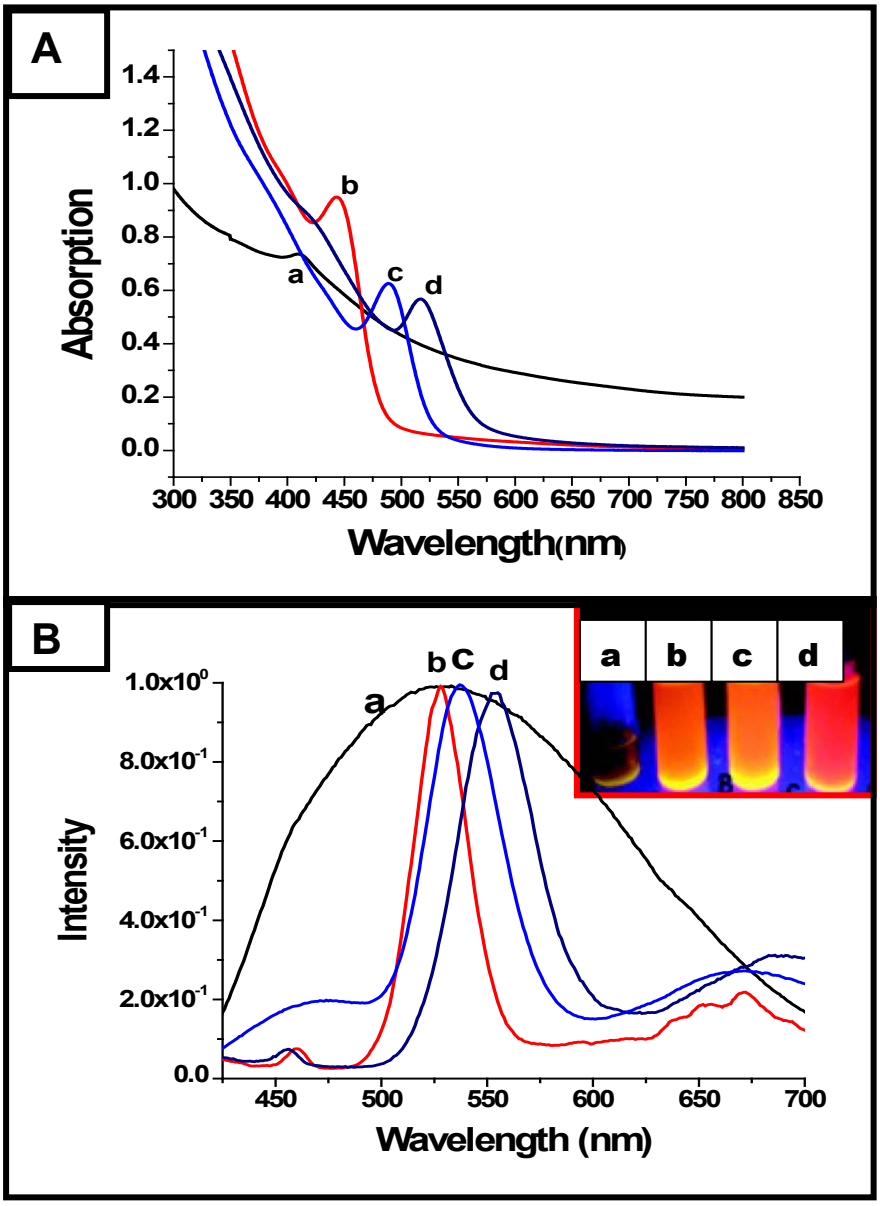

Figure 4.4(A) UV-Vis absorption spectra of CdSe with TOP and HDA in 60: 40 ratio (a) as prepared SMAD product, (b) after 6 hrs at 120°C, (c) after 6 hrs at 150°C and (d) after 6 hr of reflux at 190°C in TBT. (B) Corresponding photoluminescence spectra. Insert are the corresponding samples upon UV-Vis illumination.

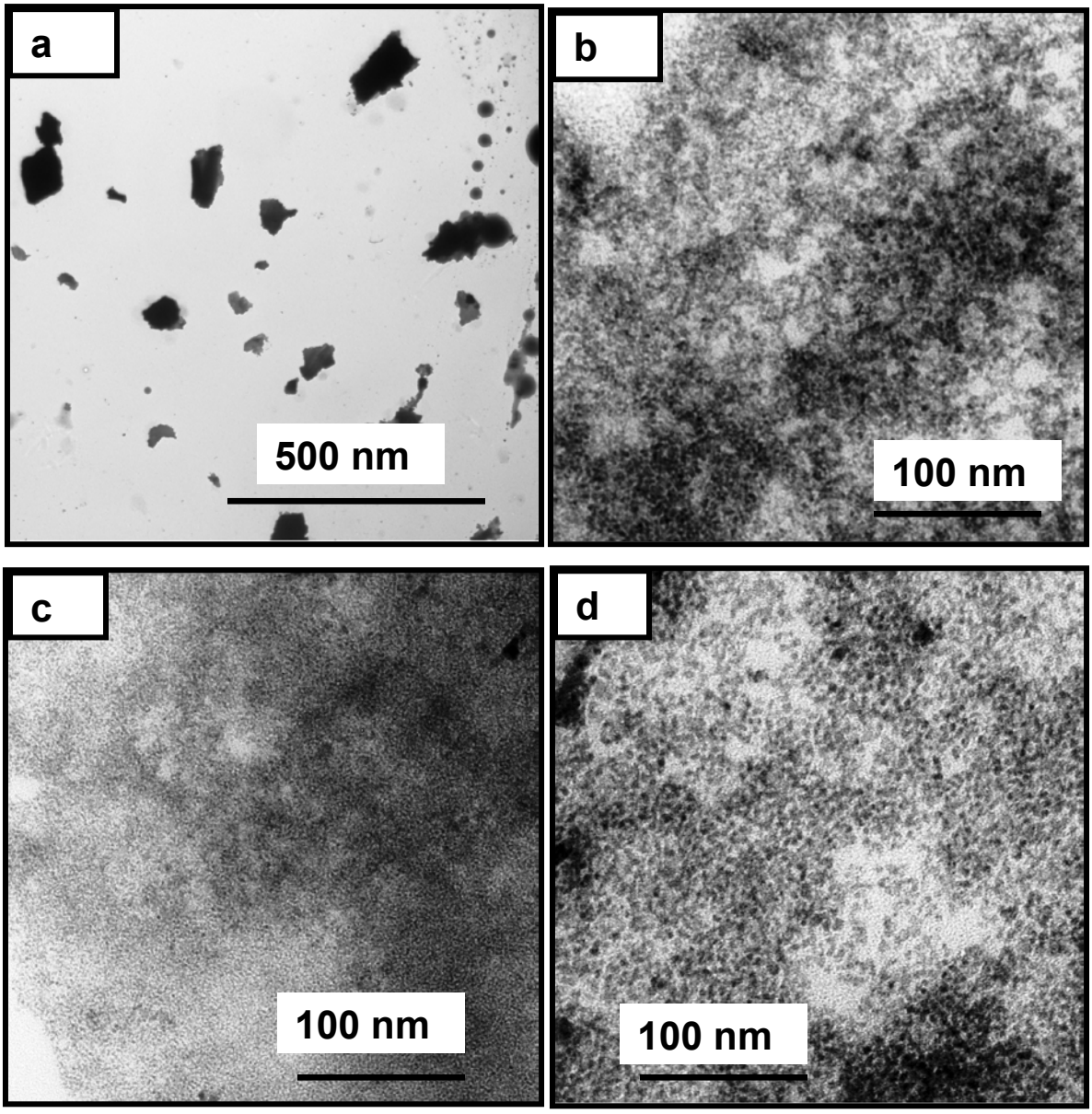

Figure 4.5 Transmission Electron Microscopy images of (a) as prepared SMAD product of CdSe with TOP and HDA in 60: 40, (b) after 6 hrs at 120°C, (c) after 6 hrs at 150°C and (d) after 6 hr of reflux at 190°C in TBT

The powder XRD data (Figure 4.6) revealed the wurtzite structure of CdSe QDs, the same as the bulk material. The transformations from narrow peaks (bulk) to broad peaks are indicative of smaller crystallite. Powder XRD data are consistent with the published PXRD data.[23]

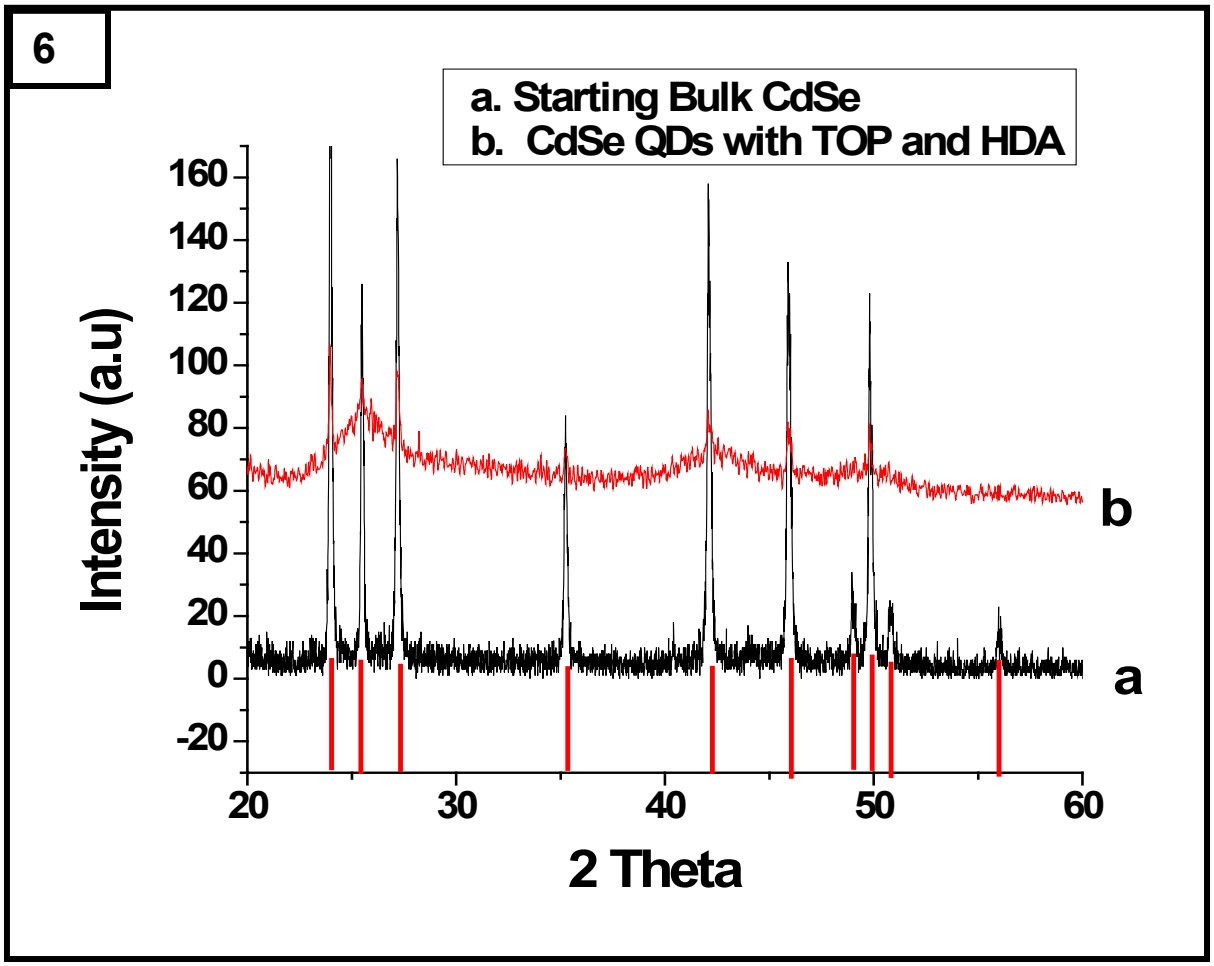

Figure 4.6 Powder XRD patterns of (a) starting bulk CdSe and (b) CdSe QDs with TOP and HDA after 6 hrs of reflux at 190°C in *t*- butyltoluene. Wurtzite lines are shown from reference 26

4.5 Summary

Firstly, the polydispersed CdSe QDs were synthesized by using the SMAD technique that involved the vaporization of the bulk CdSe followed by co-condensation with THF solvent at Liq. N_2 temperature. Secondly, quasi monodispersed CdSe QDs were obtained after subjecting the SMAD prepared polydispersed CdSe QDs to digestive ripening as a successful post-synthesis treatment.[24] The XRD data revealed that these CdSe QDs have the wurtzite structure of bulk CdSe. Moreover, we observed very significant effects of the solvents (Toluene and TBT) and mixed ligands system (TOP and HDA) on the narrowing of the particles size distribution, UV-Vis, Photoluminescence properties and QY of CdSe QDs. We found TBT as a more preferable solvent for the synthesis of monodispersed CdSe QDs in a shorter digestive ripening time (6 hrs), compared with toluene (24 hrs). This is likely due to the higher boiling point of TBT that makes digestive ripening more effective. Likewise, we observed better fluorescence properties of CdSe QDs with an appropriate combination of TOP and HDA ligands. Samples prepared by using TOPO as a protecting ligand in 1: 40 ratio yield particles with different morphology and unfortunately these results were not reproducible.

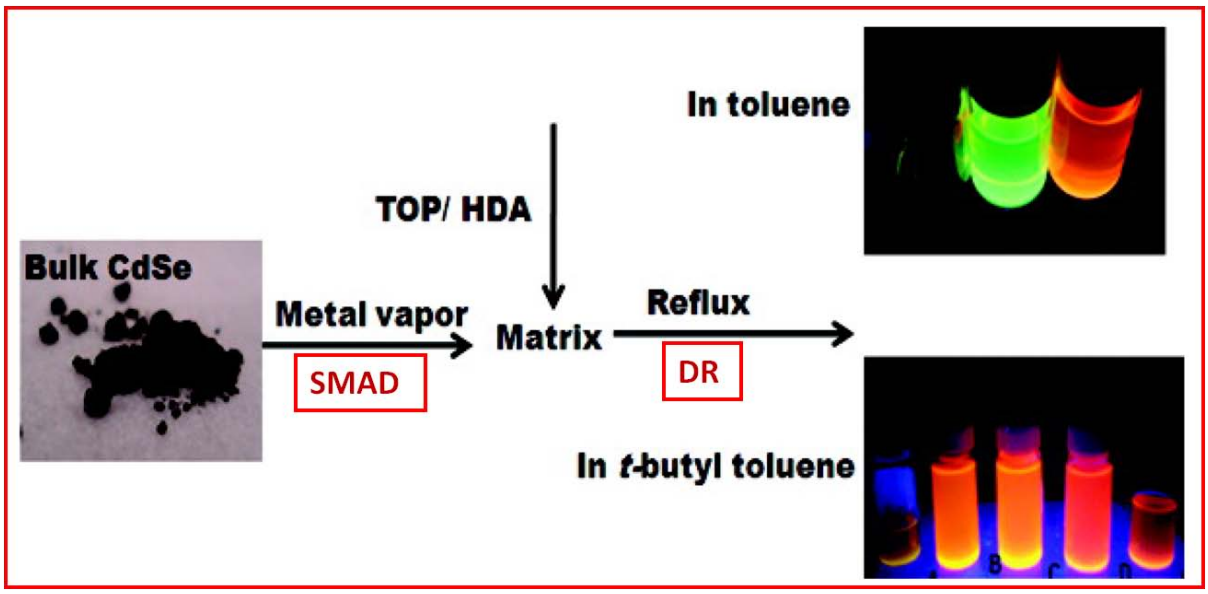

Figure 4.7 Schematic Representation of Overall Synthesis Procedure

4.6 References

(1) Bruchez, M.; Moronne, M.; Gin, P.; Weiss, S.; Alivisatos, A. P. *Science* **1998**, *281*, 2013.

(2) Dubertret, B.; Skourides, P.; Norris, D. J.; Noireaux, V.; Brivanlou, A. H.; Libchaber, A. *Science* **2002**, *298*, 2759.

(3) Huynh, W. U.; Peng, X. G.; Alivisatos, A. P. *Adv. Mater.* **1999**, *11*, 923.

(4) Huynh, W. U.; Dittmer, J. J.; Alivisatos, A. P. *Science* **2002**, *295*, 2425.

(5) Zhao, J.; Bardecker, J. A.; Munro, A. M.; Liu, M. S.; Niu, Y.; Ding, I. K.; Luo, J.; Chen, B.; Jen, A. K. Y.; Ginger, D. S. *Nano Lett.* **2006**, *6*, 463.

(6) Caruge, J. M.; Halpert, J. E.; Bawendi, M. G. *Nano Lett.* **2006**, *6*, 2991.

(7) Achermann, M.; Petruska, M. A.; Koleske, D. D.; Crawford, M. H.; Klimov, V. I. *Nano Lett.* **2006**, *6*,1396.

(8) Murray, C. B.; Norris, D. J.; Bawendi, M. G. *J. Am. Chem. Soc.* **1993**, *115*, 8706.

(9) Peng, Z. A.; Peng, X. *J. Am. Chem. Soc.* **2001**, *123*, 183.

(10) Malik, M. A.; Revaprasadu, N.; Oâ€™Brien, P. *Chem. Mater.* **2001**, *13*, 913.

(11) Cumberland, S. L.; Hanif, K. M.; Javier, A.; Khitrov, G. A.; Strouse, G. F.; Woessner, S. M.; Yung, C. S. *Chem. Mater.* **2002**, *14*, 1576.

(12) Indika, A. U.; Brock, S. L. *J. Am. Chem. Soc.* **2007**, *129*, 1840.

(13) Indika, A. U.; Brock, S. L. *J. Am. Chem. Soc.* **2006**, *128*, 7964.

(14) Kui, Y.; Shanthi, S.; Natasha, P.; Virginia, C. *Langmuir* **2004**, *20*, 11161.

(15) Sung, Y. M.; Park, K. S.; Lee, Y. J. *J. Phys. Chem. C* **2007**, *111*, 1239.

(16) Talapin, D. V.; Rogach, A. L.; Kornowski, A.; Haase, M.; Weller, H. *Nano Lett.* **2001**, *1*, 207.

(17) Klabunde, K. J.; Timms, P. L.; Skell, P. S.; Ittel, S. *Inorg. Synth.* **1979**, *19*, 59.

(18) Lin, X. M.; Sorensen, C. M.; Klabunde, K. J. *J. Nano Research* **2000**, *2*, 157.

(19) Stoeva, S.; Klabunde, K. J.; Sorensen, C. M.; Dragieva, I. *J. Am. Chem. Soc.* **2002**, *124*, 2305.

(20) Zhu, C. Q.; Peng, W.; Xin, W.; Li, Y. *Nanoscale Res. Lett.* **2008**, *3*, 213.

(21) Wang, F.; Tang, R.; Buhro, W. E. *Nano Lett.* **2008**, *8*, 3521.

(22) Kalyuzhny, G.; Murray, R. W. *J. Phys. Chem. B.* **2005**, *109*, 7012.

(23) Wang, Q.; Seo, D. K. *J. Chem. Mater.* **2006**, *18*, 5764.

(24) Klabunde, K. J.; Sorensen, C. M.; Stoeva, S. I.; Prasad, B. L. V.; Smetana, A. B.; Lin, X. M.; Corrain, C.; Schmid, G.; Toshima, N. *Metal Clusters in Catalysis and Materials Science: The Issue of Size Control, Part II Methodologies*, 2008.

CHAPTER 5 - Improvised Synthesis of CdSe and CdTe Quantum Dots by Evaporation/ Condensation SMAD Technique: Refined Digestive Ripening

5.1 Introduction

The solvated metal atom dispersion (SMAD) technique allows the synthesis of nanomaterial from the bulk material by vaporization and co-condensation.[1-7] The as-prepared polydispersed SMAD colloid products were made monodispersed in size by a unique process known as digestive ripening.[8] Digestive ripening involves the heating of polydispersed colloidal material at the boiling point (BP) of solvent in the presence of excess surface active ligand. [1-9] In the present work; we employed trioctylphosphine oxide (TOPO) and oleylamine (OA), which served both as capping agent as well as digestive ripening solvent. The general procedure for the synthesis of high quality crystalline II-VI semiconductor material is by the hot injection method, where cadmium precursor $(CH_3)_2Cd$ or CdO is dissolved in coordination ligands like trioctylphosphine oxide, hexylphosphonic acid or tetradecylphosphonic acids, and then the selenium precursor (Se dissolved in TOP) was quickly injected into the hot coordination reaction mixture, which initiated the nucleation process, and subsequent growth was carried out at a relatively lower temperature and this process was initially reported by Murray et al, and [10] later, Peng et al and Talapin et al have developed the hot injection procedure.[11-16]

One of the advancements in this process was selecting an injection temperature and a growth temperature. This high reaction temperature (>150 - 350°C) facilitates the

removal of crystalline defects and allows enhancement in the photoluminescence. In semiconductor QDs, high emission efficiency from band-edge state is required especially when these are used in laser or imaging. In general, a high band gap inorganic material coating over the QD core has been proven to enhance the QY by passivating surface nonradiative recombination sites. Typically, II-VI semiconductor QDs are covered with a high band gap ZnS shell, which was initially developed by Hines and Guyot-Sionnest.[17] These two methods (hot injection and ZnS shell covering) have been widely used to achieve narrow size particle distribution and enhance QY. In addition to the above method, other routes like layer by layer ZnS passivation,[18] CO_2 gas expanded liquids, [19]surface treatments with polymers,[20] and sonochemical process [21] were used. In current work we adopted the sonochemical procedure for the growth of ZnS shell over CdSe and CdTe QD core.

5.1.1 Advantages

The outcomes of the digestive ripening process we have developed for semiconductors are : (1) the reduction of particle growth time period (digestive ripening time) by employing ligands (Trioctylphosphine oxide (TOPO) and oleylamine (OA)) as capping agent as well as digestive ripening solvent, (2) ability to tune the photoluminescence (PL) from 410 nm to 670 nm, (3) demonstrate the versatility of the SMAD synthesis technique for other semiconductors (CdTe), (4) direct comparison of CdSe QDs growth with CdTe QDs growth based on digestive ripening time , and (5) enhanced PL quantum yield (QY) of CdSe QDs and CdTe QDs upon ZnS shell. Also the merit of this synthesis is the use of bulk CdSe and CdTe as the starting material, which avoids

usage of toxic organometallic compounds, eliminates the hot injection procedure, size selective precipitation process, and makes scale-up to large amount of material quite feasible.

5.2 Experimental Section

5.2.1 Chemicals

Bulk Cadmium Selenide(CdSe) and bulk Cadmium Telluride (CdTe) (99.9 %, Strem Chemicals Inc), Oleylamine (98%) from ACROS Organic chemicals, Trioctyl phosphine oxide (TOPO) (Reagent Plus 99%), trioctyl phosphine (TOP), tributyl phosphine (PBu_3), Zinc nitrate hexahydrate, and potassium ethylxanthate were purchased from Sigma-Aldrich and used without further purification. Tetrahydrofuran (THF), acetone, and methanol were purchased from Fisher Scientific. Tetrahydrofuran solvents were distilled and degassed four times by the standard freeze-thaw procedure prior to use. Oleyl amine was purged with argon for 2 hrs prior to use.

5.2.2 Synthesis of as-prepared SMAD Colloid

As described in reference([22]) a stationary reactor was used for the evaporation and co-condensation of bulk CdSe or CdTe. Briefly, 1g of either bulk CdSe or bulk CdTe was evaporated using water cooled copper electrodes and the generated heat during the evaporation was passivated by water cooled copper electrodes and insulating packing material (Zircar product, Inc.) around the crucible and metal basket. The optimum temperature required for the evaporation of bulk CdSe is ~ 900°C, whereas, for bulk CdTe it is less than 900°C. Initially the bulk material was charged in C9 boron nitride

crucible (R.D. Mathis # C9-BN) resting in a metal basket (R. D. Mathis # B8B # x.030 w) and the ligands were placed at the bottom of the SMAD reactor and the entire setup was then vacuum sealed. After complete evacuation, a liquid N_2 Dewar was placed around the sealed SMAD reactor. Once the vacuum attains 4 X 10^{-3} torr, initially 50 mL of distilled and degassed THF was evaporated through a solvent shower head, which was inserted into the reactor. The evaporated solvent was condensed on the wall of SMAD reactor by external liquid nitrogen cooling. After the formation of condensed solvent matrix on the walls, the metal crucible was heated by water cooled copper electrode and the heat was ramped slowly and the evaporated material was co-condensed along with the solvent on to the walls of reactor, co-condensation of evaporate material along with the solvent restricts aggregation and allows formation of small crystallites. It took nearly 3 hrs for the complete evaporation of 1g of bulk material. The frozen matrix appears like a reddish brown (Figure 5.1). Upon warming up of the frozen matrix with a heat gun, the matrix melts and slowly reaches to the bottom of the reactor and mixes well with the coordinating ligands (TOPO with OA). To ensure homogeneous colloid formation the system was vigorously stirred for 45 minutes with a magnetic stirrer. Figure 5.1(a) shows the as-prepared CdSe-THF-TOPO-OA colloidal solution after vigorous stirring. The as-prepared SMAD product was then siphoned into a Schlenk glass tube under the protection of argon (Figure5.1 (b)). *Safety and cleanliness:* Prior to synthesis the SMAD reactor was cleaned with aqua regia, base bath, acid bath and finally with copious amount of water. While working with vacuum lines it's a must to wear protective eye glasses. Both CdSe and CdTe are carcinogenic so, proper protection is necessary while handing these chemicals. Also, the acid and

base bath used in cleaning may cause severe burns, so proper acid proof gloves and protecting clothing are necessary.

5.2.3 Preparation of CdSe-TOPO-OA colloid

The THF from the as- prepared CdSe-THF-TOPO-OA colloidal solution was vacuum evaporated, leaving a THF solvent free semisolid CdSe-TOPO-OA colloid (Figure 5.1(c)). Upon gentle warming, CdSe –TOPO-OA colloid was obtained (Figure5. 1(d)). This as-prepared product was then subjected to digestive ripening. The same procedure was adopted for the synthesis of the as-prepared CdTe-TOPO-OA system.

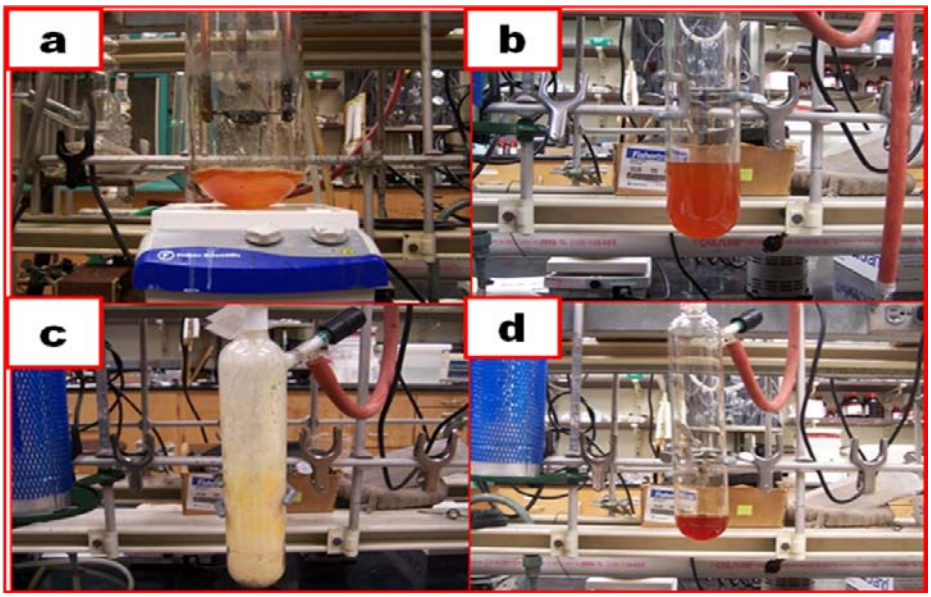

Figure 5.1(a) as-prepared SMAD CdSe-THF-TOPO-OA colloidal solution after vigorous stirring for a period of 45 minutes (b) as-prepared siphoned CdSe-THF-TOPO-OA colloidal solution (c) Semi-solid CdSe –TOPO-OA after complete vacuum evaporation of THF solvent (d) CdSe –TOPO-OA colloid after gentle warming.

5.2.4 Refined Digestive Ripening

Digestive ripening is the key step for the formation of quasi monodispersed core QDs. In previous work we used toluene and t-butyl toluene as a digestive ripening solvent for CdSe-TOPO-HDA system. However, for the current work TOPO and OA were used as digestive ripening solvent, as well as capping ligands.

5.2.5 ZnS Shell Formation on Core Quantum Dots

ZnS shell formation over a core QD (CdSe or CdTe) was carried out by a reported sonochemical procedure using zinc ethylxanthate as precursor.[21,23] In a typical ZnS shell growth, aliquots (5 mL) of freshly synthesized core QDs were placed in a reaction vessel and the reaction vessel was then placed in 100 W sonicator (Fisher Scientifics), to which freshly prepared zinc ethylxanthate (0.15 g) in tributylphosphine (3 mL) (PBu_3) solution was mixed when the sonication temperature was 60°C. The sonication was continued until the temperature of the reaction mixture reached 120°C to ensure complete passivation of the QD core with the ZnS shell. During this process aliquots of reaction mixture were collected to monitor the shell growth, and no purification steps were involved on the core solution before use. Isolation of core-shell QDs was carried out by precipitation with anhydrous methanol, followed by washing with acetone and methanol. This process was repeated to remove any un-reacted zinc ethylxanthate and excess ligands. The core-shell QDs were then vacuum dried and re-dispersed in toluene for transmission electron microscope (TEM) sample preparation. No size selective precipitation step was carried out. The yield of core QDs is about ~78-80 %.

5.3 Characterization

5.3.1 UV – Vis Spectroscopy

UV-vis absorption spectra were obtained using an in situ UV-vis optical fiber, assisted by a DH-2000 UV-vis optical spectrophotometer instrument (Ocean Optics Inc) for core QDs. The absorption spectra of core-shell QDs were obtained using a Cary 500 Scan UV–vis–NIR spectrophotometer. All samples were washed with absolute ethanol, acetone, and were dried under vacuum. The dried samples were then re-dissolved in toluene for analysis.

5.3.2 Photoluminescence Spectroscopy

Fluorescence spectra of both core QDs (CdSe and CdTe) and core-shell QDs (CdSe-ZnS and CdTe-ZnS) were measured by using a Fluoro Max- 2 instrument from HORIBA Jobin Yvon Company. These samples were all excited at 400 nm. Photoluminescence quantum yields (Q.Y) value (Φ_{em}) of QDs (CdSe and CdTe) and core-shell QDs (CdSe-ZnS and CdTe-ZnS) were measured relative to Rhodamine 6G in methanol, assuming it's PL QYs as 95% [24,25] and the % yield were calculated by using equation 1.

$$\Phi_{em} = \Phi_S (I / I_S) (A_S / A) (n^2/n_S^2) \text{.....eq -1}$$

In equation 1, I (sample) and I_S (standard) are the integrated emission peak areas, up to 480 nm excitation. A (sample) and A_S (standard) are the absorption (<.1) at 480 nm; n (sample) and n_S (standard) are the refractive indices of the solvents; and the Φ_{em} and Φ_S are the PL QYs for the sample and the standard respectively.

5.3.3 Transmission Electron Microscopy (TEM)

TEM studies were performed on a Philips CM100 operating at 100kV. The TEM samples were prepared by placing a few micro liters of precipitated, washed, vacuum dried and re-dissolved sample in toluene onto a carbon-coated Formvar copper grid and the grids were allowed to dry overnight.

5.3.4 High Resolution Transmission Electron Microscopy / Energy Dispersive X- Ray Spectroscopy

High resolutions images were performed with FEI Tecnai F20 XT Field Emission Transmission Electron Microscopy operated at 300 kV. The Energy Dispersion X-ray (EDX) analysis was carried on scanning electron microscope (SEM) mode, which is an integral part of FEI Tecnai F20 XT. The experimental conditions are as follow: Energy Resolution: 134 eV, Reference Energy: 5.9 keV, Minimum Energy: 100 eV. Detector Thickness: 3 mm, Detector Distance: 11.8 mm, Detector Angle: 14.6 deg. The facilities were provided by the Microscopy and Analytical Imaging Laboratory at University of Kansas. Washing procedure was same as described above. However, a Lacey carbon coated TEM grid was used.

5.3.5 Powder X-ray diffraction (PXRD)

Powder X-ray diffraction patterns were recorded by a Bruker D8 X-ray diffractometer with CuKα radiation. PXRD samples were prepared by the evaporation of toluene from the core or core-shell QDs /toluene dispersion loaded on XRD glass plates. The

samples were scanned from 20< 2θ < 80° at an increment of 0.01°/ min and the total acquisition time period was more than 7 hrs.

5.3.6 X-ray photoelectron spectroscopy

X-ray photoelectron spectroscopy is a powerful analytical tool, which determines the chemical composition of a surface. The chemical analysis is done by irradiating a sample with soft x-rays to ionize atoms and releasing core-level photoelectrons. The kinetic energy of the escaping are collected and analyzed by the instrument to produce a spectrum of emission intensity versus electron binding energy. Since each element has a unique set of binding energies, XPS can be used to identify the elements on the surface. Also, peak areas at nominal binding energies can be used to quantify concentration of the elements. Small shifts in these binding energies (chemical shifts) provide powerful information about sample chemical states and short-range chemistry. XPS is suitable for the analysis of both conductors and insulators.

XPS data were collected on a Kratos Axis 165 x-ray photoelectron spectrometer operating in the hybrid mode using Al Kα (1486.6 eV) radiation at 300 W. Charge neutralization was used to minimize sample charging, and the charge neutralizer settings were 2.0 amps, 1.7 V charge balance, 1.1 V bias. Survey spectra were collected with a pass energy of 160 eV, while high resolution spectra were collected with a pass energy of 20 eV. Peak fitting was performed using CASA XPS software, using peaks with a 50% Gaussian, and 50% Lorentzian line shape on a Shirley background. The facilities were provided by the Shared Experimental Facilities (SEF) at University of Maryland.

5.4 Results and Discussion

5.4.1 Cadmium Selenide – Oleyl Amine – Trioctyl Phosphine Oxide

The as-prepared SMAD product generally yields polydispersed colloid material due to little control over the particle size during vaporization and co-condensation. In previous work, the synthesized fluorescent CdSe QD from bulk by vaporization / co-condensation, followed by digestive ripening in toluene or in *t*-butyl toluene, yield particles which emits either green or yellow orange fluorescence in the wavelength ranging from 410 nm to 550 nm, and it took nearly 24 hr of digestive ripening time in toluene and 16 hrs of digestive ripening time in *t*-butyl toluene. In the current, refined digestive ripening we used TOPO and OA in 30:20 ratio to the bulk starting material and these ligands act as both digestive ripening solvent as well as capping agent. The as-prepared CdSe-TOPO-OA-THF (Figure5.1 (a)) colloid material is a homogeneous single phase. In order to obtain CdSe-TOPO-OA colloid, the THF solvent was vacuum evaporated resulting a semi-solid CdSe-TOPO-OA (Figure 5.1(b)) and the semi-solid nature of the CdSe-TOPO-OA can be explained by the fact that TOPO exists as a solid at room temperature, whereas OA is liquid. The yield of CdSe QD is nearly ~80% with variations in batch to batch synthesis and the 20% loss was due to either condensation of vaporized material onto copper electrodes, or possibly to losses in handling. In previous work, we used TOPO and HDA as coordinating ligands, where as in current work we replace HDA with OA. Compared to TOPO, OA is a weaker ligand and binds less strongly to the CdSe, and thereby affects the growth process. [25,26] In this work we also employed OA as a solvent, as others have done.[15,27] In the present work, the as-

prepared CdSe exhibited a broad fluorescence, but within 90 minutes of digestive ripening, the PL becomes sharper and can be tuned to 670 nm. The reduction of digestive ripening time is attributed to the higher boiling point of these ligands /Solvents. The poor-fluorescence behavior of the as-prepared CdSe is due to aggregation of small crystallites, which is evident from the TEM image (Figure 5.3(a)).

During digestive ripening these aggregates of small crystallites (Figure 5.3(a)), breakdown or dissolve completely to form small particles (Figure 5.3(b)) and grow into quasi monodispersed particles (Figure 5.3 (b- d) and Figure 5.4 (e-f)). It is important to note that in digestive ripening bigger particles will break down into smaller particles and the smaller particles will tend to grow bigger and finally the system will reach a thermodynamic equilibrium size, and the PL data of CdSe can be correlated with the digestive ripening phenomenon. Figure 5.4 (g) are the samples of CdSe collected at various times with progress of digestive ripening and then exposed to UV-Vis.

Table 5.1 tabulates the UV-Vis, PL of CdSe and particle mean size with respect to digestive ripening time. The UV-Vis spectra are broad, but show small absorption features that slowly shifts to longer wavelength. The PL peaks sharpen and also shifts to longer wavelength with time (Figure 5.2 (a-f) and Table 5.1).

Digestive Ripening Time (Min)	10	20	30	40	50	60	70	80	90
UV-vis absorption wavelength λ max (nm)	487	495	507	515	531	549	576	591	651
PL wavelength λ max (nm)	539	542	551	557	566	572	586	600	667
Particle mean size (nm)	2.4	2.6	2.8	3.0	3.4	3.6	4.0	5.0	7.3

Table 3 Change in the wavelength of UV-Vis, photoluminescence and particle size of CdSe QDs with digestive ripening time

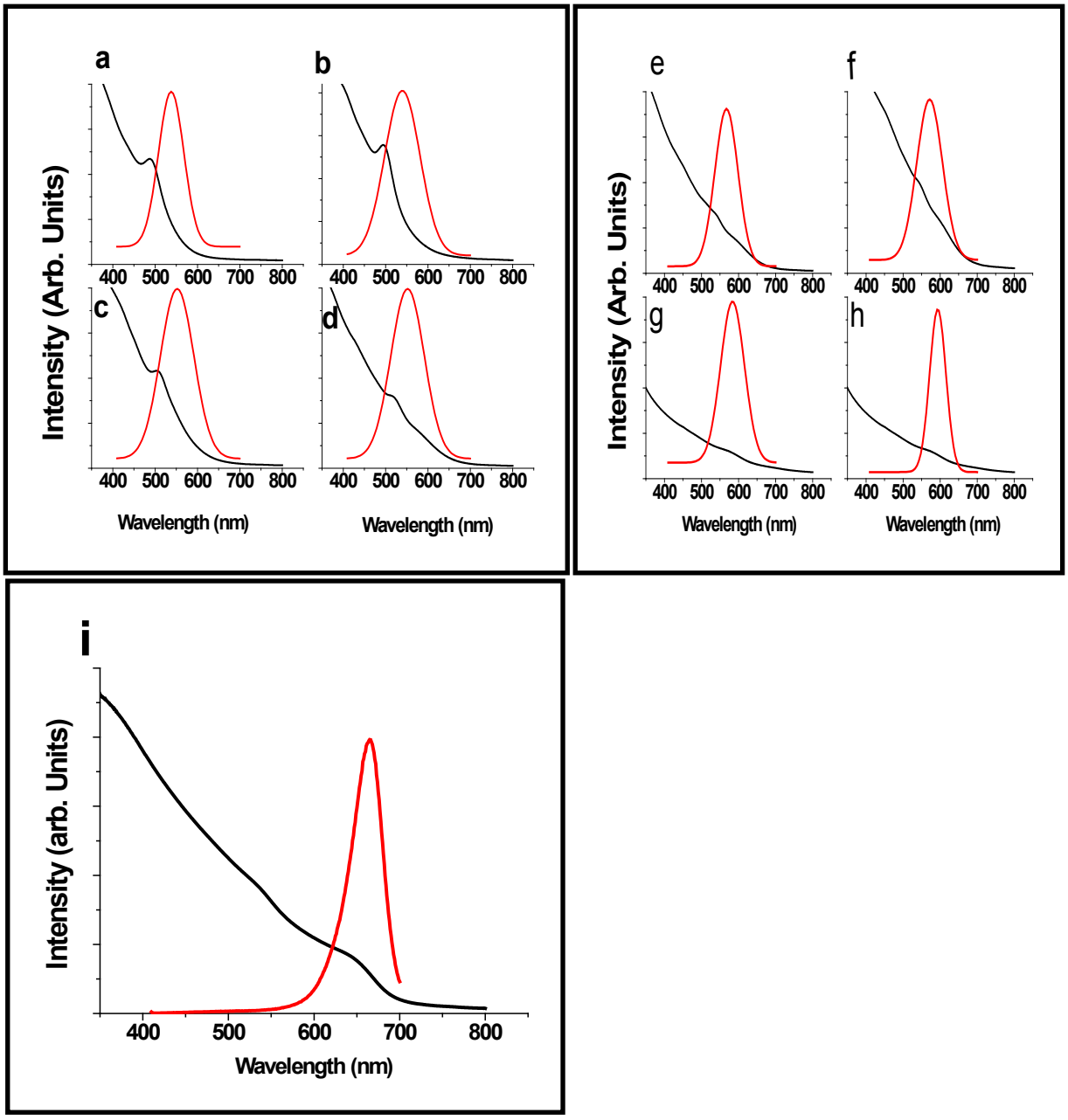

Figure 5.2(a- i) UV-Vis absorption spectrum and corresponding PL of CdSe QD samples collected at 10, 20, 30, 40, 50, 60, 70, 80 and 90 minutes of digestive ripening.

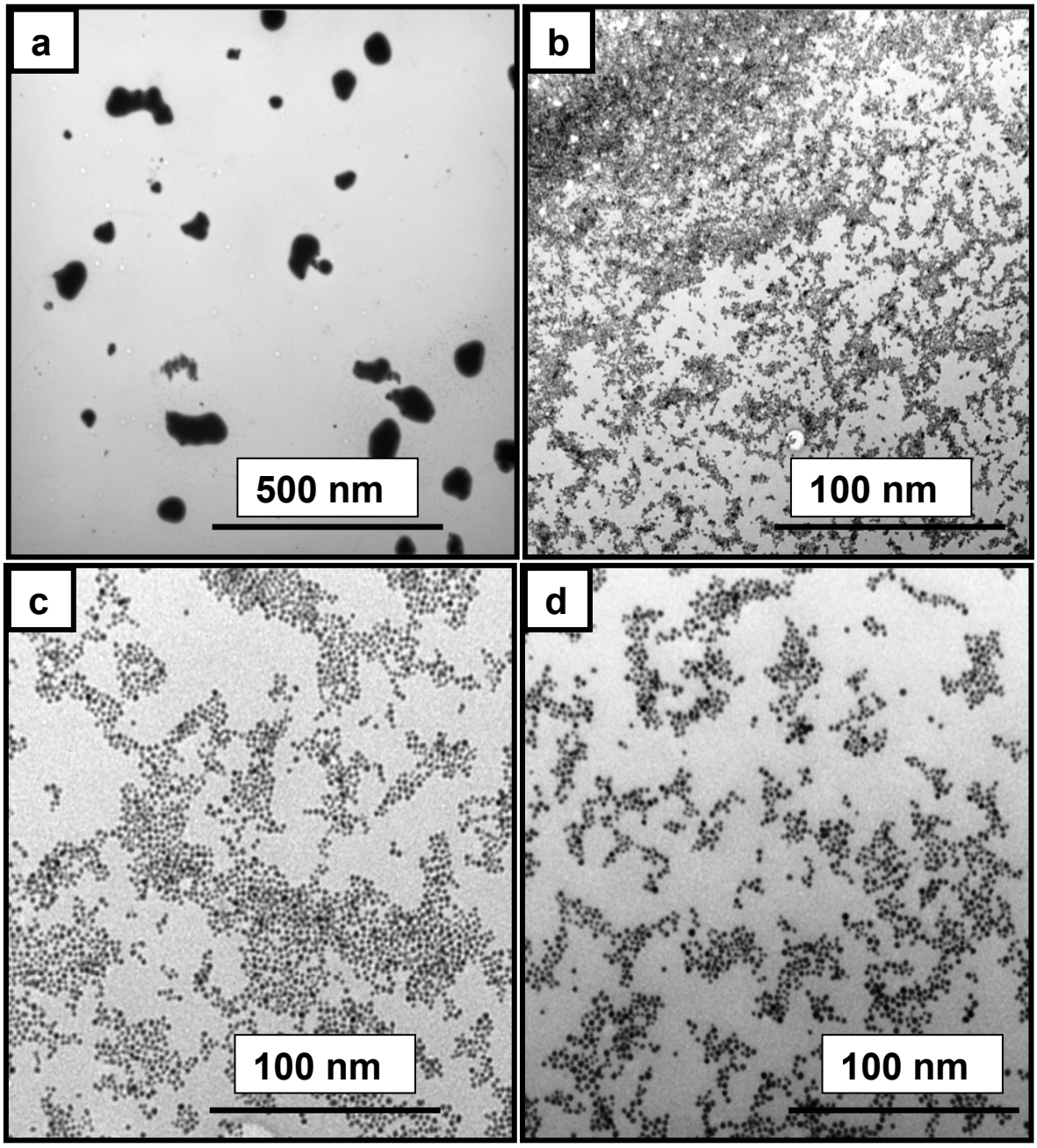

Figure 5.3 TEM images of (a) as-prepared SMAD product, (b) after 10 min (c) after 20 Min and (d) after 40 Min of digestive ripening.

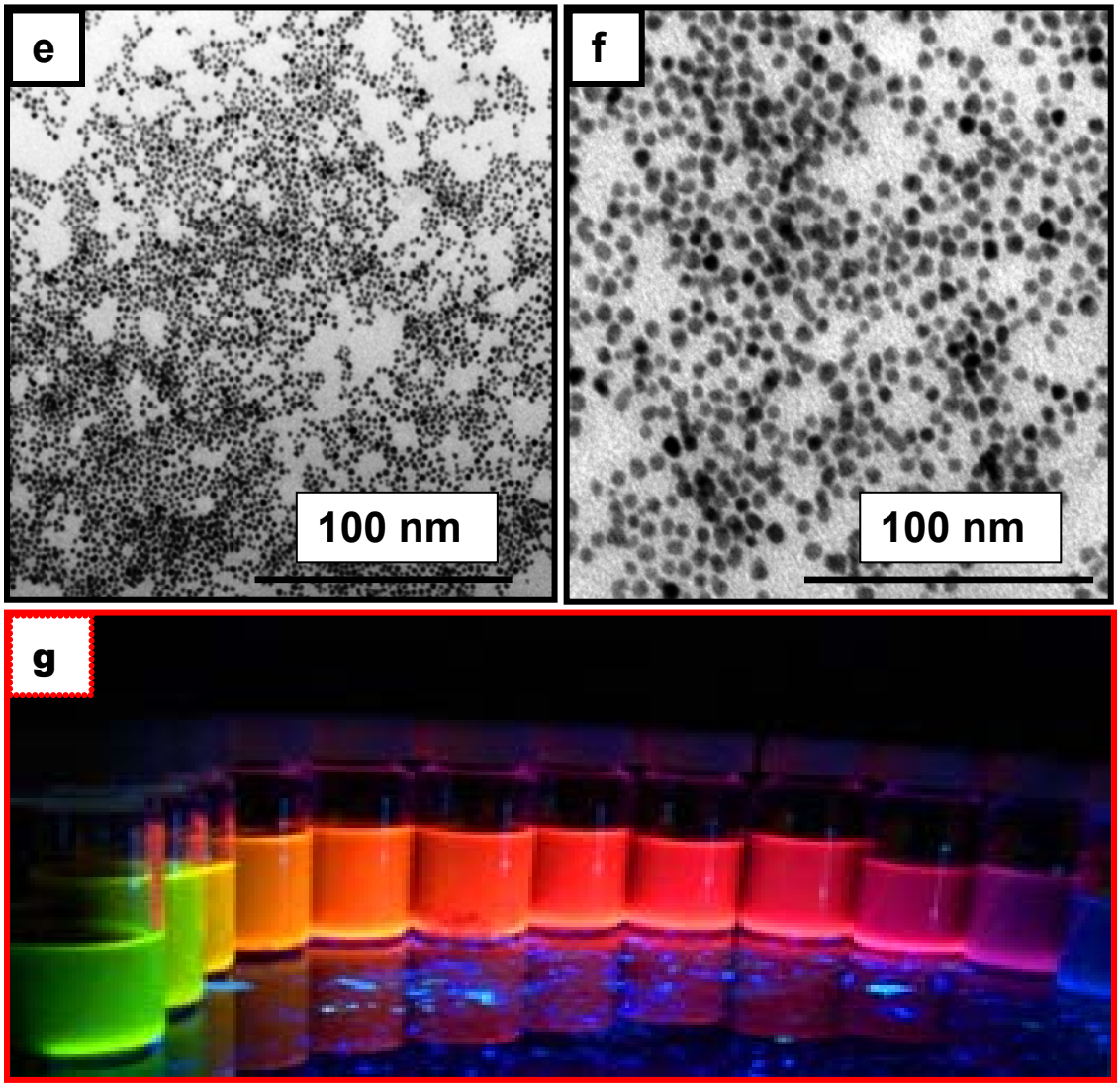

Figure 5.4 TEM images of CdSe QDs, (e) after 60 Min and (f) after 90 Min of digestive ripening and (g) Corresponding CdSe QDS samples upon exposure to UV-Vis illuminator.

5.4.2 Cadmium Telluride – Oleyl Amine – Trioctyl Phosphine Oxide

In case of CdTe, a similar trend was observed where; the as- prepared SMAD product has broad fluorescence but upon digestive ripening the fluorescence narrows and shifts. Under the same reaction conditions (Like that of CdSe-OA-TOPO) the PL of CdTe can be tuned to 667 nm but compared to CdSe it took only 60 minutes. The as - prepared SMAD product is light yellow and turns brighter yellow color, then red and, finally into dark red color, which indicates rapid breakdown of aggregated crystallites and dramatic growth of CdTe nanocrystals in the first 30 minutes of digestive ripening. After 30 minutes the growth rate decreased, indicating the formation of larger particles. The as-prepared SMAD product absorption spectrum (Figure 5.5) reveals broad electronic transitions, indicating high crystallinity of CdTe. Upon digestive ripening these electronic transitions merge into a broad peak, which implies formation of larger particles, and this phenomenon has been observed when mixed ligands were employed. [28,29] Figure 5.6 shows the PL of CdTe QDs with the progress of digestive ripening time. As observed with CdSe, CdTe also reaches an equilibrium size; where the initial FWHM was broad but as digestive ripening time progresses the FWHM has narrowed. Figure 5.7(a-b) shows the as-prepared SMAD product TEM images. Note the aggregated small crystallites, but upon digestive ripening these aggregates breakdown into smaller particles and then grow in size (Figure5. 7(c-d) and Figure 5.8(e-h). Figure 5.9 shows the corresponding samples collected at various time intervals from the same batch and these samples were exposed to the UV-Vis illuminator. Table 5.2 shows the progressive growth of particle size and the PL of CdTe with digestive ripening time.

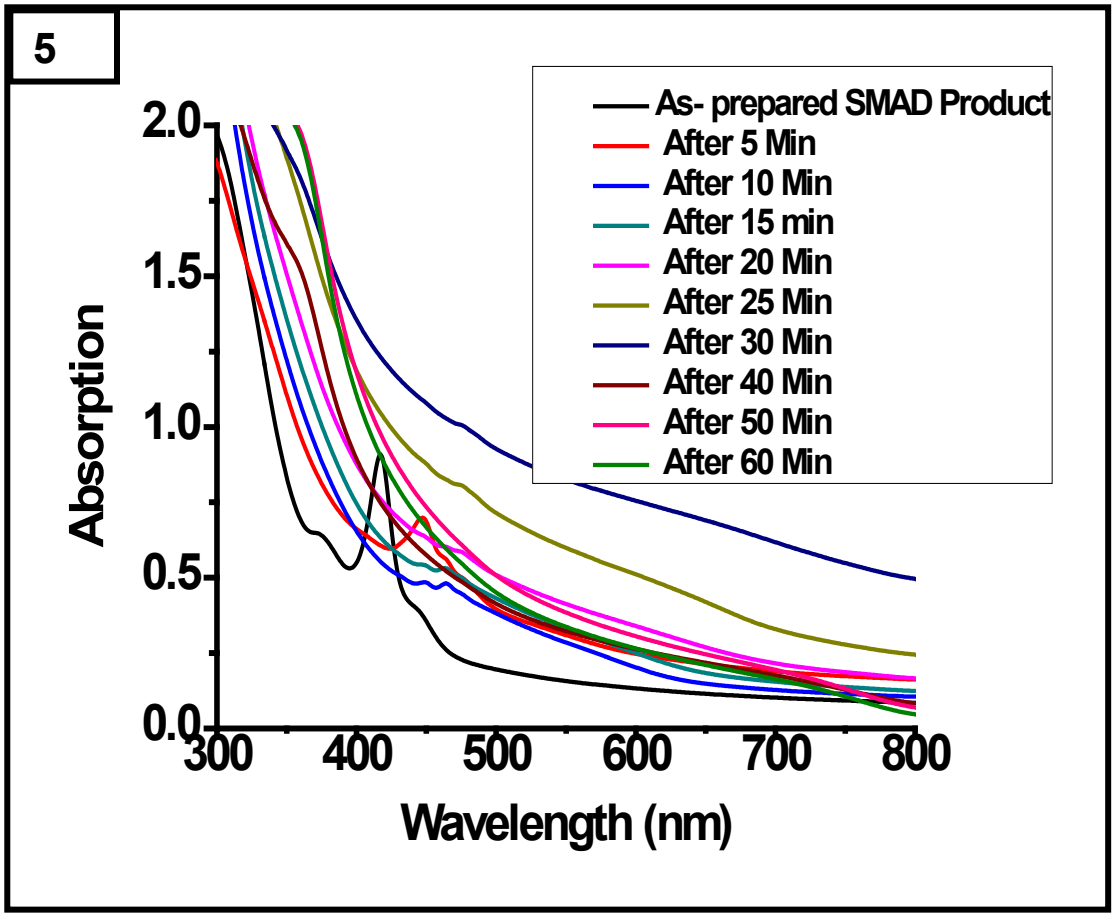

Figure 5.5 UV-Vis absorption spectrum of CdTe QD samples collected at 10, 20, 30, 40, 50, and 60 minutes of digestive ripening.

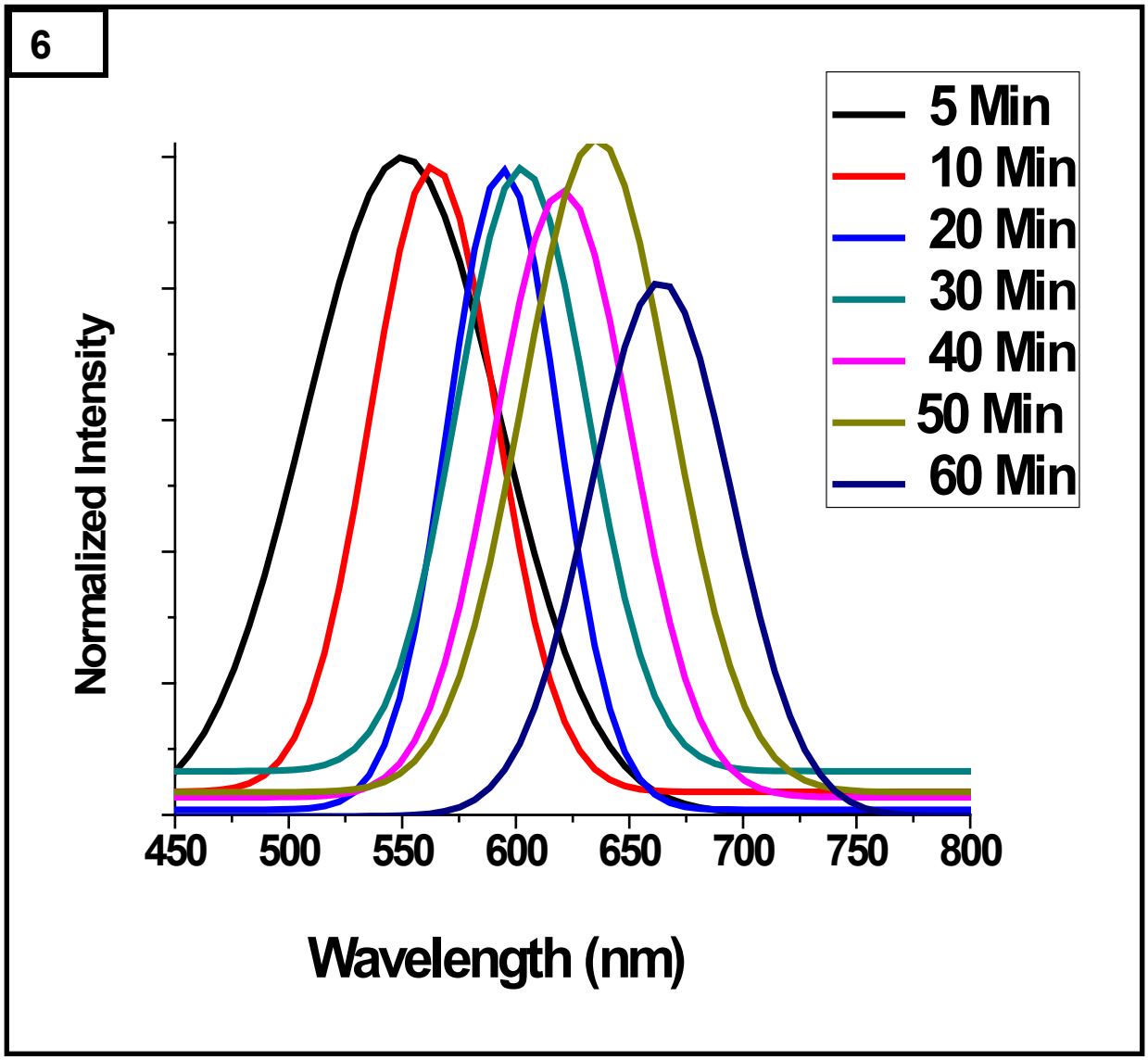

Figure 5.6 Photoluminescence spectrum of CdTe QD samples collected at 5, 10, 20, 30, 40, 50, and 60 minutes of digestive ripening.

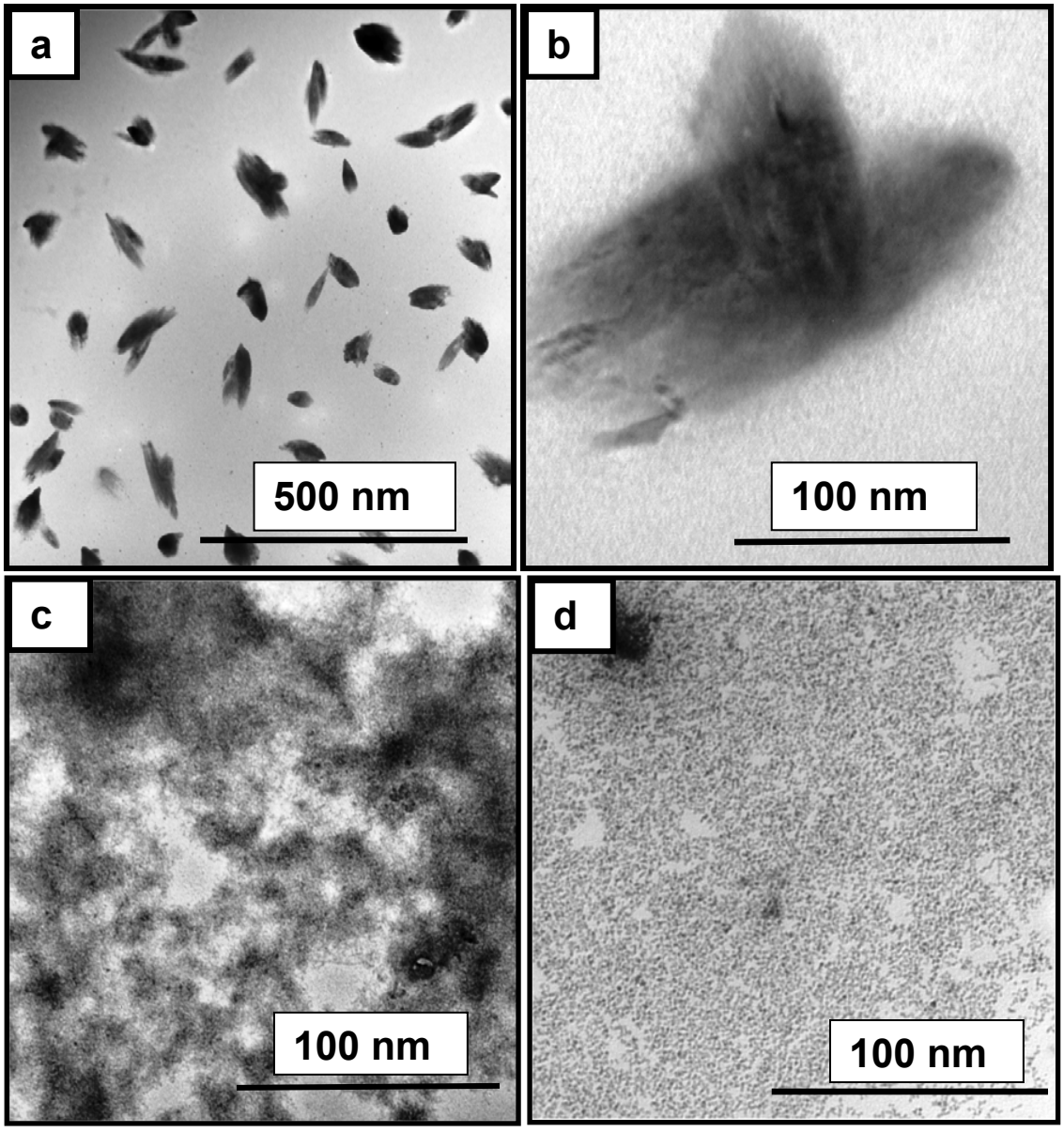

Figure 5.7 TEM images of CdTe QDs, (a, b) as- prepared SMAD product before digestive ripening, (c) after 10 Min of digestive ripening, and (d) after 20 Min of digestive ripening.

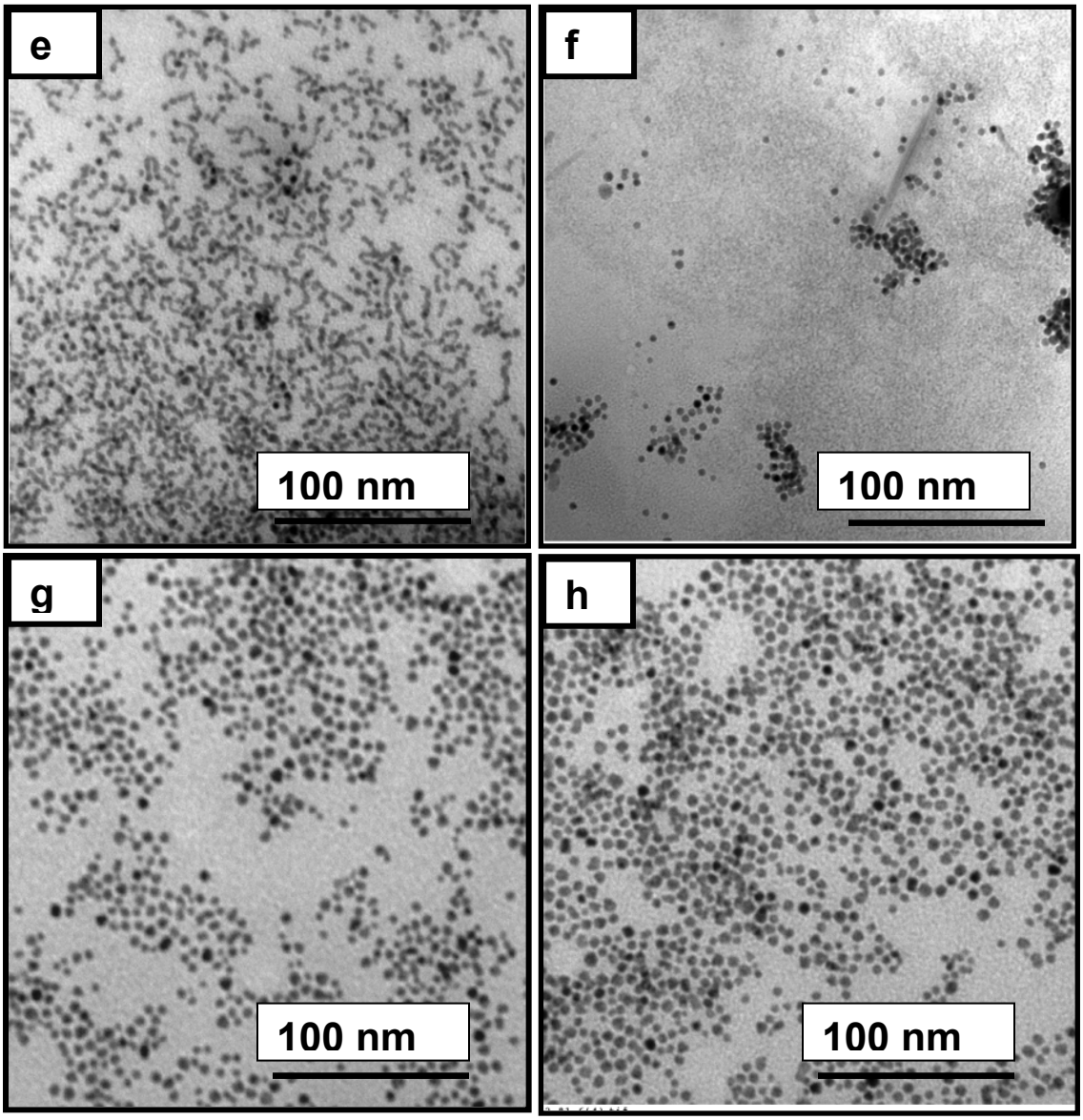

Figure 5.8 TEM images of CdTe QDs, (e) after 30 Min and (f) after 40 Min of digestive ripening, (g) after 50 min and (h) after 60 min of digestive ripening.

Figure 5.9 Corresponding CdTe QDS samples upon exposure to UV-Vis illuminator

Digestive Ripening Time (Min)	5	10	20	30	40	50	60
PLwavelength λ max (nm)	549	560	592	602	620	635	663
Particle Mean Size (nm)	2.9	3.2	4.5	5.0	5.2	5.3	7.2

Table 4 Change in wavelength of UV-Vis, photoluminescence and particle size of CdTe QDs with digestive ripening time

5.4.3 Cadmium Selenide Core – Zinc Sulfide Shell QDs

Over coating of semiconductor QDs with a high band gap inorganic material enhances the photoluminescence QY by passivating surface recombination sites.[17] Surface coating not only protects the core nanomaterial from photooxidation but also from physical and chemical stress. Figure 5.10 illustrates a schematic representation of shell coating on semiconductor QDs.[17]

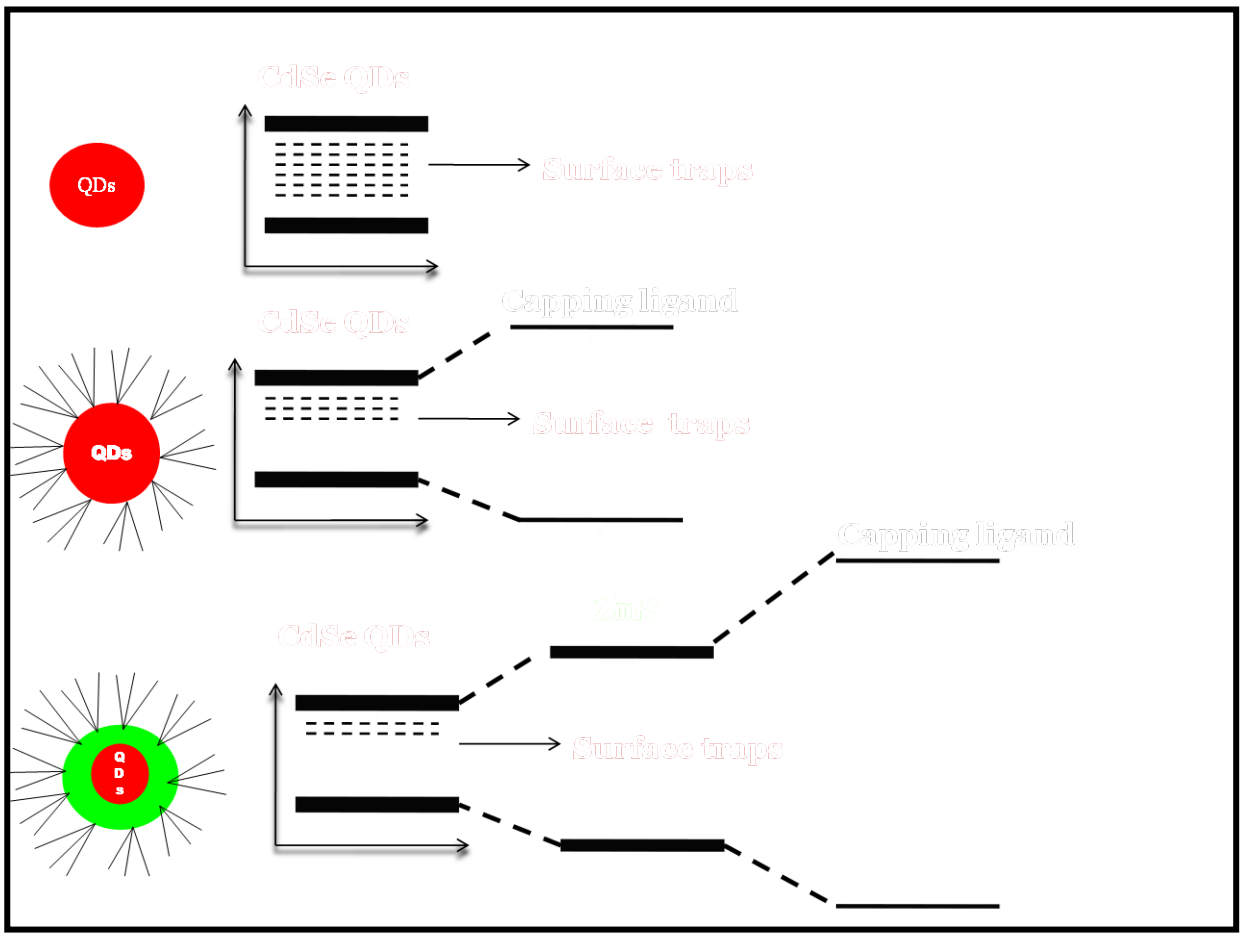

Figure 5.10 Schematic illustrates of shell coating on semiconductor QDs. [17]

The evolution of the PL from the CdSe-ZnS is depicted in Figure 5.11- 13. It is clearly shown that the PL peak becomes sharp and more symmetrical than that of the core. The red-shift is due to the further growth in the shell thickness.

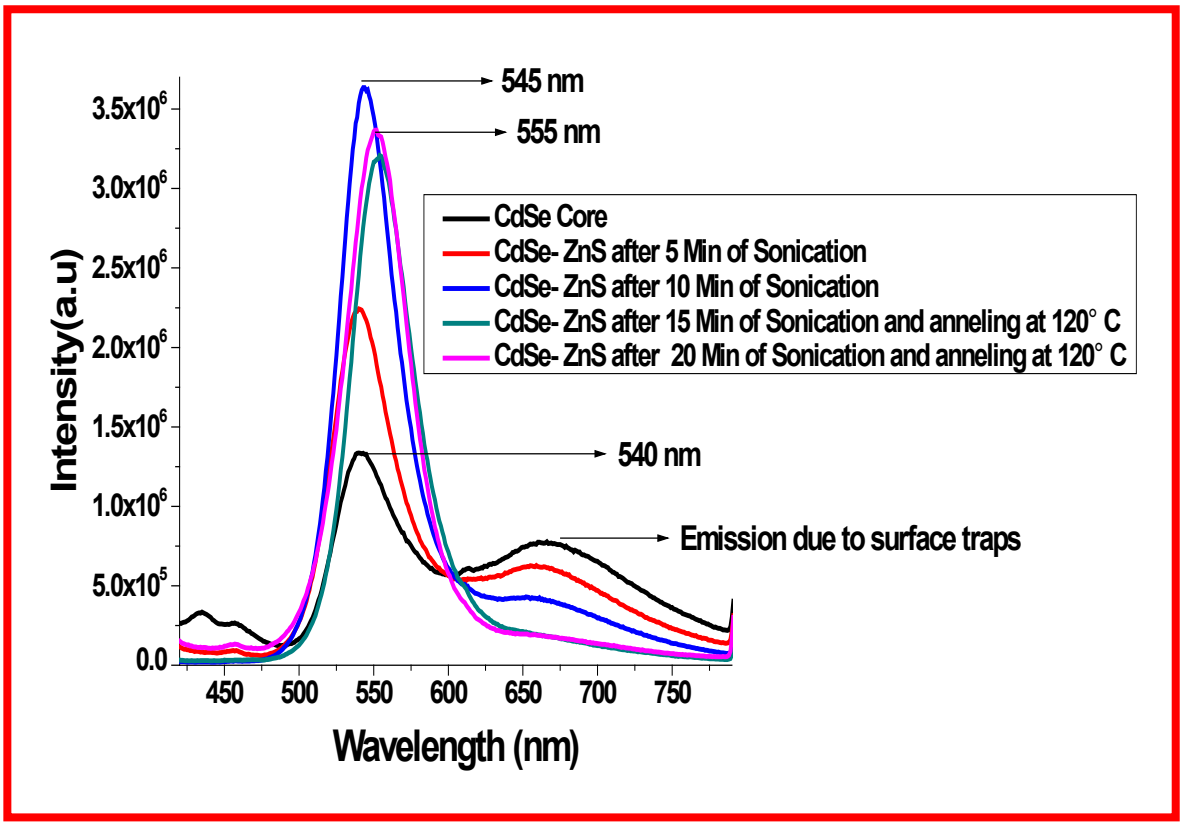

Figure 5.11 Shell coating on digestively ripened CdSe QDs. The broad emission band from 625-700 nm wavelength in core CdSe QDs is due to surface traps but upon ZnS shell growth, the emission due to surface traps was reduced and simultaneously enhanced PL can be seen. The PL shift from 540 nm to 545 nm and then to 555 nm indicates the growth of shell material on the CdSe Core.

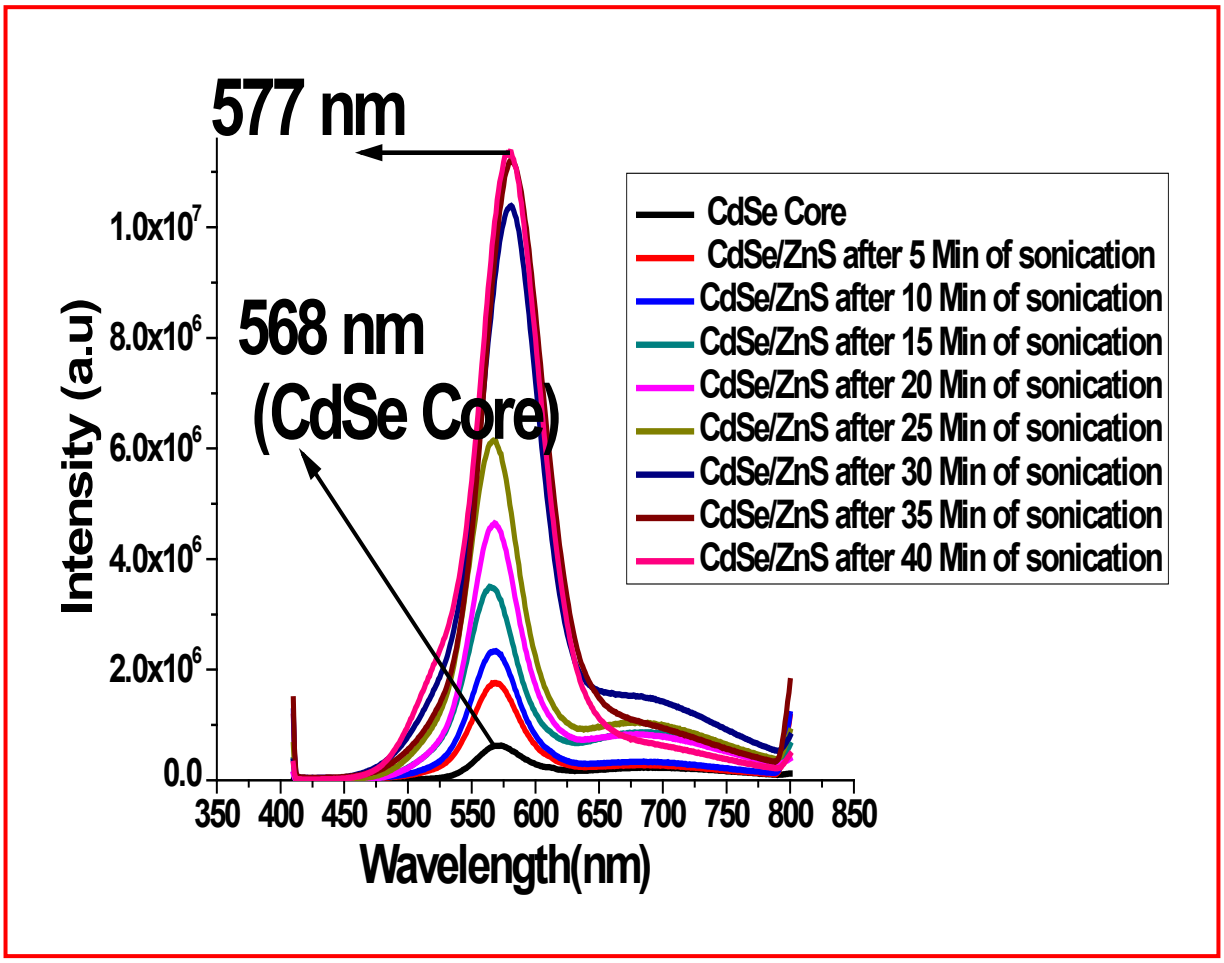

Figure 5.12 shell coating on digestively ripened CdSe QDs (568 nm emission) and after ZnS shell growth the PL peak is not only enhanced, but also there is a considerable shift (577).

The initial broadening in PL (Figure 5.13) is obviously from the growth of shell material, which is due to increase in particle size and further shell growth resulted in a red-shift (from 568 nm to 577 nm) of PL. [30]

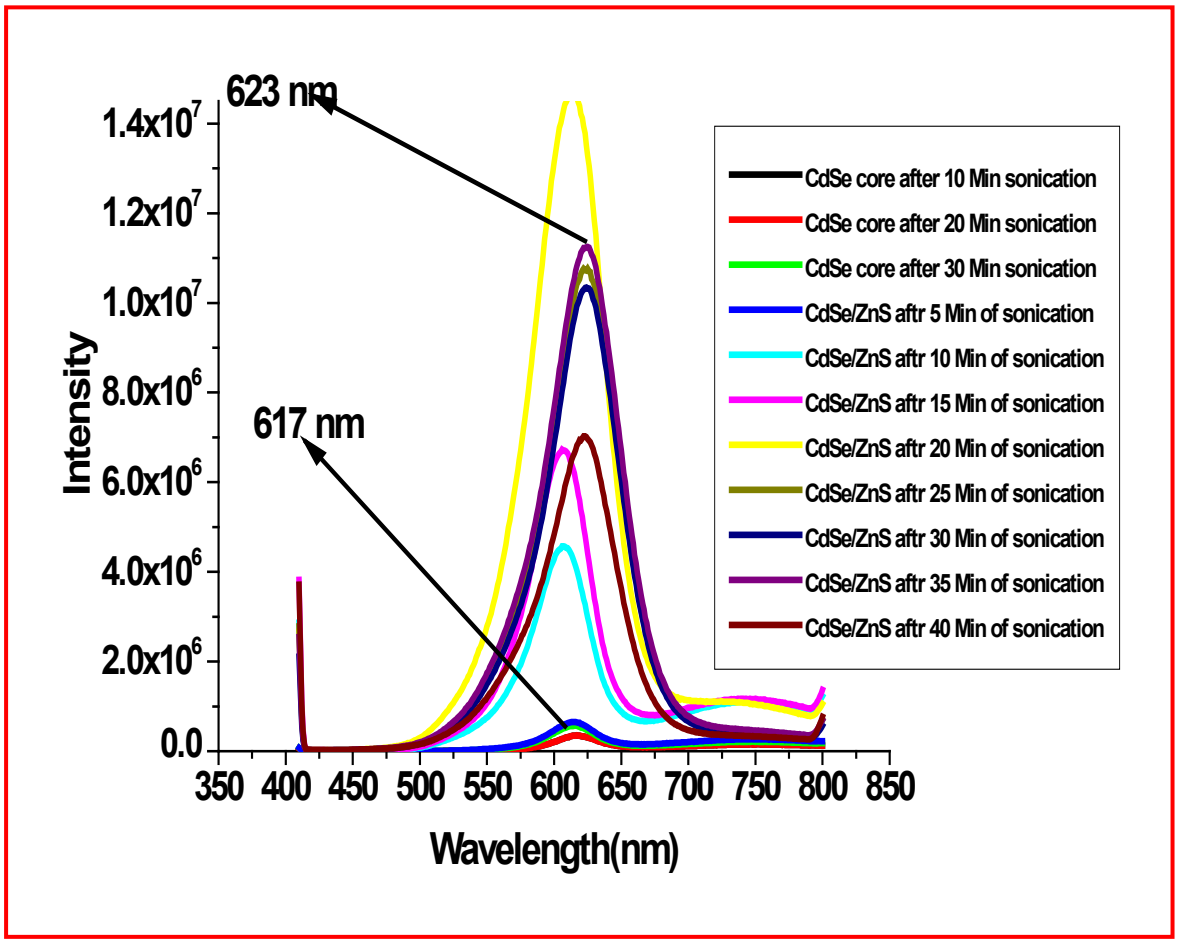

Figure 5.13 Photoluminescence of CdSe QDs (617 nm emission) core and enhanced photoluminescence from the CdSe-ZnS Core-Shell.

Figure 5.13 – 15 are the HRTEM images of CdSe and CdSe/ZnS core-shell quantum dots. The lattice mismatch between the CdSe and ZnS is 12%, and resolving this by using TEM is challenging, [30-33] but by measuring the average particle size on the HRTEM images of core, and by subtracting the average particle size measured on the HRTEM images of the core-shell will give an estimated shell thickness.

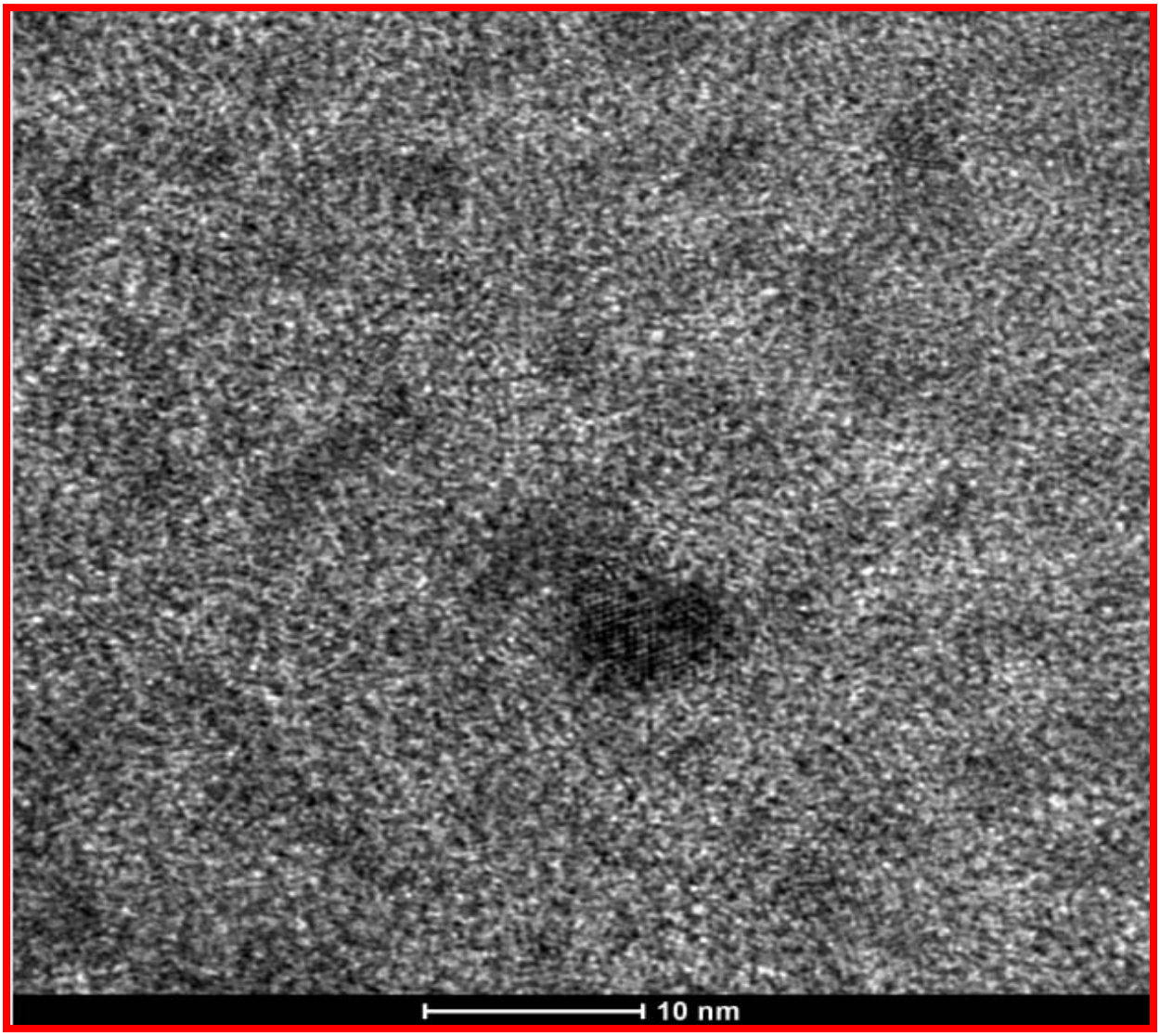

Figure 5.14 HRTEM image of CdSe QDs showing the crystalline nature after 30 minutes of digestive ripening.

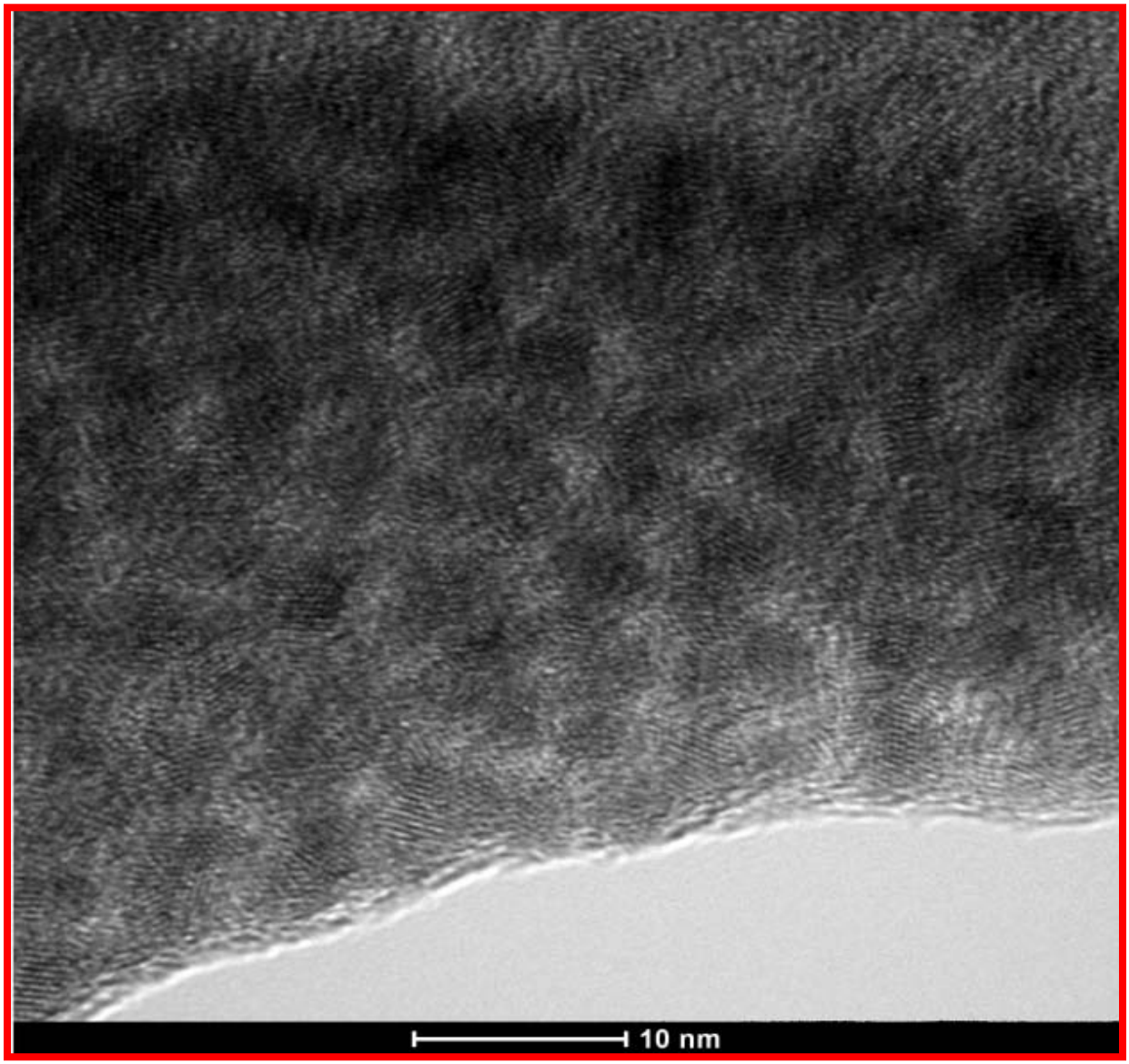

Figure 5.15 HRTEM image of CdSe/ ZnS Core-Shell QDs. CdSe QDs were obtained after 30 minutes of digestive ripening.

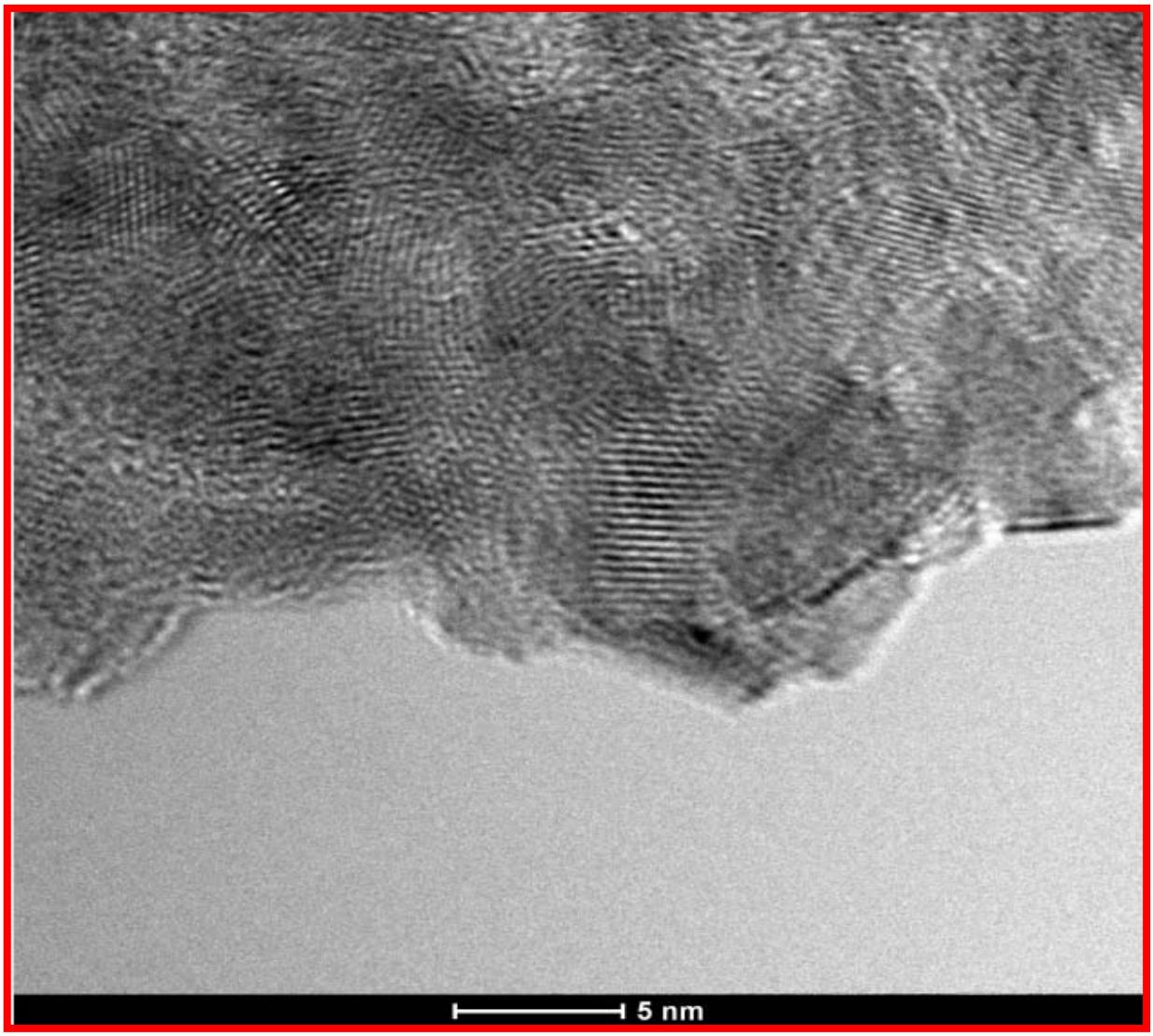

Figure 5.16 HRTEM image of CdSe/ ZnS Core-Shell QDs showing the crystalline lattice. CdSe QDs was obtained after 40 minutes of digestive ripening

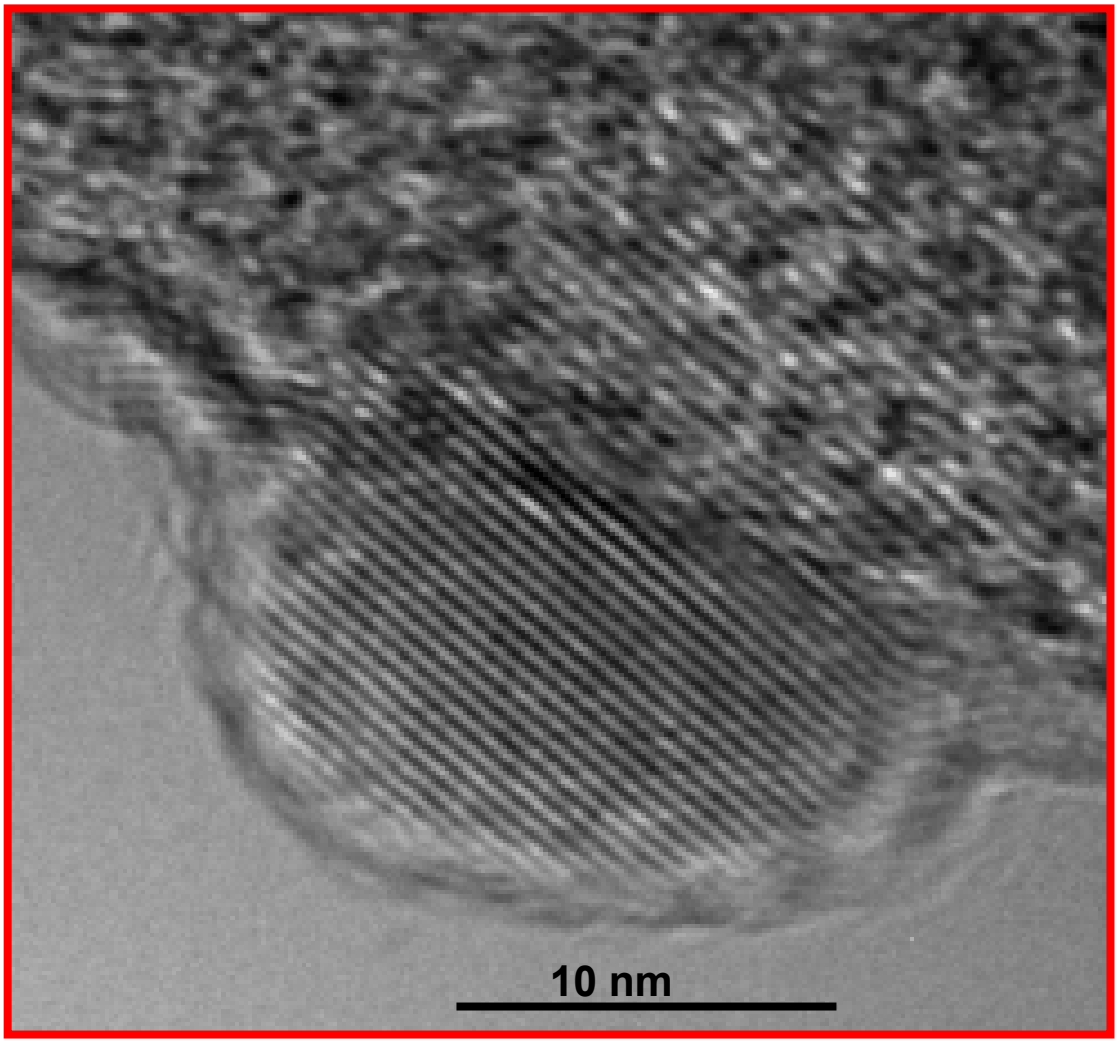

Figure 5.17 HRTEM image of CdSe/ ZnS Core-Shell QDs showing the crystalline lattice.The CdSe QD was obtained after 90 minutes of digestive ripening.

The average diameter of particle size measured on HRTEM image of CdSe/ZnS core-shell (Figure 5.15) is 4.8 nm and the average diameter measured on the core (Figure 5.14) is 3.6 nm. Therefore, the average shell thickness on these particles is 1.2 nm. Both core and core-shell QDs were characterized by Energy Dispersion spectroscopy (EDX) as show in Figure 5. 18 -19 and the EDX measurements were measured in the scanning transmission electron microscopy (STEM) mode.

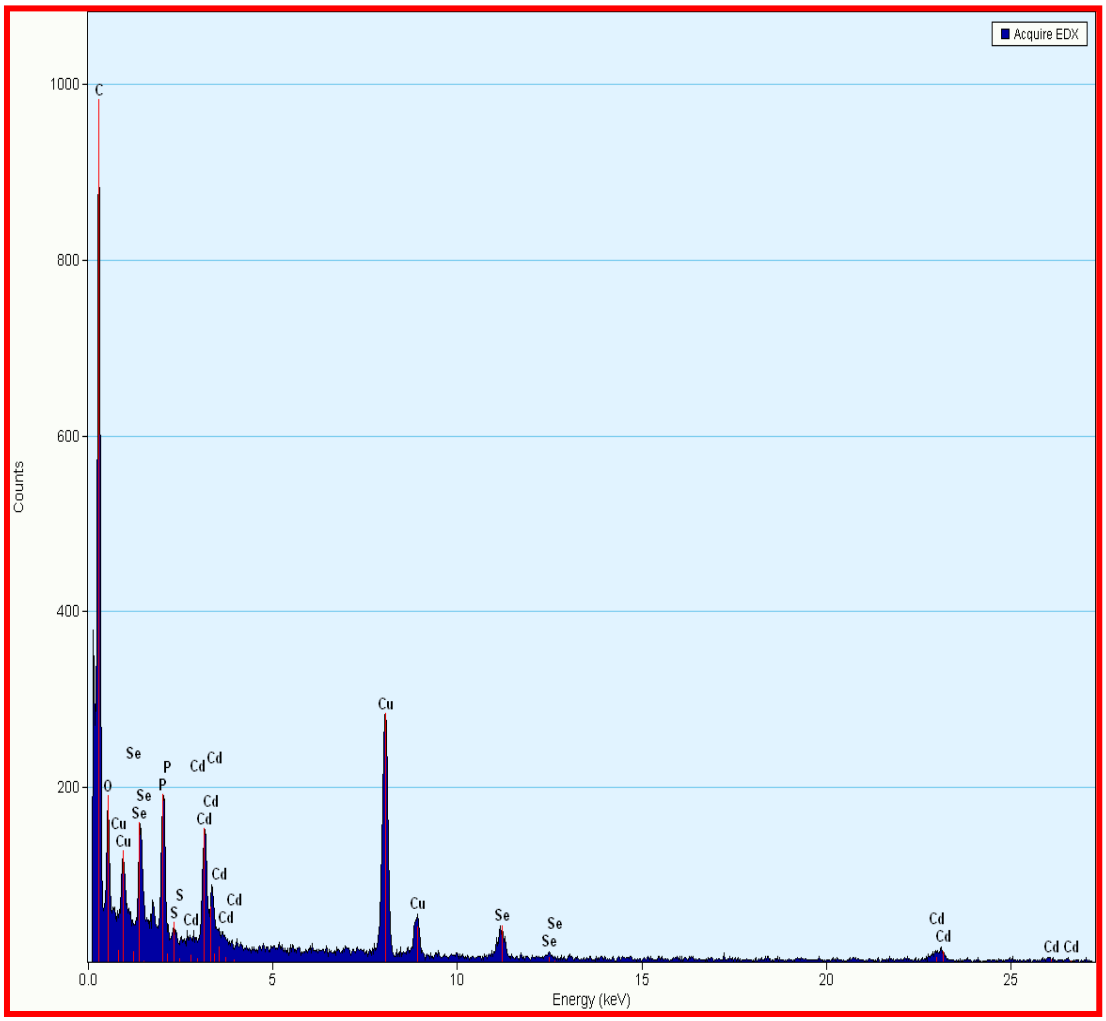

Figure 5.18 Energy Dispersion spectroscopy (EDX) spectrum of CdSe QDs, which shows all the characteristic peaks of cadmium and selenide and the rest of the peaks are from the lacey copper coated TEM grid.

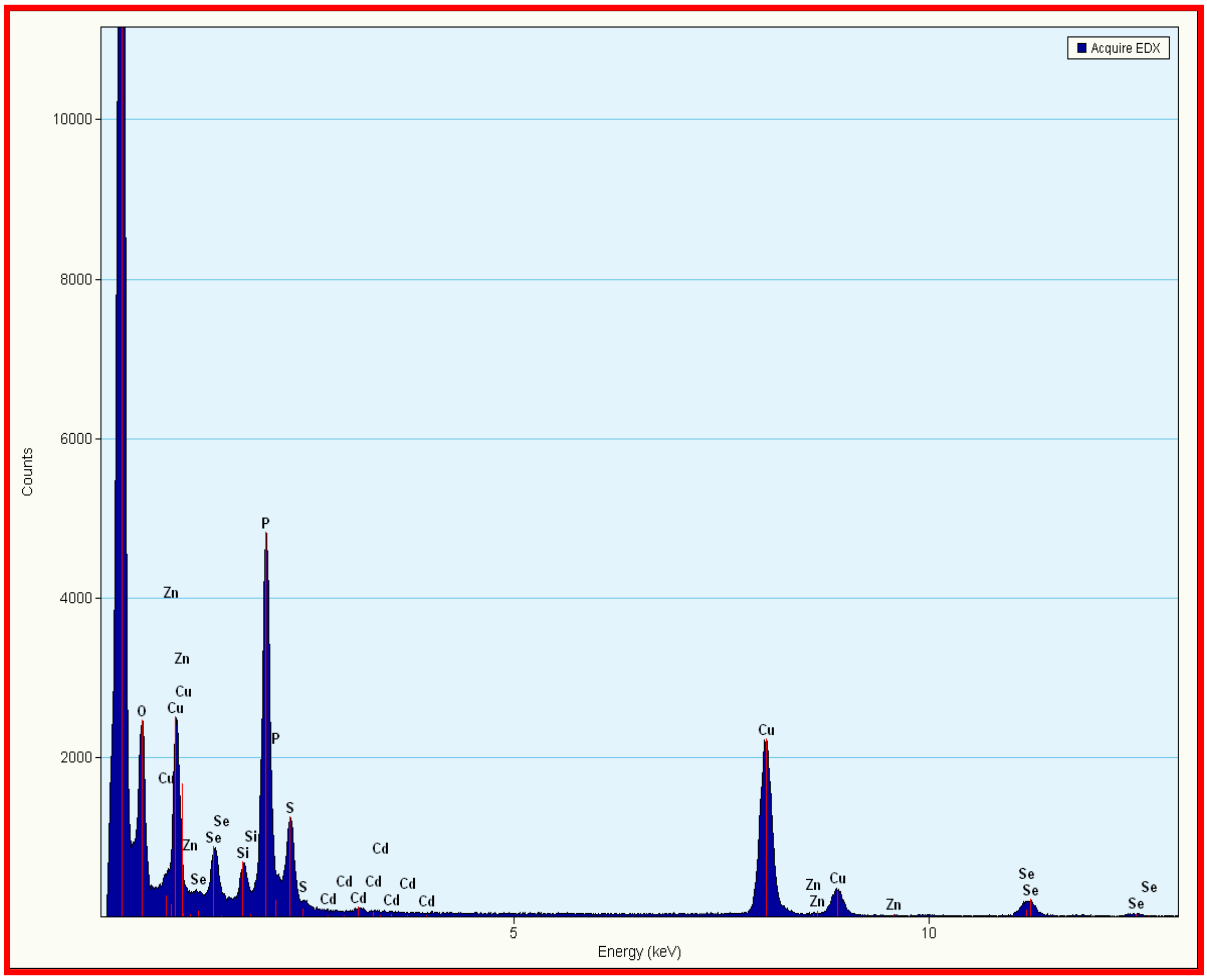

Figure 5.19 Energy Dispersive spectroscopy (EDX) spectrum of CdSe- ZnS core-shell QDs. All the characteristic peaks of cadmium, selenide, zinc and sulfur are present. The rest of the peaks are from the lacy carbon coated copper TEM grids.

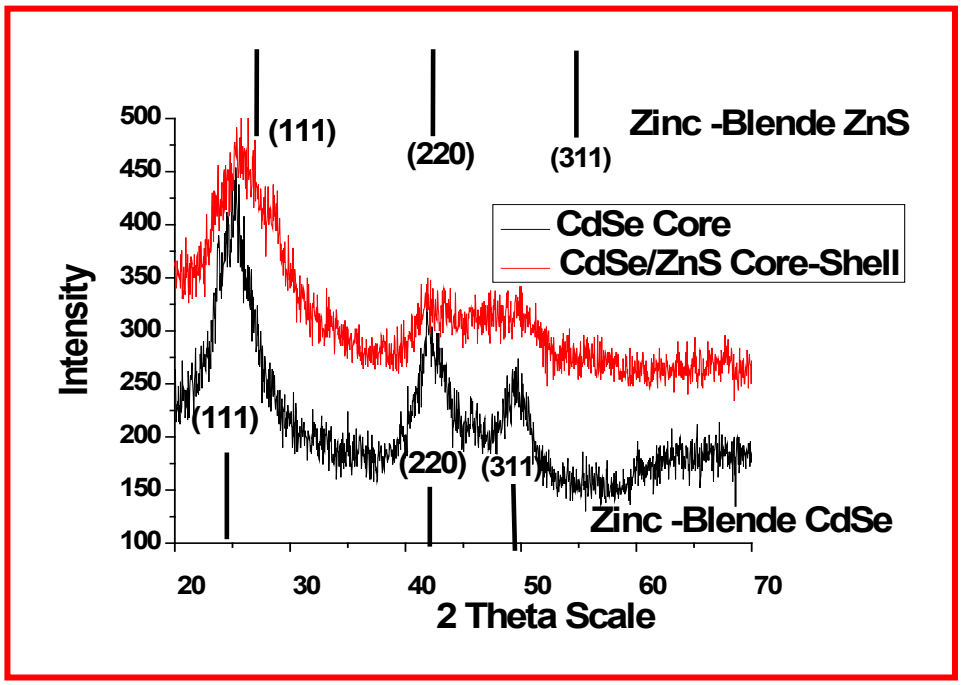

Figure 5.20 The XRD patterns of CdSe (Black lines) showing the characteristic features of zinc blend crystalline structure and CdSe/ZnS (Red lines) showing the characteristic features of zinc blend structure and the vertical bars (bottom) corresponds to JCPDS file No. 77-2100 and (top) JCPDS file No. 19-0191.

After ZnS shell growth the XRD patterns of CdSe core was slightly shifted to higher 2-theta angle, which supports the formation of ZnS shell over the CdSe core. Further, broadening in XRD patterns (Figure 5.20) represents the finite crystalline size of the core. It is interesting to note that when lower boiling point solvents (toluene (BP 110° C), t-butyl toluene (BP 190°C)) were used to digest as-prepared SMAD product, the particles retain the crystalline nature of the bulk starting material i.e wurtzite (hexagonal) crystalline structure. [1]

However, when digestive ripening was carried out at an elevated temperature (250 °C) in presence of ligands, the particles attained a Zinc blend (cubic) crystal structure. [34] Further, the measured quantum yield was enhanced from 36 % to 60 % upon adding a ZnS shell. It is important to note that when toluene was used as digestive ripening solvent the measured QY was 11% and a 28% QY was achieved with t-butyltoluene. [1] With the higher temperature, the higher QY must be due to removal of crystalline defects. The HRTEM images (Figure 5.14- 17) do show that the particles have good crystalline nature of both core and core-shell particles, and these were synthesized under the higher temperature digestive ripening conditions.

To further characterize the core-shell structure, we carried out the XPS studies to investigate the surface composition of CdSe and CdSe/ZnS QDs. In Figure 5.21(a), the two strong peaks located at 405.2 and 412 eV correspond to Cd 3d binding energy of CdSe, and the peak at 54. 3 eV in Figure 5.21(b), correspond to Se 3d binding energy of CdSe.[35,36] The XPS spectrum of CdSe/ZnS core/shell NCs shows typical peaks for ZnS, with Zn 2p3/2 and S 2p3/2 located at 1022 and 161.5 eV, respectively. Based on XPS data, the growth of ZnS shell on CdSe core is conformed.

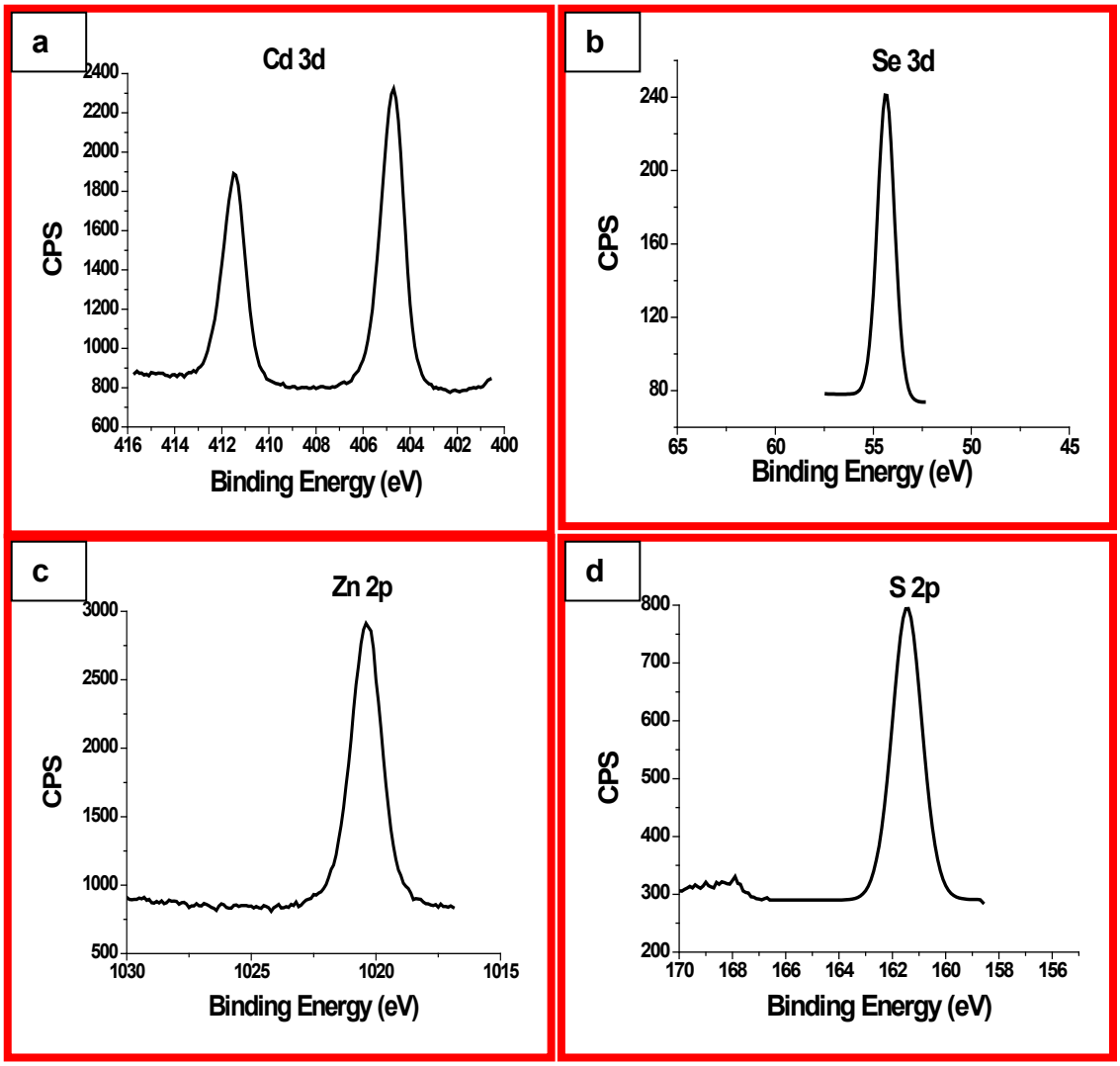

Figure 5.21(a) XPS spectra of Cd, (b) Se, (c) Zn and, (d) S binding energy (eV) of CdSe-ZnS QDs respectively

The lattice parameters for CdTe c = 6.477 Å, and for ZnS c = 6.257 Å [37] and the lattice mismatch CdTe core and ZnS shell is found to 19.8 %. [38] Figure 5.22 is the PL of the CdTe/ZnS core shell. The measured QY of CdTe and CdTe/ZnS is 38 % and 60% respectively.

In order to confirm the formation of ZnS shell on CdTe, energy dispersive X-ray spectroscopy (EDX), and the powder XRD measurements were made. The EDX spectrum in Figure 5.23 shows the existence of Cd and Te and Figure 5.24 shows the existence of Te, Cd, Zn and S in CdTe/ZnS sample. The sulfur peak at 2.3 keV and the Zn peak at 8.9 keV in EDX spectrum indicate the existence of a ZnS shell layer on the CdTe core. These results of the EDX spectrum further confirm the formation of the core/shell QDs.

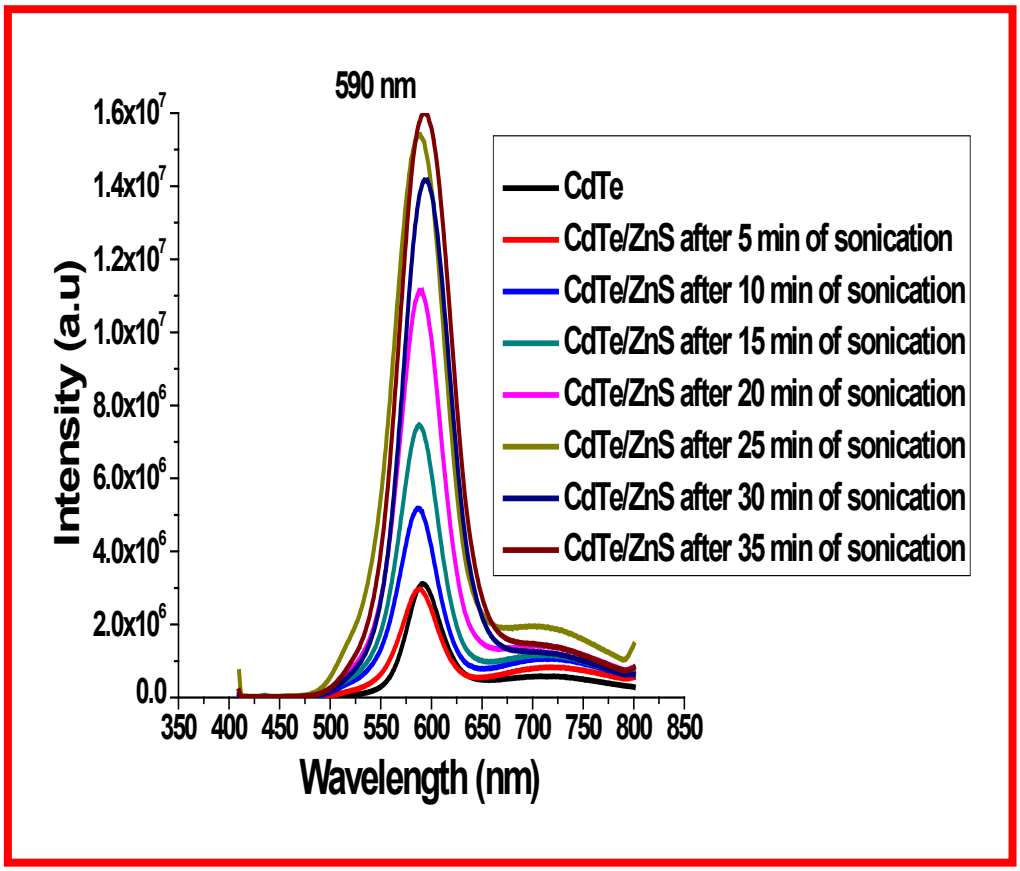

Figure 5.22 Photoluminescence spectrum of CdTe core and CdTe/ZnS shell with sonication time.

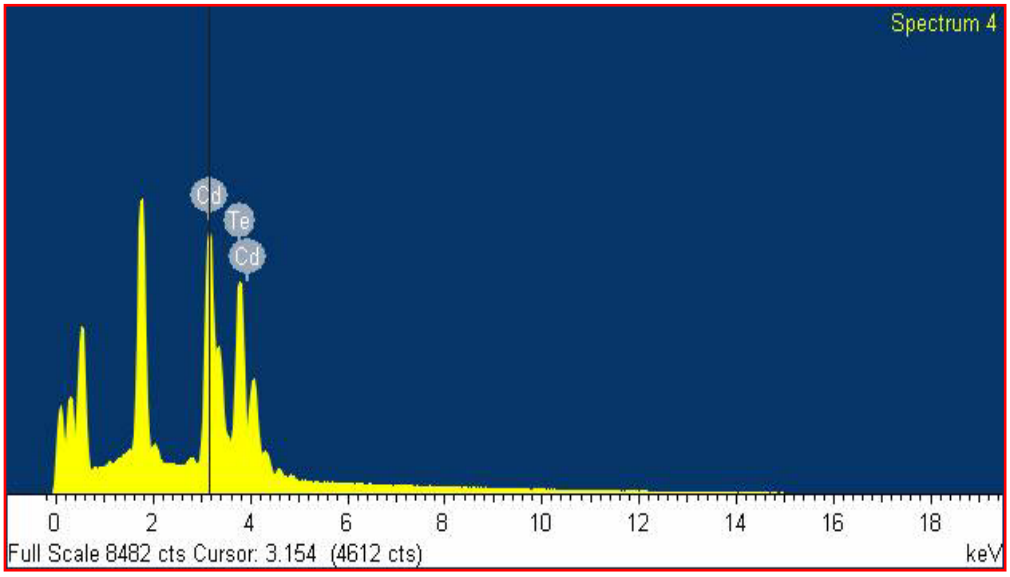

Figure 5.23 The energy dispersive X-ray spectroscopy (EDS) measurement showing the existence of cadmium and tellurium.

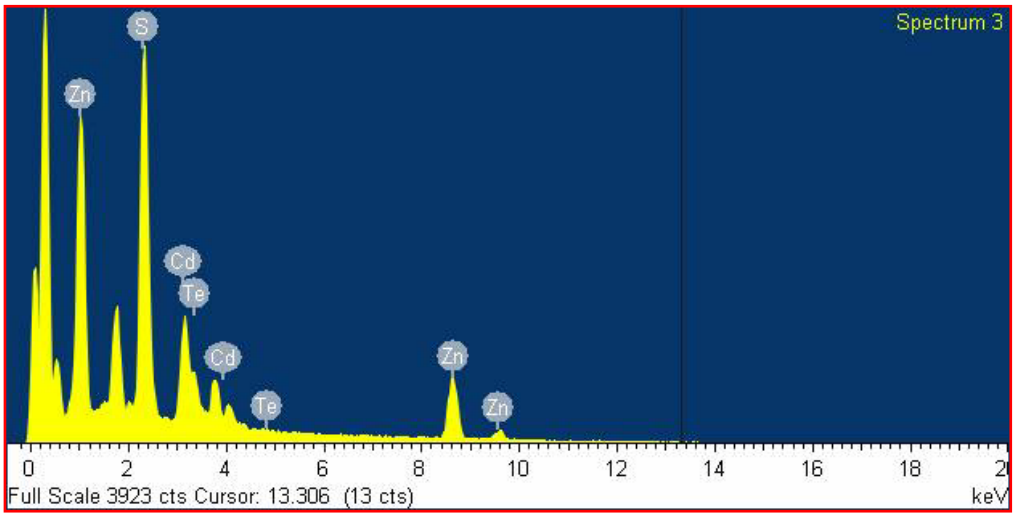

Figure 5.24 The energy dispersive X-ray spectroscopy (EDS) measurement showing the existence of cadmium, tellurium, zinc and sulfur.

The powder XRD patterns of CdTe and CdTe/ZnS core-shell are shown in Figure 5.25. The characteristic zinc blend planes of 111, 220, and 311 located at 24.40°, 41.60°, and 47.90° for CdTe core and at 24.94°, 41.72°, and 48.76° for CdTe/ZnS in 10–60° 2Θ range are observed. The position of the XRD peaks of CdTe cores matched well with those of bulk CdTe cubic structure (JCPDS NO. 15-0770). After growth of ZnS shell on the CdTe core, the peak position shifted to higher angles towards the positions of bulk ZnS cubic structure peaks (JCPDS NO. 05-0566), which substantiates the formation of CdTe/ZnS core-shell.

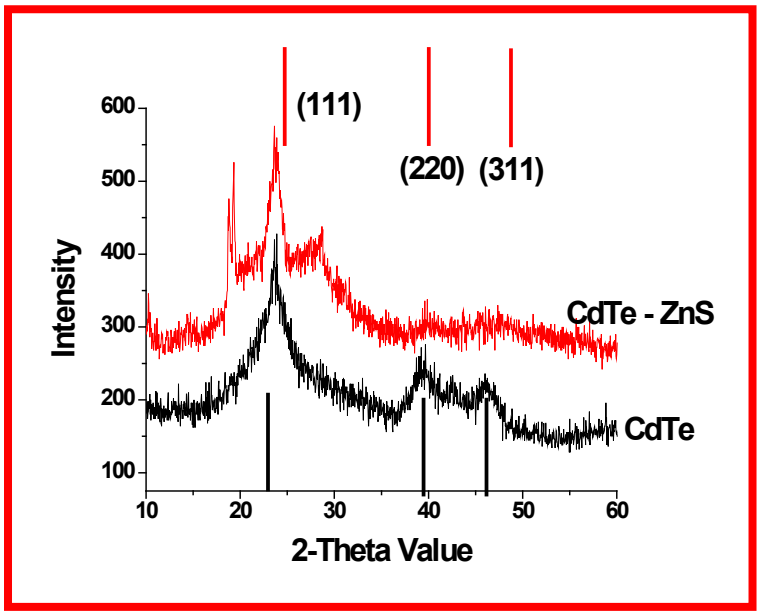

Figure 5.25 The characteristic zinc blend planes of 111, 220, and 311 locating at 24.40°, 41.60°, and 47.90° for CdTe core and at 24.94°, 41.72°, and 48.76° for CdTe/ZnS in the 10–60° 2Θ range.

To further characterize the CdTe/ ZnS core-shell structure, we carried out the XPS studies to investigate the surface composition of CdTe and CdTe/ZnS QDs. In Figure

5.25(a), the two strong peaks located at 404.89 and 412 eV correspond to Cd 3d binding energy of CdTe QD, and the peak at 571.77, 581.91eV in Figure 5.25(b), correspond to Te 3d binding energy of CdTe. In Figure 5.25(c) the strong peaks 1020.84, 1044.08 eV correspond to Zn 2p and 161.48 eV in Figure 5.25 (d) correspond to S binding energy of CdTeZnS QDs. These data of XPS provide the direct evidence of the formation of CdTe/ZnS QDs.

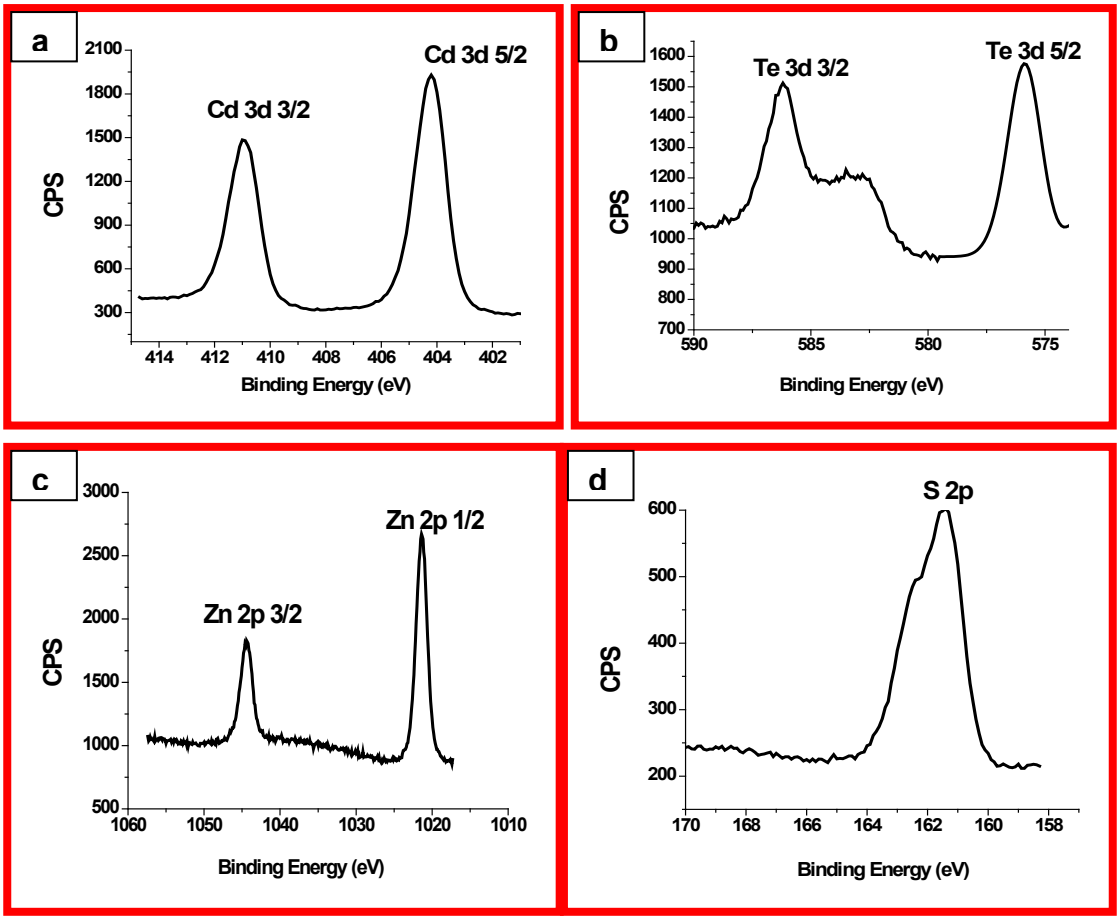

Figure 5.26(a) XPS spectra of Cd, (b) Te, (c) Zn and, (d) S binding energy (eV) of CdTe-ZnS QDs respectively

5.5 SUMMARY

1. Demonstration of the ability of SMAD technique for the gram-scale synthesis of semiconductor cadmium selenide and cadmium telluride.

2. Extending the digestive ripening phenomenon for cadmium telluride.

3. By employing ligands as capping agent and digestive ripening solvent, high temperature (250 °C) was achieved and more rapid digestive ripening occured

4. Compared to CdSe, the digestive ripening of CdTe was much faster.

5. Enhanced QY was obtained due to high digestive ripening condition, and promoted the more crystalline nature of the particles, and thereby enhanced QY.

6. Further enhancement of QY (40 to 60%) was achieved by coating core nanoparticles with a high band gap inorganic ZnS shell.

7. Formation of ZnS over the core is evident from PL, XRD, EDX, and XPS analysis.

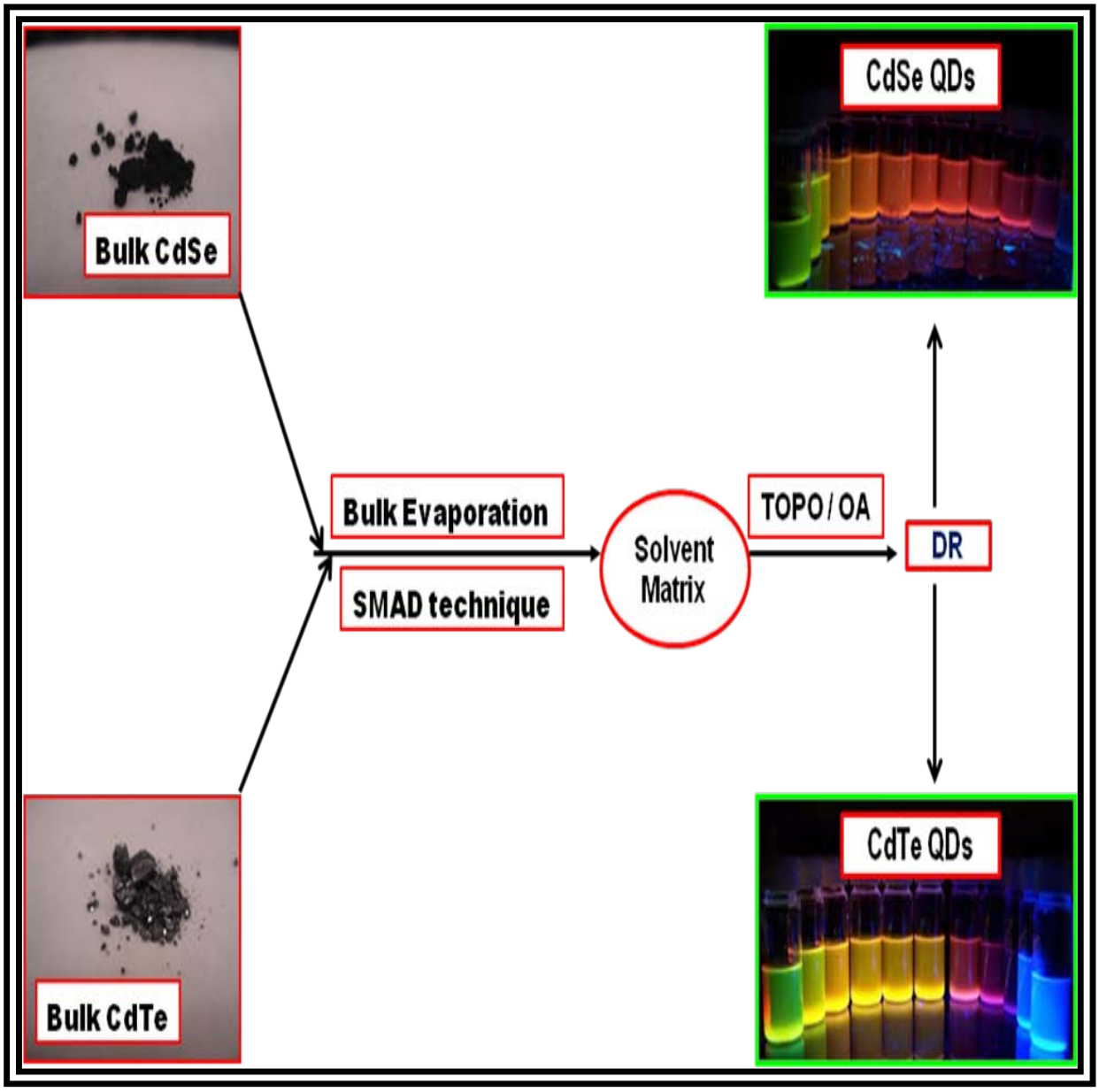

Figure 5.27 Schematic Representation of Overall Synthesis Procedure

5.6 References

(1) Cingarapu, S.; Yang, Z.; Sorensen, C. M.; Klabunde, K. J. *Chem. Mater.* **2009**, *21*, 1248-1252.

(2) Heroux, D.; Ponce, A.; Cingarapu, S.; Klabunde, K. J. *Adv. Funct. Mater.* **2007**, *17*, 3562-3568.

(3) Ponce, A. A.; Klabunde, K. J. *J. Mol. Catal. A: Chem.* **2005**, *225*, 1-6.

(4) Smetana, A. B.; Klabunde, K. J.; Sorensen, C. M. *J. Colloid Interface Sci.* **2005**, *284*, 521-526.

(5) Stoeva, S.; Klabunde, K. J.; Sorensen, C. M.; Dragieva, I. *J. Am. Chem. Soc.* **2002**, *124*, 2305-2311.

(6) Stoeva, S. I.; Smetana, A. B.; Sorensen, C. M.; Klabunde, K. J. *J. Colloid Interface Sci.* **2007**, *309*, 94-98.

(7) Kalidindi, S. B.; Jagirdar, B. R. *Inorg. Chem. (Washington, DC, U. S.)* **2009**, *48*, 4524-4529.

(8) Lin, X. M.; Sorensen, C. M.; Klabunde, K. J. *J. Nanopart. Res.* **2000**, *2*, 157-164.

(9) Klabunde, K. J. S., C. M.; Stoeva, S. I.; Prasad, B. L. V.; Smetana, A. B.; Lin, X. M.; " Metal Clusters in Catalysis and Materials Science: The issue of size control, Part II methodologies," Corrain, C.; Schmid, G.; Toshima, N.; editor, Elsevier Sci, Amsterdam, (2008) Chap ii, "Digestive Ripening" 233- 252

(10) Murray, C. B.; Norris, D. J.; Bawendi, M. G. *J. Am. Chem. Soc.* **1993**, *115*, 8706-15.

(11) Battaglia, D.; Li, J. J.; Wang, Y.; Peng, X. *Angew. Chem., Int. Ed.* **2003**, *42*, 5035-5039.

(12) Peng, X.; Manna, U.; Yang, W.; Wickham, J.; Scher, E.; Kadavanich, A.; Allvisatos, A. P. *Nature (London)* **2000**, *404*, 59-61.

(13) Peng, Z. A.; Peng, X. *J. Am. Chem. Soc.* **2001**, *123*, 183-184.

(14) Qu, L.; Peng, Z. A.; Peng, X. *Nano Lett.* **2001**, *1*, 333-337.

(15) Talapin, D. V.; Rogach, A. L.; Kornowski, A.; Haase, M.; Weller, H. *Nano Lett.* **2001**, *1*, 207-211.

(16) Yu, W. W.; Peng, X. *Angew. Chem., Int. Ed.* **2007**, *46*, 2559.

(17) Hines, M. A.; Guyot-Sionnest, P. *J. Phys. Chem.* **1996**, *100*, 468-71.

(18) Talapin, D. V.; Mekis, I.; Gotzinger, S.; Kornowski, A.; Benson, O.; Weller, H. *The Journal of Physical Chemistry B* **2004**, *108*, 18826-18831.

(19) Dorvel, B. R.; Keizer, H. M.; Fine, D.; Vuorinen, J.; Dodabalapur, A.; Duran, R. S. *Langmuir* **2007**, *23*, 7344-7355.

(20) Wang, X.-S.; Dykstra, T. E.; Salvador, M. R.; Manners, I.; Scholes, G. D.; Winnik, M. A. *J. Am. Chem. Soc.* **2004**, *126*, 7784-7785.

(21) Murcia, M. J.; Shaw, D. L.; Woodruff, H.; Naumann, C. A.; Young, B. A.; Long, E. C. *Chem. Mater.* **2006**, *18*, 2219-2225.

(22) Klabunde, K. J. T., P. L.; Skell, P. S.; Ittel, S. Inorg. Synth. 1979, 19, 59-86, Shriver, D.; Ed.

(23) Nair, P. S.; Radhakrishnan, T.; Revaprasadu, N.; Kolawole, G.; O'Brien, P. *Journal of Materials Chemistry* **2002**, *12*, 2722-2725.

(24) Zhu, C.-Q. W., Peng.; W, Xin.; Li, Y. Nanoscale. Res. Lett. 2008, 3, 213 -220.

(25) S.L. Cumberhand, K. M. H., A. Javier, G.A. Khitrov, G.F. Strouse, S.M. Woessner, C.S. Yun, Chem. Mater. 2002, 14, 1576 -1584

(26) Sung, Y.-M. P., K-S.; Lee, Y –J. J. Phys. Chem. C. 2007. 111, 1239- 242.

(27) Zhong, X.; Feng, Y.; Zhang, Y. *The Journal of Physical Chemistry C* **2006**, *111*, 526-531.

(28) Talapin, D.; Rogach, A. L.; Kornowski, A.; Haase, M.; Weller, H. *Nano Lett.* **2001**, *1*, 207.

(29) Qu, L.; Peng, X. *J. Am. Chem. Soc.* **2002**, *124*, 2049.

(30) Zhu, C. Q.; Wang, P.; Wang, X.; Li, Y. *Nanoscale Res. Lett.* **2008**, *3*, 213-220.

(31) Dabbousi, B. O.; Rodriguez-Viejo, J.; Mikulec, F. V.; Heine, J. R.; Mattoussi, H.; Ober, R.; Jensen, K. F.; Bawendi, M. G. *J. Phys. Chem. B* **1997**, *101*, 9463-9475.

(32) Hines, M. A.; Guyot-Sionnest, P. *J. Phys. Chem. B* **1998**, *102*, 3655.

(33) Mekis, I.; Talapin, D. V.; Kornowski, A.; Haase, M.; Weller, H. *J. Phys. Chem. B* **2003**, *107*, 7454-7462.

(34) Xie, C.; Chen, W.; Wang, J. *Frontiers of Chemical Engineering in China* **2007**, *1*, 377-380.

(35) Quan, Z.; Wang, Z.; Yang, P.; Lin, J.; Fang, J. *Inorganic Chemistry* **2007**, *46*, 1354-1360.

(36) Zhu, C.-Q.; Wang, P.; Wang, X.; Li, Y. *Nanoscale Research Letters* **2008**, *3*, 213-220.

(37) Trindade, T.; O'Brien, P.; Pickett, N. L. *Chemistry of Materials* **2001**, *13*, 3843-3858.

(38) Smith, A. M.; Mohs, A. M.; Nie, S. *Nat Nano* **2009**, *4*, 56-63.